

Tailoring Toll-like Receptor 8 Ligands for Balancing Immune Response and Inflammation

Inaugural-Dissertation

to obtain the academic degree

Doctor rerum naturalium (Dr. rer. nat.)

submitted to the Department of Biology, Chemistry, Pharmacy

of Freie Universität Berlin

by

DORA ŠRIBAR

2021

I hereby declare that I have completed the present work myself and have used no tools other than those listed here.

The following work was done from August 2016 to January 2021 under the supervision of Prof. Dr. Gerhard Wolber from the Institute of Pharmacy of Freie Universität Berlin.

1st Reviewer: Prof. Dr. Gerhard Wolber

2nd Reviewer: Prof. Dr. Günther Weindl

date of defence: 09.06.2021.

Acknowledgements

I would first like to thank Gerhard. I feel privileged (and a bit spoiled) by the working and academic environment you provided during my doctoral project. I especially appreciate your efforts to provide the best available infrastructure for our projects and support the healthy working atmosphere.

My thesis would not be complete without the remarkably skilled work of Maria and Ana. The immense recognition goes to them and their supervisors Günther and Matej for the smooth and open collaboration on our projects.

I also want to thank *Deutscher Akademischer Austauschdienst, Berlin School of Integrative Oncology* and *Frauenförderung des Fachbereichs Biologie Chemie und Pharmazie* for their financial support and the numerous opportunities to meet inspiring professionals and academics from all over the world.

A significant role in my doctoral journeys played colleagues from my group. I want to thank the more experienced members Manuela and Marcel for their support and advices for my projects. I salute comrades from the first floor: David&David, Kathrin, Szymon and Tessa. Memes, bad puns and lively scientific discussions lifted my spirits numerous times. Also, special thanks go to David M and Szymon for their suggestions for the thesis. Lihua, thank you for all the help and kind support during my time in the group. I also want to thank Petra for the help with administration, occasional German language practice and all the chocolate surprises in the past four years. Vielen Dank für alles, Petra.

To all friends who accompanied me through the journey. Especially Kosta and Milica, who generously let me hijack their spell-checker account for the past few months.

Finally, I want to thank my family for their unconditional support. Especially my parents, who said that they would financially support me as long as I study, and regretted immediately. To Ivana, who was the only one to consider my bar plots an art. And to Vedran, for being the biggest psychological and academic support, and especially for making me laugh in the most stressful moments.

Contents

Abbreviations.....	i
1 Introduction.....	1
1.1 Toll-like receptors	1
1.2 Functional significance of Toll-like receptor 8	3
1.3 Structural insights into Toll-like receptor 8 function	4
1.4 Toll-like receptor 8 in signalling pathways	7
1.5 The function of Toll-like receptor 8 in diseased states	8
1.6 Recent development of drugs targeting Toll-like receptor 8.....	10
2 Research aim.....	13
3 Computational methods	14
3.1 Molecular docking.....	14
3.2 Molecular dynamics simulations.....	16
3.3 Three-dimensional (3D) pharmacophores.....	18
3.3.1 Three-dimensional (3D) pharmacophores-based virtual screening.....	19
3.3.2 Dynamic pharmacophores	19
3.4 Shape-based similarity search	19
4 Results.....	21
4.1 Structural analysis of Toll-like receptor 8.....	21
4.1.1 Overview of the structure	21
4.1.2 Analysis of the dimerisation interface	26
4.1.3 Comparison to evolutionary related Toll-like receptors.....	28

4.2	Computationally-assisted identification of novel Toll-like receptor 8 modulators....	31
4.2.1	Overview of previously reported TLR8 modulators	32
4.2.2	Binding of small-molecule agonists	34
4.2.3	Systematic development of the three-dimensional pharmacophore for TLR8 agonist binding.....	36
4.2.4	Pharmacophore-based virtual screening	37
4.2.5	Experimental validation of the hits from pharmacophore-based virtual screening	39
4.2.6	Virtual screening based on shape- and atom-based similarity search	41
4.2.7	Experimental validation of the hits from shape- and atom-based similarity search	42
4.2.8	Experimental assessment of the anti-inflammatory activity for the active compounds	44
4.2.9	Binding of small-molecule antagonists	45
4.2.10	Prediction of binding poses for discovered antagonists with the pyrimidine scaffold	47
4.3	Optimisation of novel Toll-like receptor 8 antagonists.....	50
4.3.1	Optimisation strategy.....	51
4.3.2	Synthesis and pharmacological evaluation of the analogues.....	51
4.3.3	Prediction of the binding poses for the synthesised compounds	54
5	Discussion	57
5.1	Overview of the structure of Toll-like receptor 8.....	57
5.2	Computationally-assisted identification of novel Toll-like receptor 8 modulators....	59
5.3	The paradigm of the agonist binding.....	61
5.4	Pharmacological characterisation of the compounds	63

5.5	Elucidation of the binding mode for antagonists.....	64
6	Conclusion and outlook	65
7	Experimental section.....	67
7.1	Data collection and preparation.....	67
7.1.1	Ligand data	67
7.1.2	Protein data	67
7.2	Analysis of the protein structure	67
7.3	Analysis of the ligand properties.....	67
7.4	Molecular docking for binding pose prediction	68
7.5	Three-dimensional pharmacophore modelling.....	68
7.6	Virtual screening workflow	68
7.7	Shape- and atom-based similarity search	69
7.8	Molecular dynamics simulations.....	70
7.9	Analysis of protein dimerisation interface	70
7.10	Dynophore analysis	71
7.11	Experimental methods	71
7.11.1	The purity of commercial compounds.....	71
7.11.2	Pharmacological characterisation	72
7.11.3	General synthetic procedure	72
8	Summary	74
9	Zusammenfassung.....	75
10	List of publications	77
10.1	Publications	77
10.2	Conference posters	77

11 Bibliography	78
Appendix.....	94
Tables	94
Figures	113
List of figures.....	122
List of tables.....	127

Abbreviations

AP-1	activator protein 1
APC	antigen-presenting cells
DAMP	damage-associated molecular pattern
ELISA	enzyme-linked immunosorbent assay
ERK	extracellular signal-regulated kinases
GA	genetic algorithm
HEK	human embryonic kidney cell line
HPLC	high performance liquid chromatography
IFN	interferon
IL	interleukin
IRAK	interleukin-1 receptor-associated kinase
IRF	interferon regulatory factor
IRF	interferon regulatory factor
LRR	leucine-rich repeat
MAPK	mitogen-activated protein kinase
MD	molecular dynamics
NF- κ B	nuclear factor kappa-light-chain-enhancer of activated B cells
OD	optical density
PAMP	pathogen-associated molecular pattern
PDB	protein data bank

PRR	pattern-recognition receptors
RMSD	geometrical root mean square difference
ROC	receiver operating characteristic curve
ROCS	rapid overlay of chemical structures
SAR	structure-activity relationships
SD	standard deviation
SEAP	secreted embryonic alkaline phosphatase
SLE	systemic lupus erythematosus
SMILES	simplified molecular-input line-entry system representations of molecules
TAB	TAK1 binding proteins
TAK	transforming growth factor β -activated kinase 1
TIR	cytoplasmic Toll/IL-1 receptor domain
TLR	Toll-like receptors
TNF	tumour necrosis factor
TPSA	topological polar surface area
TRAF	tumour necrosis factor receptor-associated factor

1 Introduction

1.1 Toll-like receptors

The immune system recognises potential threats, e.g. microorganisms, parasites and cancer cells, and subsequently activates its elaborate defence machinery. The innate immune system represents a fast first-line response. It recognises highly conserved structures from a large variety of microorganisms [1, 2]. The highly conserved structures are called pathogen-associated molecular patterns (PAMPs). PAMPs are components of the bacterial cell wall, bacterial flagella or viral nucleic acids [3]. In addition, endogenous molecules, so-called damage-associated molecular patterns (DAMPs) can activate the innate immune response. DAMPs include molecules from damaged or dying cells or extracellular matrix, e.g. heat-shock proteins, uric acid and various proteoglycans [4]. PAMPs and DAMPs act as ligands for pattern-recognition receptors (PRRs) [5, 6]. PRRs localise primarily on the cells of the innate immune system, e.g. dendritic cells and macrophages. Upon recognition of PAMPs and DAMPs, PRRs activate intracellular signalling cascades. The activation of the signalling cascades leads to the secretion of pro-inflammatory molecules and early host response to infection. Subsequently, activation of PRRs activates and shapes adaptive immunity (Figure 1) [7].

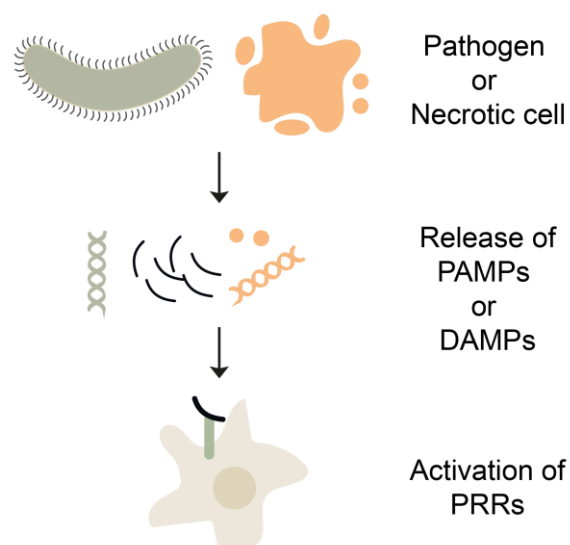


Figure 1. Pattern-recognition receptors (PRRs) recognise pathogen-associated molecular patterns (PAMPs) and damage-associated molecular patterns (DAMPs) from pathogens and endogenous cells.

Introduction

Toll-like receptors (TLRs) are among the most extensively studied PRR families [8] and can be divided into two subfamilies: Cell membrane TLRs include TLR1, TLR2, TLR4, TLR5, TLR6, and TLR10, whereas intracellular TLR3, TLR7, TLR8, TLR9 localise to the endosomal membranes. Every TLR recognises specific PAMP. For example, TLR5 recognises bacterial flagellin, and TLR7 recognises single-stranded RNA (ssRNA) (Table 1) [9].

Table 1. Toll-like receptors, their localisation in cells and their respective natural ligands [9].

TLR	Localisation	Ligand
TLR1	Cell membrane	Triacyl lipopeptides
TLR2	Cell membrane	Peptidoglycan
TLR3	Endosomal membrane	Double-stranded RNA
TLR4	Cell membrane	Lipopolysaccharide
TLR5	Cell membrane	Flagellin
TLR6	Cell membrane	Diacyl lipopeptides
TLR7	Endosomal membrane	Single-stranded RNA
TLR8	Endosomal membrane	Single-stranded RNA
TLR9	Endosomal membrane	CpG DNA
TLR10	Cell membrane	Unknown

Binding of PAMPs or DAMPs to the extracellular domains activates TLRs. Extracellular domains are located on the extracellular side of the plasma membrane or in the endosomal compartments. After the activation, cytoplasmic domains of TLRs interact with and recruit various downstream molecules. Subsequently, this activates downstream signalling pathways [10]. Recent studies have shown that impaired TLR-mediated signalling plays an essential role in developing cancer [11], infections [12], autoimmune disorders [13] and

Introduction

allergic diseases [14] [15]. Therefore, TLR-targeting drugs represent a promising therapy for infections, allergic rhinitis, different cancers, ischemia-reperfusion injury, systemic lupus erythematosus, psoriasis and sepsis [16-18]. Despite their therapeutic potential, only two TLR ligands are currently in clinical use: Imiquimod, a drug for treating genital warts [19], and monophosphoryl lipid A, a vaccine adjuvant [20, 21].

Sparse information on ligand binding and receptor activation has prohibited the rational design of TLR-targeted drugs. Recently, researchers have elucidated how TLR8 rearranges into the activated form after ligand binding [22]. Therefore, TLR8 is a promising drug target for computer-aided drug design.

1.2 Functional significance of Toll-like receptor 8

Human TLR8 is an essential sensor for RNA from viruses and bacteria [23-25], as well as host RNA [26-30]. TLR8 recognises degradation products of uridine-rich ssRNA rather than specific RNA sequences [31]. Because the receptor itself cannot discriminate between degraded host RNA and foreign RNA, its localisation plays an essential role. In particular, endosomal localisation enables the recognition of RNA from the endocytosed pathogen. In contrast, host RNAs are rapidly degraded in the extracellular environment and fail to reach endosomal compartments [32].

The gene for TLR8 is located on chromosome X and encodes two isoforms. The longer isoform has an extended 19-amino acid N-terminus. The shorter isoform is the prevalent form responsible for the canonical TLR8 function in the immune system [33, 34]. Location on chromosome X might explain gender-specific differences in susceptibility to different diseases, e.g. systemic lupus erythematosus (SLE) [35, 36] or infections [37]. Interestingly, a recently reported method for sexing mice sperm has creatively exploited TLR8's location on chromosome X [38].

Immune cells, e.g., monocytes, macrophages and myeloid dendritic cells, express TLR8 [39, 40] (Figure 2). Activation of TLR8 in these cells induces a potent antiviral and antibacterial immune response, which includes the production of type I interferons (IFNs) and nuclear factor kappa-light-chain-enhancer of activated B cells (NF- κ B)-dependent cytokines, and activation of antigen-presenting cells (APCs) [41, 42]. Furthermore, activation of TLR8 in regulatory T-

Introduction

cells reverses their suppressive activity [43]. Reversal of suppression in regulatory T-cells further enhances immune response activation.

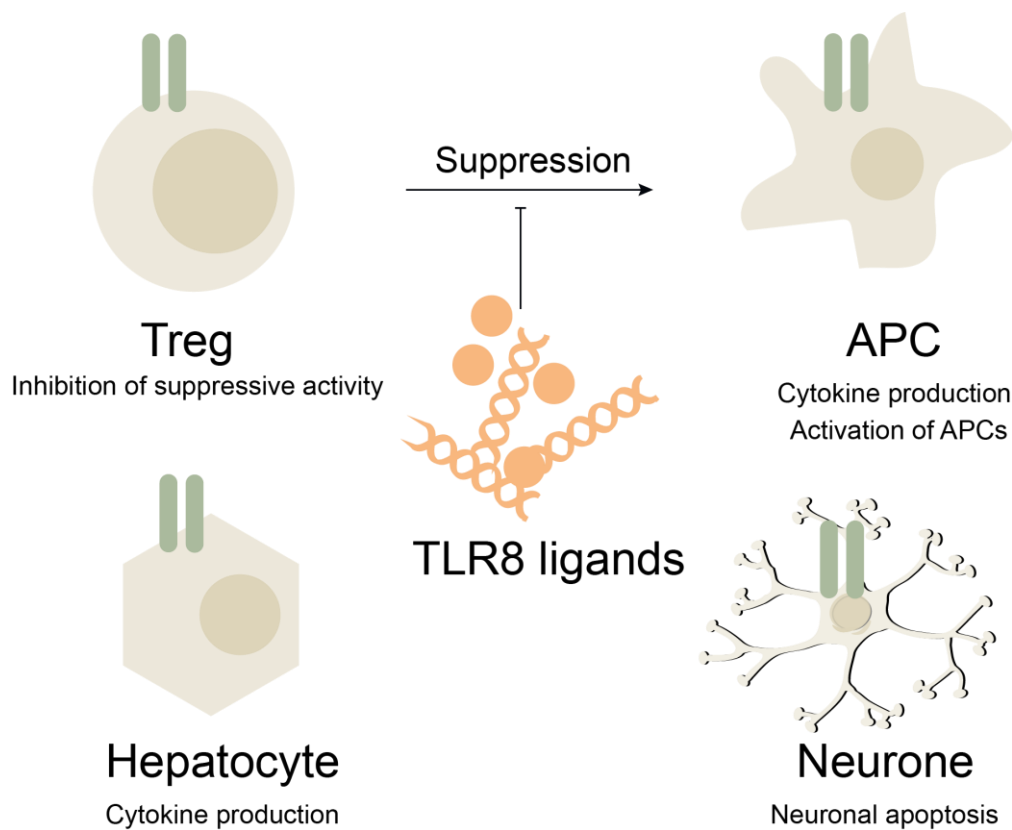


Figure 2. Roles of TLR8 in antigen-presenting cells (APC), Treg (T regulatory cells), hepatocytes and neurons.

Other cell types also express TLR8. For example, TLR8 in hepatocytes recognises and inhibits replication of the Hepatitis C Virus [44] (Figure 2). In neurons, TLR8-mediated signalling negatively regulates neurite outgrowth and induces neuronal apoptosis [45]. Unfortunately, the detailed role of TLR8 outside of the immune system is currently unknown.

1.3 Structural insights into Toll-like receptor 8 function

TLR8, as other TLRs, is a type I transmembrane glycoprotein composed of the extracellular, transmembrane and cytoplasmic signalling domain [8, 46] (Figure 3A). The N-terminal, extracellular domain (ectodomain) of TLR8 is composed of leucine-rich repeat (LRR) modules, which form a characteristic horseshoe-shaped structure. The ectodomain consists of about 800 amino acid residues and is responsible for binding ligands (Figure 3B). The transmembrane domain consists of the single transmembrane helix consisting of about 20

Introduction

uncharged, mostly hydrophobic amino acid residues. C-terminal cytoplasmic Toll/IL-1 receptor (TIR) domains interact with TIR domains of the downstream molecules. TIR domains of TLR8 are composed of ~150 amino acids [22]. Additionally, TLR8 has an extended inserted loop region in the ectodomain, so-called Z-loop, which consists of about 30 amino acids. Proteolytic cleavage at the Z-loop enables the dimerisation of the receptor [47] (Figure 4). The functional form of the receptor is a homodimer.

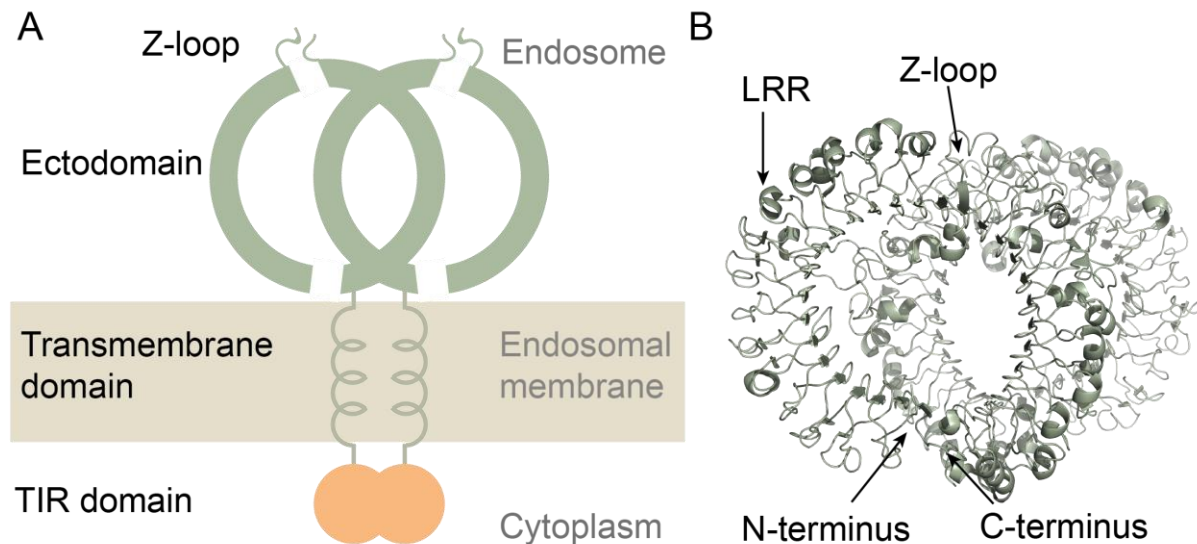


Figure 3. Structure of TLR8. Schematic representation of the TLR8 ectodomain, transmembrane domain and cytoplasmic TIR domain (A). Cartoon representation of the ectodomain (B) with leucine-rich repeats (LRR) and Z-loop (PDB ID: 3W3J) [22].

Recently published crystal structures have shed light on how different ligands bind to TLR8 and consequently activate the downstream signalling pathways [22]. As previously mentioned, TLR8 recognises partially degraded uridine-rich ssRNAs. Lysosomal enzymes degrade ssRNAs to the uridine and short oligonucleotides [48]. Uridine binds to the small pocket on the dimerisation interface of TLR8. However, binding of the uridine alone is not enough to introduce a sufficiently large structural rearrangement to activate the receptor (Figure 4). Simultaneously, short oligonucleotides bind to the allosteric binding site on the concave surface of the ectodomain. Allosteric binding synergistically introduces extensive structural rearrangement that activates the receptor (Figure 4) [31]. Synthetic small-molecule agonists bind to the same uridine-binding pocket. In contrast to uridine, binding of synthetic ligands alone can directly introduce a sizable structural change that activates the receptor [22].

Introduction

However, the exact structural mechanism responsible for the observed differences in activation by natural and synthetic ligands has not been yet elucidated.

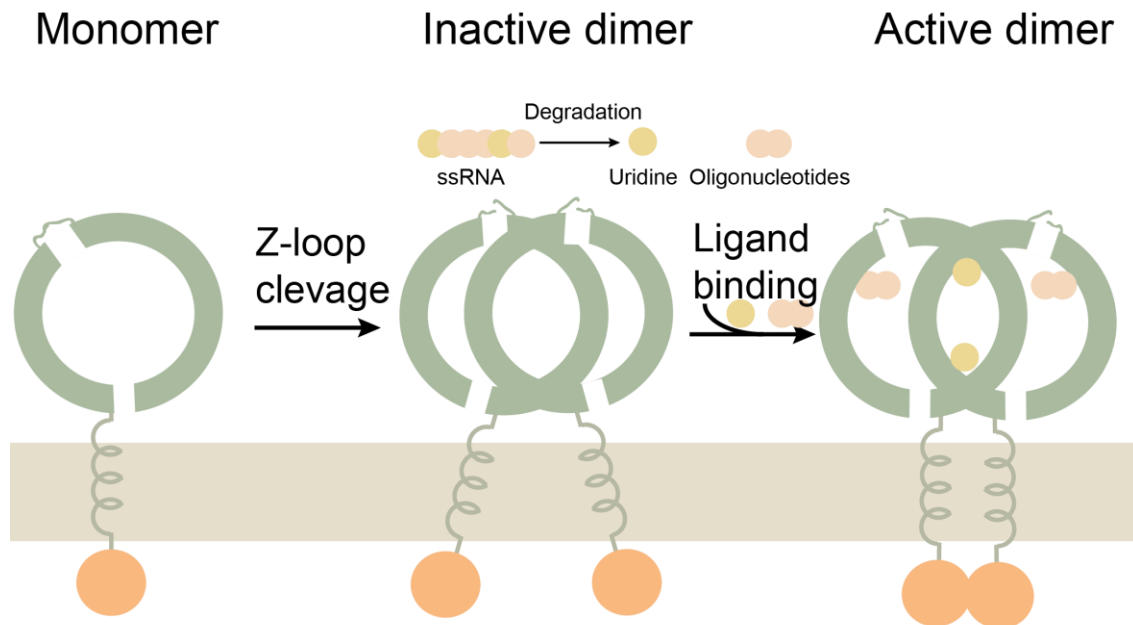


Figure 4. Schematic representation of the dimerisation of TLR8 monomers upon Z-loop cleavage, and subsequent activation of the dimer by the binding of natural ligands.

More recent work has shown that small-molecule antagonists stabilise the preformed TLR8 dimer in its inactive state, preventing the activation by the agonists (Figure 5) [49].

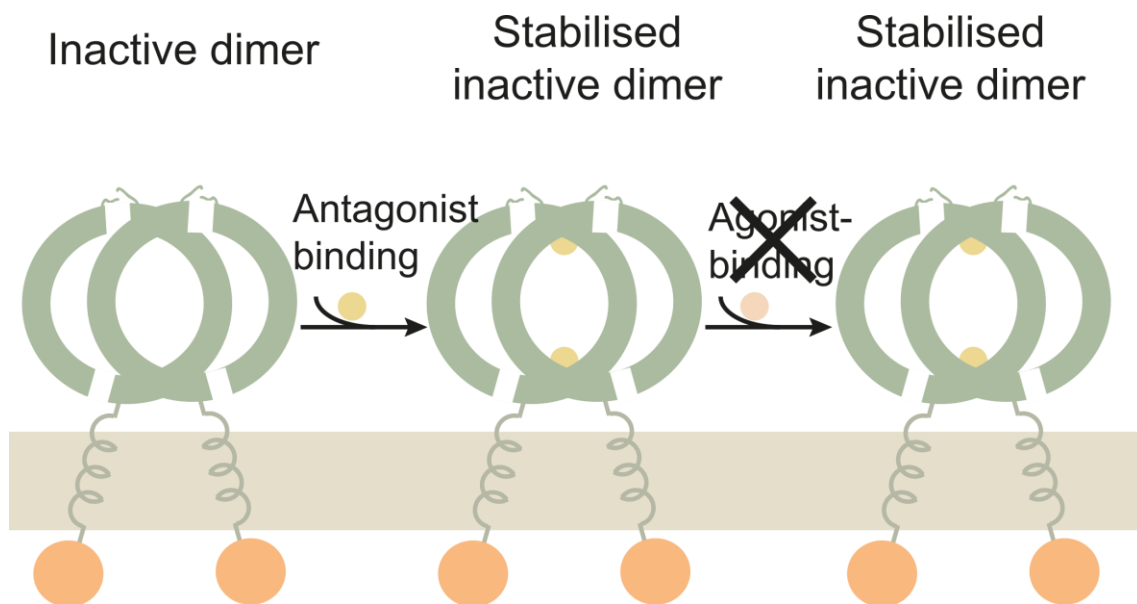


Figure 5. Schematic representation of the stabilisation of inactive state by small-molecule antagonists.

1.4 Toll-like receptor 8 in signalling pathways

Ligand binding to the extracellular domain of TLR8 introduces a structural change in TIR domains of TLR8. TLR TIR domains can then associate with TIR domains of cytoplasmic adaptors (Figure 6) [50]. The primary role of adaptor proteins, which lack intrinsic enzymatic activity themselves, is to mediate binding between two or more proteins in the larger signalling complexes. Myeloid differentiation primary response 88 (MyD88) is the most notable adaptor with TIR domains. MyD88 interacts with the members of the interleukin-1 receptor-associated kinase (IRAK) family. MyD88 first activates and interacts with IRAK4, which leads to subsequent activation and recruitment of IRAK1 and IRAK2 [51, 52]. MyD88, IRAK4, IRAK1 and IRAK2 form a mydosome. Mydosome promotes activation of tumour necrosis factor receptor-associated factor (TRAF) 6 [53]. TRAF6 in return activates transforming growth factor β -activated kinase 1 (TAK1), which forms a complex with a TAK1 binding proteins (TAB1-3) [54-57].

At this point, the activated TAK1 can either activate NF- κ B or mitogen-activated protein kinase (MAPK) signalling pathways. NF- κ B is bound to the inhibitor of κ B (I κ B) in the cytoplasm, which keeps it inactivated. Phosphorylation of I κ B by I κ B kinases (IKK) results in its degradation and release of NF- κ B. NF- κ B then moves to the nucleus and induces the expression of pro-inflammatory genes [58]. Alternatively, activation of MAPK signalling pathway results in the activation of p38, c-Jun N-terminal kinases (JNK) and extracellular signal-regulated kinases 1 and 2 (ERK1 and ERK2), and subsequent activation of activator protein 1 (AP-1) family transcription factors [59]. Activation of transcription factors NF- κ B and AP-1 induces transcription of pro-inflammatory cytokines, such as tumour necrosis factor α (TNF- α), interleukin 6 (IL-6), IL-8, and IL-1 β and IL-12. Besides, activation of TLR8 leads to the production of type I IFNs through the formation of Myd88, IRAK1, IRAK2, IRAK4, TRAF3 and TRAF6 complex, and subsequent translocation of interferon regulatory factor 7 (IRF7) to the nucleus [60].

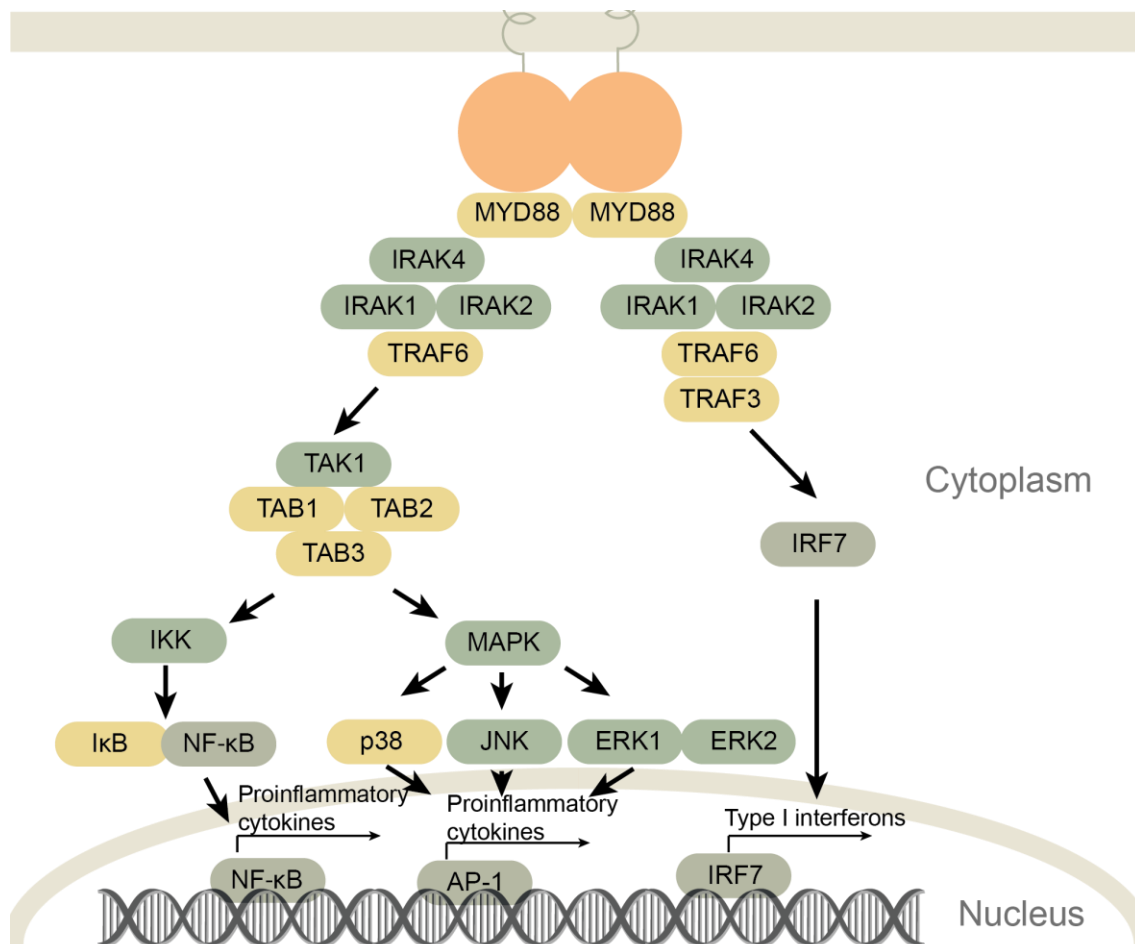


Figure 6. Overview of TLR8-mediated signalling pathways. Upon activation of the receptor, downstream signalling cascades, which involve various adapter molecules and kinases, transmit the signal. As a result, transcription factors NF-κB, AP-1, and IRF7 activate subsequent transcription of genes coding for pro-inflammatory cytokines and type I interferons.

All signalling pathways described above apply to the cells of the immune system. However, it is still unclear whether other cell types show the same or similar signalling pathways upon TLR8 activation. For example, TLR8-mediated responses in neurons presumably involve alternative pathways [45].

1.5 The function of Toll-like receptor 8 in diseased states

Initial research focused on the role of TLR8 in infectious diseases [12, 61, 62]. Upon activation of TLR8, APCs start to secrete various pro-inflammatory cytokines, such as TNF- α , IL-12 and type I IFNs. Type I IFNs upregulate major histocompatibility complex class I (MHC-I) and co-stimulatory molecules [12]. Activated APCs migrate into lymphoid organs and provide naive T-cells with the antigen that stimulates specific T-cell receptors (TCRs), co-

Introduction

stimulatory molecules that prevent the development of tolerance and polarising factors that promote response by T Helper Cell Type 1 (Th1). Th1 responses are crucial for the effective elimination of viruses or bacteria. Insufficient Th1 responses may contribute to chronic infectious diseases [63].

In allergies and asthma, usually harmless environmental antigens induce a strong response by T Helper Cell Type 2 (Th2) [64]. As already mentioned in the previous paragraph, the activation of TLR8 promotes Th1 response, which can counteract Th2 responses [65]. Thereby, activation of TLR8 shifts the balance between Th1 and Th2 towards the reduction in the allergic reaction (Figure 7A) [66]. TLR8 may also lead to SLE development by recognition of host RNA [67, 68]. In contrast, more recent studies have shown that TLR8 deletion accelerates autoimmunity in mice through a TLR7-dependent mechanism [68, 69]. Similarly, studies have indicated the role of TLR8 in rheumatoid arthritis [70, 71], antiphospholipid syndrome [72, 73], inflammatory bowel disease [74] and systemic sclerosis [75].

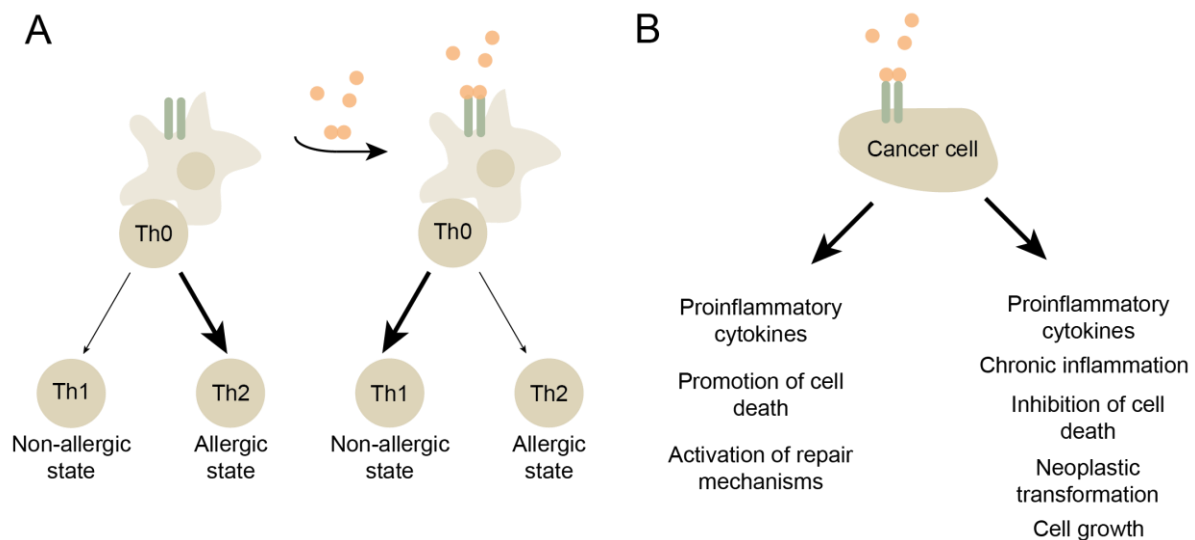


Figure 7. Aberrant TLR8 signalling is involved in various pathological conditions. In allergic disorders and asthma (A) activation of TLR8 shifts the allergic state, characterised by T-helper cell type 2 cells response (Th2), into the non-allergic Th1 response. In cancer (B), TLR8 activation in, e.g pancreatic and lung cancer cells, leads to the secretion of pro-inflammatory cytokines and cell death inhibition, which promotes chronic inflammation and neoplastic transformation in pre-cancerogenic and cancerogenic cells. The opposite effect is observed in squamous carcinoma, where TLR8 activation leads to cell death and subsequent activation of the repair mechanisms.

The role of TLR8 in cancer is controversial. We still mostly do not know why and how tumour cells control or utilise TLR activation. However, the opposite effects of the NF- κ B

Introduction

signalling in cancer have been observed (Figure 7B) [76-79]. In basal cell carcinoma and melanoma, TLR8-mediated response can activate dendritic and natural killer cells and start a strong immune response against the tumour [11, 18, 79-82]. Besides, TLR8-mediated response suppresses regulatory T cells, which leads to enhanced antitumor activity [43]. Simultaneously, some cancer cells or cell lines, such as cervical cancer cells, human head and neck squamous cell carcinoma cell lines or lung cancer cells lines, also express TLR8 [83-85]. In some cancer cells, such as squamous carcinoma cell lines, the activation of TLR8 promotes cell death and suppresses metastasis. On the other hand, the TLR8-mediated inflammatory response in pre-cancerogenic or cancerogenic cells, e.g. in multiple myeloma, pancreatic and lung cancer, can promote chronic inflammation and cell-survival, which results in neoplastic transformation and growth of malignant cells (Figure 7B) [84, 86, 87]. Furthermore, tumour-secreted miRNAs can act as paracrine agonists of human TLR8, thereby activating pro-metastatic inflammatory response and leading to tumour growth and metastasis [88]. The observed complex downstream effect of TLR8 signalling in cancers is a consequence of multiple factors. Most notably, the TLR8-mediated response highly varies between different cell types, organs, tumour stages and even testing conditions, and depends on the role that antitumour immune responses play in a particular tumour [89].

Finally, TLR8 may contribute to the development of neurological diseases. Recent work showed that activation of TLR8 in neurons negatively impacts stroke outcome by promoting neuronal apoptosis and T cell-mediated post-stroke inflammation [90]. Besides, TLR8 stimulates the production of inflammatory mediators and neuronal hyper excitability in neuropathic pain [91].

1.6 Recent development of drugs targeting Toll-like receptor 8

In recent years, a significant amount of research has focused on drugs that target TLR8. Investigated therapeutic approaches include both inhibition and activation of the receptor activity. Motolimod, a small molecule agonist of TLR8, is in clinical trials for the treatment of allergic rhinitis and different cancers (Figure 8) [65, 92]. IMO8400, an oligonucleotide-based antagonist of TLR7, TLR8 and TLR9, is currently investigated for the treatment of SLE and psoriasis [93]. Additionally, several chemotypes are in preclinical studies.

Introduction

Reported TLR8 agonists include 2,3-diaminofuro[2,3-*c*]pyridines [94], benzazepines such as motolimod [95], quinoline-2-amines [96], 1H-benzimidazol-2-amines [97], imidazol-2-amines [98] and pyrimidine-2,4-diamines [99] (Figure 8). These compounds show promising adjuvant properties in animal models. Simultaneous activation of multiple TLRs may induce even more potent immune response, leading to superb adjuvant properties [100]. Several dual TLR7/TLR8 agonists have been reported, including substituted imidazo/thiazolo/oxazolo/pyrazolo[4,5-*c*]quinolines-4-amines [101-104], 2,4-diaminoquinazolines [105] and pyrimidine-2,4-diamines [100, 106] (Figure 8). Simultaneous activation of TLR7, TLR8 and TLR9 by small-molecule agonist elicited a robust immune response in Henrietta Lacks (HeLa) cells [107].

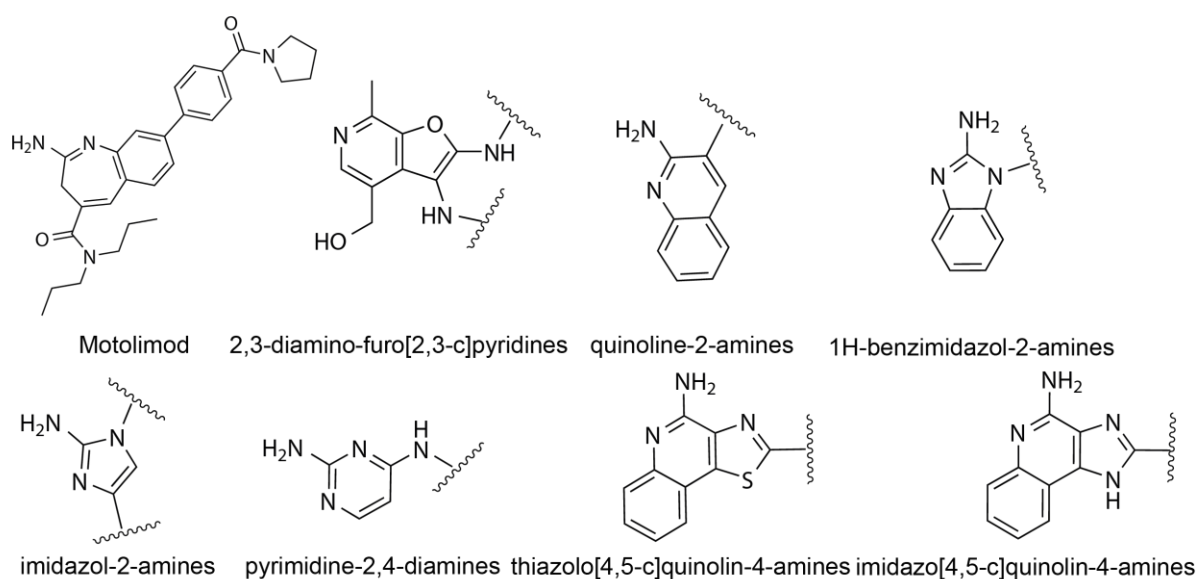


Figure 8. Previously described TLR8 agonists.

3H imidazoquinolines [108] and dimeric constructs of imidazoquinoline linked at the C2 position [101] were reported as dual TLR7/TLR8 antagonists, and more recently pyrazolo[1,5-*a*]pyrimidines and 4-phenyl-1-(2H)-phthalazinones [49, 109] were discovered as selective TLR8 antagonists (Figure 9). These compounds show potent anti-inflammatory effects in models for various autoimmune disorders [49, 109].

Introduction

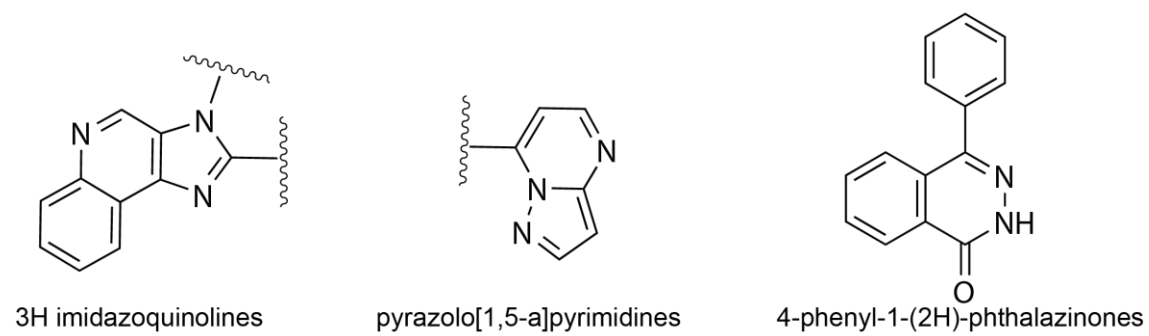


Figure 9. Previously described TLR8 antagonists.

2 Research aim

Modulators of TLR8-mediated responses are promising drug candidates. Some modulators have already been in clinical trials for the treatment of cancers and allergic rhinitis, and use as vaccine adjuvants [65, 92, 95]. Unfortunately, most of them did not reach clinical use because of an insufficient therapeutic effect or severe side effects. We need to find more highly active and selective chemotypes for TLR8 modulators, both agonists and antagonists. In addition to therapeutic potential, novel chemical entities provide useful tools to study TLR8-mediated signalling pathways. TLR8 crystal structure is solved, and several modulators are known from previous drug screens. Therefore, TLR8 represents a promising target for systematic and rational computer-aided development of new drug candidates. In this case, computational techniques can study events on a molecular level and rationalise mechanisms of action, thereby providing the basis for tailored drug development.

The overall research aim is to discover novel small molecule TLR8 modulators. Furthermore, we will try to understand their mechanism of action. Our study on TLR8 will help us understand the processes necessary for modulating other TLRs and facilitate the future design of small molecule TLR modulators.

Main objectives of the project are:

- Investigation and rationalisation of binding of different ligands to TLR8 and subsequent activation or inhibition of the receptor
- Development of predictive models for discovery of new small molecule TLR8 modulators
- Identification and optimisation of potential TLR8 modulators
- Experimental characterisation of the potential TLR8 modulators (in collaboration) and interpretation of the results in the context of the developed models

3 Computational methods

In the past thirty years, computational methods have become an essential part of drug discovery projects. Computational methods offer better hit rates than traditional high-throughput and combinatorial chemistry campaigns due to a higher degree of rationalization and mechanistic orientation [110, 111]. They are useful tools for optimising physicochemical properties of hit compounds by rationalisation of structure-activity relationship. Furthermore, computational methods enable prioritisation for experimental testing from larger numbers of compounds. Finally, they have become useful tools for the design of entirely new compounds [110]. Since computational methods are an essential part of this PhD project, the background of the employed methods will be described in the following sections.

3.1 Molecular docking

Molecular docking is an established method for predicting conformation and orientation of the ligand in the macromolecular binding site (Figure 10). Algorithms for molecular docking usually consist of two steps: (1) generation of ligand conformations in the binding site (so-called *poses*) and (2) scoring and ranking of the generated poses [112]. Some commonly used docking tools are DOCK [113], AutoDock [114], Glide [115], GOLD [116], AutoDock Vina [117] and FlexX [118].

Computational methods

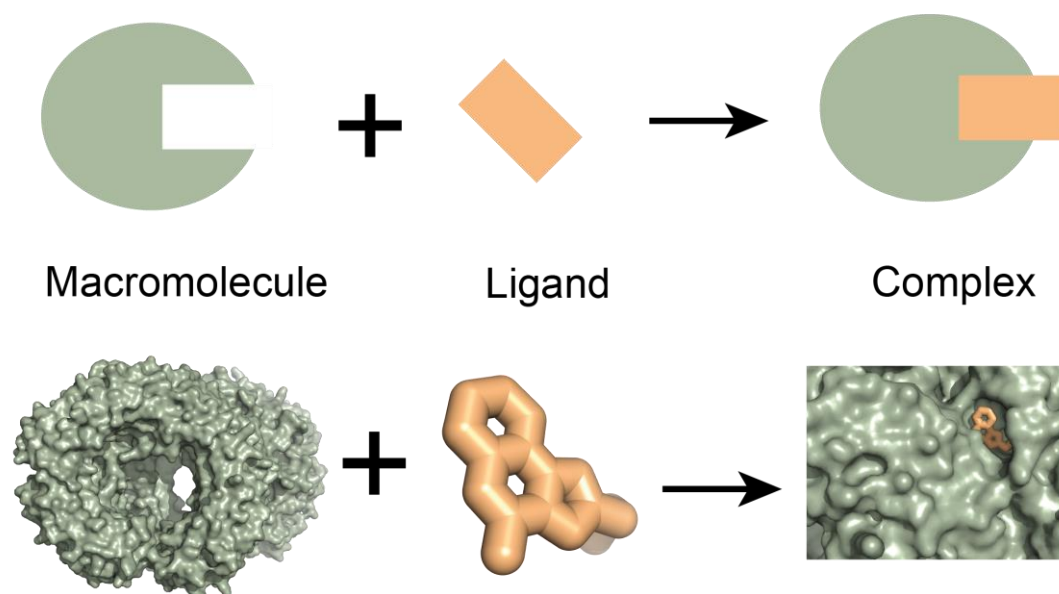


Figure 10. A simple representation of molecular docking. Molecular docking is a method for the prediction of the ligand conformation and orientation in the macromolecular binding site.

The Software GOLD implements the genetic algorithm (GA) to generate the binding poses. GA uses concepts from the theory of evolution and natural selection [116]. Individual structural parameters, analogous to genes, describe the translation, orientation and conformation of the ligand to the protein. A group of these structural parameters, analogous to the chromosome, encodes a particular binding pose. In the first step, the algorithm generates several initial poses (chromosomes) by randomly assigning values for the structural parameters. A GA refers to the group of poses as population. Generated poses are then evaluated based on the corresponding scoring function. The scoring function measures the "fitness" of the pose (or chromosome). The "fittest" poses propagate to the next population of the poses. In particular, these poses are subjected to different genetic operations, analogously to crossovers and mutations. The procedure transmits favourable structural parameters from parent to child population, promoting the generation of "fitter" chromosomes. The GA includes many rounds, and after some time, may converge to a pose that corresponds to the global "fitness" minimum [119].

Scores that measure the "fitness" of the calculated poses include force-field-based, empirical and knowledge-based scoring function [112]. Force-field-based scoring functions, such as GoldScore, use classical force fields to calculate the ligand-binding energy [120, 121]. Empirical scoring functions, such as ChemScore, use regression analysis on a set of ligand-

Computational methods

protein complexes with known binding affinities to obtain parameters for the calculation of ligand-binding energy [122]. Knowledge-based functions, such as ASP, use statistical analysis of ligand-protein complexes from crystal structures to get the interatomic contact frequencies and distances between the ligand and protein [123]. The interatomic contact frequencies are converted into energy components for the calculation of ligand-binding energy. Current scoring functions identify correct binding poses in many cases [124, 125]. However, the calculation of the scores is subject to several assumptions and simplifications. Therefore, evaluation of individual docking poses should not be solely based on score-based rankings [126]. Instead, evaluation should include visual inspection and/or statistical analysis [124].

Molecular docking methods usually consider a macromolecular target as a rigid structure. However, we can also account for the flexibility of the macromolecule. In particular, we can obtain different conformations of the macromolecule from experiments or molecular dynamics simulations. Afterwards, we can separately dock ligands in multiple conformations.

3.2 Molecular dynamics simulations

Atomic-level structures from experiments, such as from X-ray crystallography or cryo electron microscopy (cryo-EM), provide valuable insight into how molecules function. However, molecules are in constant motion, and available experimental methods cannot fully address this. One possibility to investigate local conformational flexibility is to use computer simulation to account for the dynamics of molecules. Molecular dynamics (MD) simulations use Newton's laws of motion to describe time-dependent behaviour of water, ions, small molecules and macromolecules, or complex systems, such as ribosomes [127-129], or proteins embedded in the membranes [130] (Figure 11). Subsequently, they can capture functionally relevant states.

MD simulations use current positions of the atoms, their velocities, and accelerations, resulting from the forces acting on them, to predict their arrangement in space during a given time period. Atomic coordinates from experimentally solved structures or comparative modelling data provide the atoms' initial positions [131]. The atoms' initial velocities in the system are often derived from the Maxwell – Boltzmann distribution for a given temperature. Finally, forces acting on atoms are calculated with molecular mechanics force fields [132]. The term “force field” is a common name for a set of parameters for different types of atoms and a function that uses these parameters to compute the potential (steric, conformational) energy of

Computational methods

a molecule based on its geometry. Parameters for each atom type are derived from experimental data or quantum mechanical calculations [133].

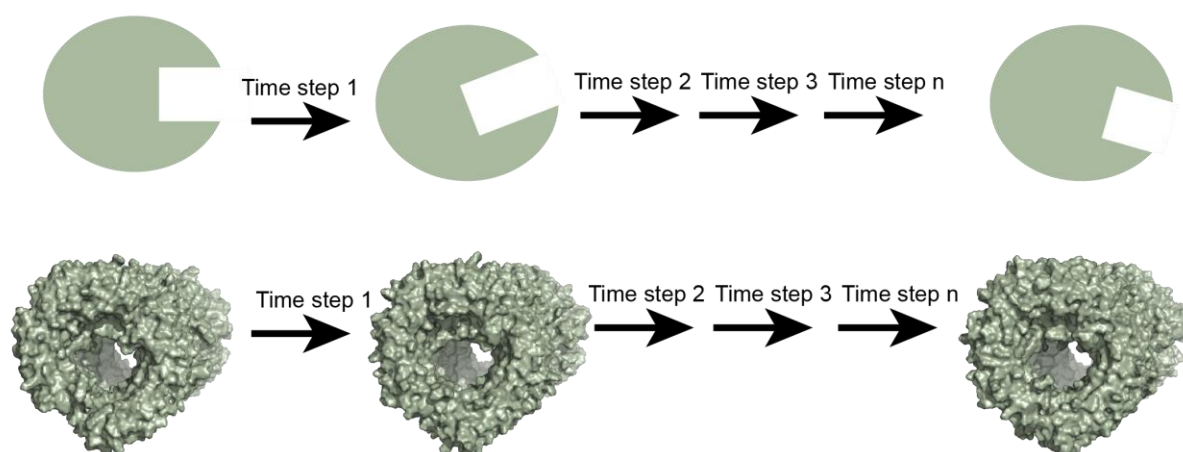


Figure 11. A simple representation of a molecular dynamics simulation. Molecular dynamics simulations are atomic-level computer simulations that capture the dynamic behaviour of different molecular systems through time.

The equation for the calculation of potential energy sums up different force terms, e.g. Coulomb's law calculates electrostatic interactions, while spring-like terms describe bond stretching [134]. By deriving the expression for the energy of all atoms' total interactions in the system and using Newton's second law, a set of Newton's equations of motion is obtained. The solution of the equations provides the time-dependent position of atoms in the system, so-called trajectory. The solution of equations of motion assumes that the forces acting on the atom are constant during the selected time step. The smaller the time step is, the more acceptable is the approximation. A time step of 1 fs (10^{-15} s), which corresponds to one-tenth of the C-H bond's stretching period, is usually sufficient [131, 135]. In summary, by one small step through time, MD simulations repeatedly calculate the forces acting on each atom and then use those forces to update each atom's position and velocity.

The resulting trajectory describes the atomic-level configuration of the system at different time points during the simulated period. The trajectory can be used to calculate various thermodynamic and dynamic properties of the system, such as temperature, pressure, kinetic energy or diffusion. The most routinely derived parameters for investigation of the system are the geometrical root mean square difference (RMSD) between two structures and the root mean square fluctuation (RMSF). The RMSD shows how a protein structure deviates from a reference structure as a function of time. The time-averaged RMSF indicates the flexibility of

Computational methods

different regions of a protein [136]. The most popular tools for MD simulations are Amber [137], CHARMM [138], GROMACS [139], NAMD [140] and Desmond [141].

3.3 Three-dimensional (3D) pharmacophores

Three-dimensional (3D) pharmacophore models describe the type and location of the chemical moieties essential for the ligand-target interaction. In pharmacophores, chemical moieties are categorised as more general features. Pharmacophoric features commonly include aromatic rings, hydrophobic moieties, hydrogen bond acceptors, hydrogen bond donors, and positively and negatively charged groups [142]. 3D pharmacophores also include the location of the interaction and direction in case of hydrogen bonds (Figure 12A) [143].

Structure-based pharmacophores are generated from the information about the binding site, with the focus on the interactions between the ligand and the macromolecule. For example, LigandScout [144], Flap [145] and Catalyst [146] generate pharmacophores from the protein-ligand complexes. Additionally, pharmacophores can be developed using ligand-based approach. Ligand-based pharmacophores consist of common features in a set of ligands known to bind to the target of interest [147], and can be derived in LigandScout [144], PHASE [148] or Pharao [149].

3D pharmacophores are often used for virtual screening. Due to their intuitive representation, 3D pharmacophores are useful for the descriptive investigation of ligand-target interaction patterns.

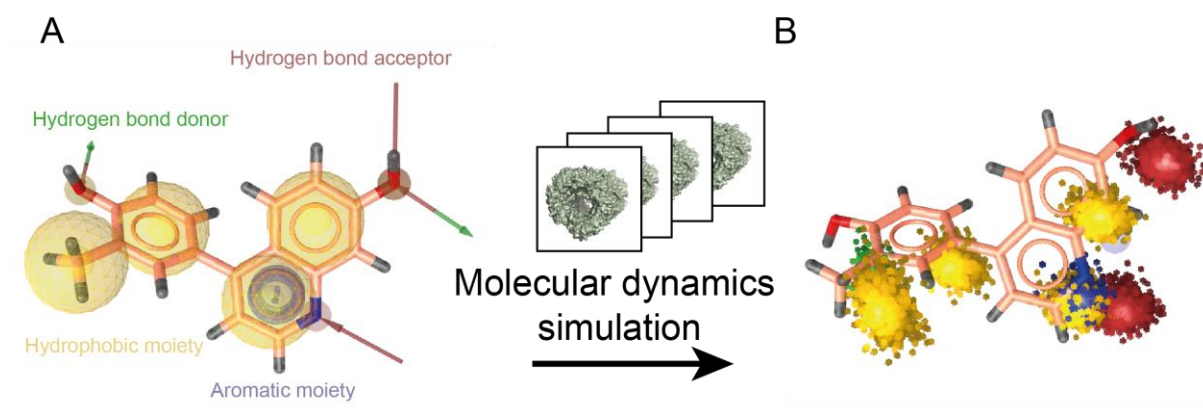


Figure 12. 3D pharmacophores describe the nature and location of the chemical moieties in ligands involved in interactions with macromolecular targets (A). The molecular interaction pattern between

Computational methods

ligand and macromolecular target through molecular dynamics simulation can be described with dynophores (B).

3.3.1 Three-dimensional (3D) pharmacophores-based virtual screening

Pharmacophore-based virtual screening searches molecular libraries for molecules with the desired pharmacophore. Molecules that contain desired pharmacophore will more likely be active against a specific target. The abstract representation of the pharmacophore substantially reduces the computational complexity of virtual screening and bears the potential to identify novel ligands with diverse scaffolds and functional groups [150].

We can evaluate the quality of the 3D pharmacophore model using molecules with known activity against the target. If inactive molecules are unavailable, we can use decoy molecules. A decoy is a presumably inactive molecule with similar physicochemical properties to the active molecules. 3D pharmacophore performance describes how well the pharmacophore identifies and classifies molecules as active or inactive [151]. For example, the receiver operating characteristic (ROC) curve is a standard tool for assessing virtual screening results. The ROC curve displays the increase of false positives versus the increased true positives. The ROC curve's Y-coordinate represents the true-positive rate, whereas the X-coordinate denotes the appropriate false-positive rate [152].

3.3.2 Dynamic pharmacophores

The traditional approach in pharmacophore modelling exploits the static information on ligand-target interaction. Since both ligand and macromolecular targets represent dynamic entities, we should account for the ligand-target interaction patterns' dynamics. Dynophores, developed in our lab, detect a pharmacophoric pattern in the binding site throughout a complete molecular dynamics simulation and report the specific interaction occurrence time and frequency (Figure 12B) [153-155].

3.4 Shape-based similarity search

Similar molecules usually exhibit similar properties. Thus, the assessment of similarity between small molecules is a useful tool in the discovery and development of various drugs. In recent years, shape similarity has become incredibly valuable in virtual screening, molecular target prediction, drug repurposing and scaffold hopping [156].

Computational methods

Rapid Overlay of Chemical Structures (ROCS) is one of the most popular methods for assessing molecular shape similarity. ROCS represents molecules as a set of overlapping Gaussian spheres [157-159]. The algorithm finds and quantifies the maximum volume overlap between two molecules. Besides, ROCS includes chemical features to improve shape-based superposition.

4 Results

The chapter consists of three parts. The first part (section 4.1) gives an overview of the most relevant structural features implicated in the function of TLR8. The second part (section 4.2) shifts the focus to the binding of the small molecules to TLR8. We investigated interactions between the known ligands and the TLR8 and used it to develop the most plausible pharmacophore model. Subsequently, we employed the developed pharmacophore model to identify novel modulators of TLR8. The third part (section 4.3) describes a follow-up study where we studied analogues of the identified modulators (section 4.2).

4.1 Structural analysis of Toll-like receptor 8

The main goal was to study relevant structural features in available crystal structures of TLR8. The focus was on the dimerisation interface because of its role in the binding of ligands and subsequent activation of the receptor. Additionally, we studied the conservation of the relevant structural features across the closely related TLRs.

4.1.1 Overview of the structure

At the beginning of the study, several structures of unliganded TLR8 and TLR8 co-crystallised with agonists were available (Table S 1) [22, 31, 96, 98, 104, 160, 161]. The solved structures only include the ectodomain of human TLR8. Therefore, throughout this chapter, when referring to the structures, TLR8 will depict the ectodomains of human TLR8. Furthermore, since the functional form of TLR8 is a homodimer, the term TLR8 will also refer to the dimeric form, if not otherwise explicitly stated. The residues of the second monomer are denoted with an asterisk (*) throughout the manuscript.

Co-crystallised agonists include quinoline-based synthetic small-molecules, uridine and dinucleotides (Table S 1). The agonists show low micromolar or nanomolar affinity towards TLR8 [22, 31, 96, 98, 104, 160, 161]. Uridine and synthetic small-molecule agonists bind to the dimerisation interface of the two monomers. The binding pocket is surrounded with the residues from leucine-rich repeats 11-14 (LRR11–14) in the first monomer, and LRR16*–18* in the second monomer [22, 31] (Figure 13). The binding of small-molecule agonists is described in detail in section 4.2.2.

Results

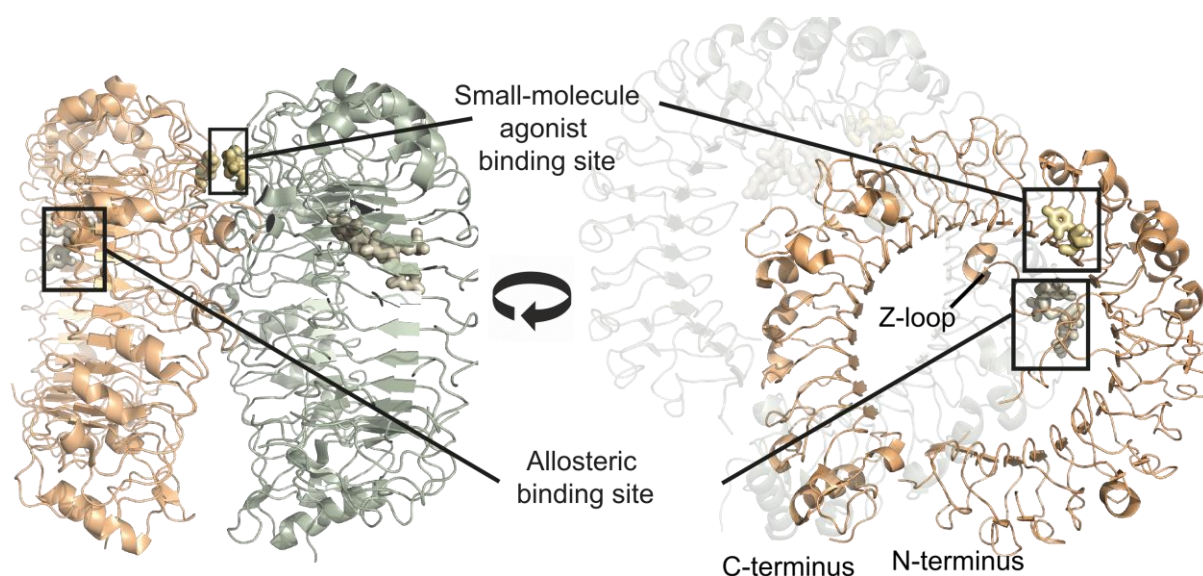


Figure 13. Overview of TLR8 (PDB ID: 4R09) (orange and green cartoons for the two monomers) with the depicted binding sites for small-molecule (yellow sticks) and dinucleotide (grey sticks) agonists, side view (left) and front view (right).

The second, allosteric binding site for the dinucleotides is located on the concave surface of the TLR8 and is surrounded by LRR10–13, and the ordered region of the Z-loop (Figure 13). The binding site residues include highly hydrophilic and charged residues, such as Lys314, Asp343, Arg370, His373, Arg375, His469 and Arg472. The allosteric binding site is more exposed and spacious than the binding pocket for small molecules on the dimerisation interface [31]. Overall conformations of the TLR8s activated by different agonists are almost identical, showing root-mean-square deviation for alpha carbons (RMSD) up to 0.5 Å. The exception is TLR8 bound to solely uridine, which shows RMSD of 1 Å to other activated forms of TLR8 (PDB ID: 4R0A) (Figure 14).

Results

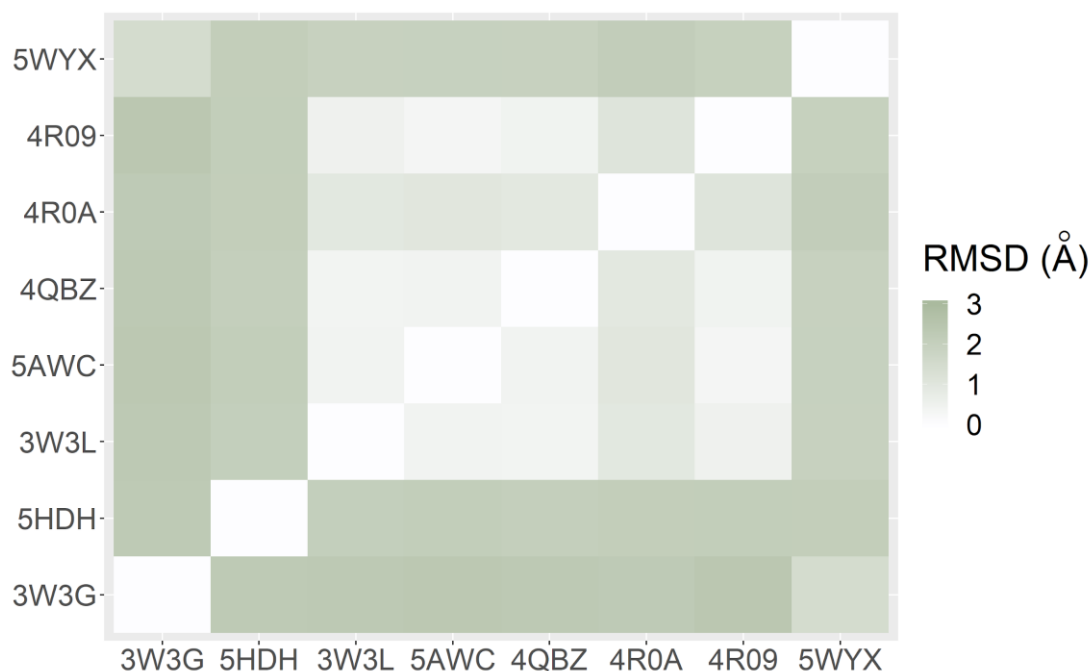


Figure 14. Heatmap of average root-mean-square deviation (RMSD) values for alpha carbons between superimposed structures of TLR8 monomers. For the sake of clarity, only representative structures were selected: unliganded TLR8 (PDB ID: 3W3G), unliganded TLR8 with uncleaved Z-loop (PDB ID: 5HDH), small-molecule agonist-bound TLR8 (PDB ID: 3W3L, 5AWC and 4QBZ), uridine-bound TLR8 (PDB ID: 4R0A), dinucleotide- and uridine- bound TLR8 (PDB ID: 4R09) and small-molecule antagonist-bound TLR8 (PDB ID: 5WYX).

Interestingly, the most significant difference between uridine-bound TLR8 and other active forms is in the loop region of LRR24 and LRR25 near the C-terminal end of TLR8 (Figure 15).

Results

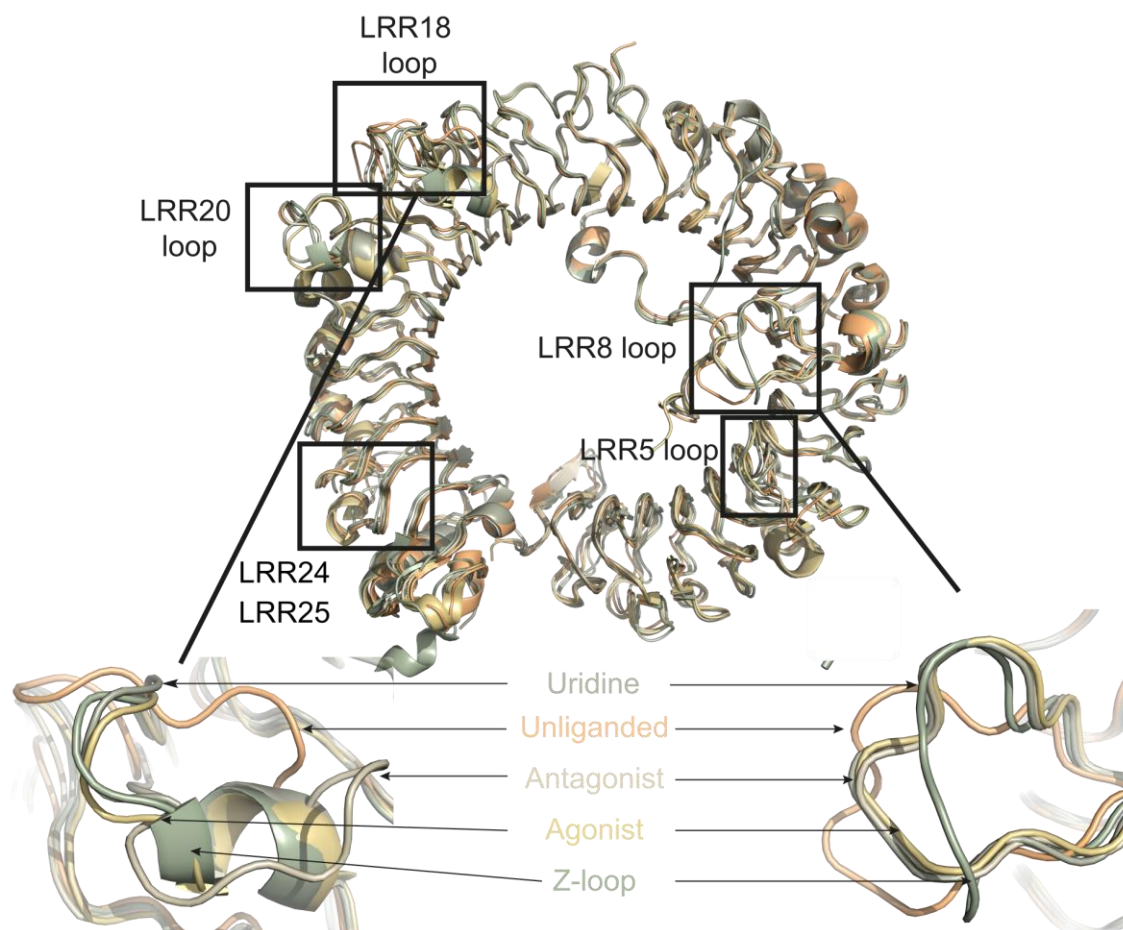


Figure 15. Superposed crystal structures of unliganded (PDB ID: 3W3G), small-molecule agonist-bound (PDB ID: 3W3J), uridine-bound (PDB ID: 4R0A), small-molecule antagonist-bound (PDB ID: 5WYZ) and TLR8 with uncleaved Z-loop (PDB ID: 5HDH). Frontal view of the lateral face of TLR8, with enlarged view on loops in LRR18 and LRR8.

During this study, two more structures were crystallised in a complex with nanomolar affine antagonists [49] (Table S 1). The co-crystallised pyrazolopyrimidine and quinoline derivatives also bind to the lateral, dimerisation side of receptors (Figure 16). The binding pocket residues partially overlap with the residues involved in the binding of the agonists. The surrounding residues are located on LRR8, LRR11, LRR12, LRR13, LRR15*, LRR16* and LRR18*. The antagonistic binding pocket is described in detail in section section 4.2.9. The overall conformation of unliganded TLR8 (PDB ID: 3W3G) is similar to small-molecule antagonist-bound TLR8 (PDB ID: 5WYZ and 5WYX). The most significant differences between unliganded and small-molecule antagonist-bound TLR8 are in the loop regions of the leucine-rich repeats 8 and 18 (LRR8 and LRR18) (Figure 15). Both loops are close to the binding site for antagonists. Therefore, local conformational changes in the loops are induced

Results

upon the binding of the antagonists and enable additional interaction with the antagonists. The most significant differences between TLR8 activated by different agonists and TLR8 bound to antagonists are in the loops of LRR5, LRR18 and LRR20. Interestingly, the loop from LRR8 accommodates the same conformation in both agonist- and antagonist- bound TLR8 (Figure 15).

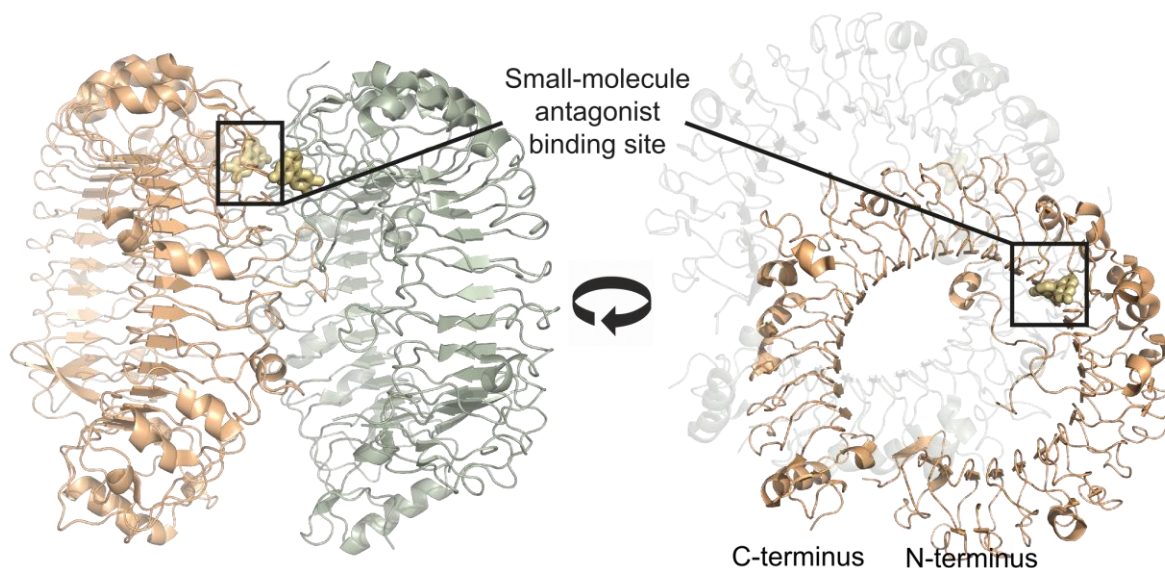


Figure 16. Overview of TLR8 (PDB ID: 5WYZ) (orange and green cartoons) with depicted binding sites for small-molecule (yellow sticks) antagonists, side view (left) and front view (right).

Finally, TLR8 with the uncleaved Z-loop has been crystallised as a monomer, compared to other dimeric forms of TLR8 [47]. Functionally inactive TLR8 with uncleaved Z-loop (PDB ID: 5HDH) has the highest overall conformational diversity to other structures. Z-loop passes the ascending lateral face of TLR8 and presumably affects the conformations of lateral loops, including LRR8 and LRR18 (Figure 15).

All TLR8 monomers are superposed well with the highest overall root-mean-square deviation (RMSD) of 3 Å (Figure 14 and Table S 1). Main conformational differences are in the loops located on the lateral side of TLR8 (Figure 15). Therefore, the binding of the ligands introduces limited conformational changes in the monomers. However, the binding of the agonists opens up the TLR8 dimer structure by 15 Å in the top lateral face of the ectodomain (Figure 4). The opening of the dimer consequently brings two C-termini closer, from around 53 Å in the inactive state to 30 Å in the active state [22] (Figure 13 and Figure 16). Therefore, binding of the ligand may induce the rearrangement of the two monomers and activation of the receptor primarily by the reorganisation of the dimerisation interface.

Results

4.1.2 Analysis of the dimerisation interface

We wanted to study the dimerisation interface between the two TLR8 monomers because of the vital role in the activation of the receptor. We focused on the intermolecular interactions between the two TLR8 monomers and their differences in the receptor's different forms. Interactions through molecular dynamics simulations (MD) were analysed in the unliganded TLR8, antagonist- and agonist- bound TLR8 (Table S 2 and Figure S 4). For the analysis, we selected crystal structures of the dimeric TLR8 with the highest average resolution.

In the unliganded TLR8 structure, the dimerisation interface is characterised by hydrophobic contacts and hydrogen bonds clustered in several patches across the interface (Figure 17). The hydrogen bonding network includes interaction between residues from LRR18 in the first monomer and LRR8* in the second monomer. The additional patch includes hydrophobic contacts and hydrogen bonding between residues from LRR14 and LRR15, and LRR11*, LRR12* LRR13* and LRR14*.

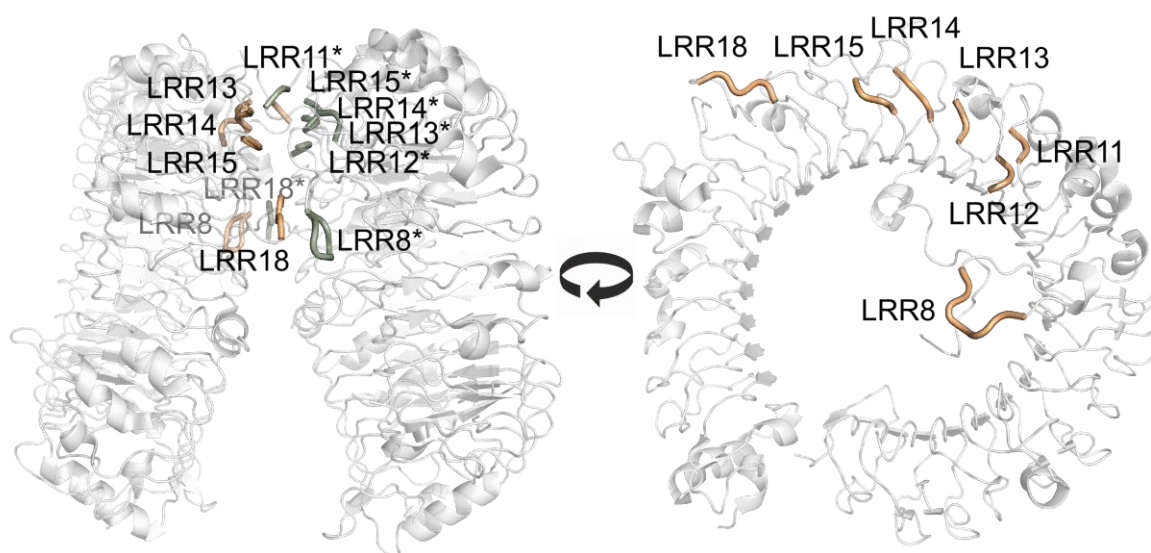


Figure 17. Overview of unliganded TLR8 (PDB ID: 3W3G) (grey cartoons) with depicted dimerisation patches (orange and green cartoons for each monomer), side view (left) and front view of the monomer (right).

Binding of the antagonist affects the conformation of the surrounding residues. Interestingly, binding of the antagonist results in a minor reorganisation of the interface and leads to the increase of hydrophobic contacts between the monomers (Table S 2). The most prominent patches are between LRR18 and Z-loop*, and LRR15 and LRR11*, LRR12* and

Results

LRR13* (Figure 18). Most of the interactions between two monomers from the unliganded form are now replaced with ligand-mediated contacts.

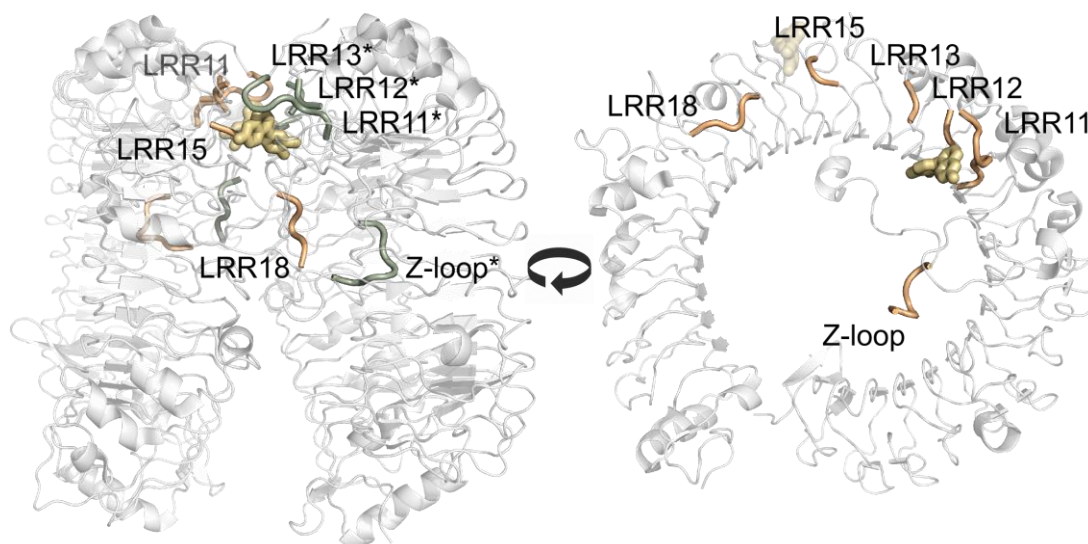


Figure 18. Overview of the antagonist-bound TLR8 (PDB ID: 5WYZ) (grey cartoons) with depicted dimerisation patches (orange and green cartoons for each monomer), side view (left) and front view of the monomer (right). The antagonist (yellow sticks) is also depicted.

In contrast to the inactive unliganded and antagonist-bound TLR8, active agonist-bound TLR8 is characterised by extensive hydrogen bonding networks between two monomers (Table S 2). The extensive contacts are between residues from LRR20 and LRR5*, LRR19 and LRR18 from the first monomer and LRR8* from the second monomer (Figure 19). Additionally, near the agonist binding site, residues from LRR16 interact with the residues from LRR13* and LRR14*.

Results

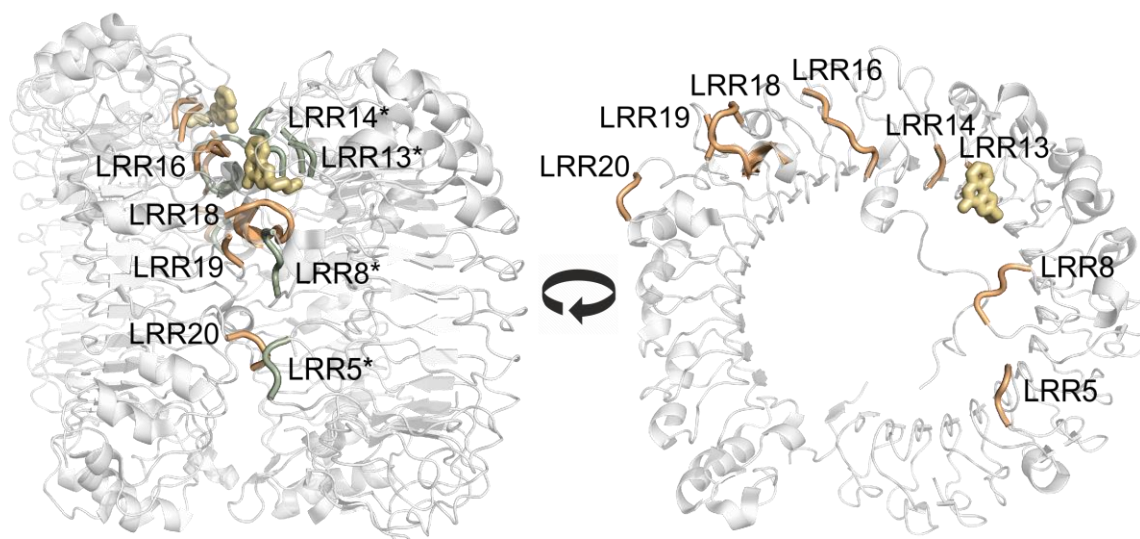


Figure 19. Overview of the agonist-bound TLR8 (PDB ID: 3W3J) (grey cartoons) with depicted dimerisation patches (orange and green cartoons for each monomer), side view (left) and front view of the monomer (right). The agonist (yellow sticks) is also depicted.

4.1.3 Comparison to evolutionary related Toll-like receptors

To further assess the functional importance of the features studied in the previous sections, we compared the protein sequences of human TLR8 with structurally related TLRs using multiple sequence alignment. We included TLR3, TLR7 and TLR9 from humans and TLR8 from the mouse, rat, pig, cow, sheep, horse and cat. TLR8 from mice, rats and pigs are particularly interesting since they exhibit species selectivity. Most notably, mouse and rat TLR8 are not activated by CL075, CL097 and R848 [162]. On the other hand, porcine TLR8 is activated by imiquimod and gardiquimod, which do not activate human TLR8 [163].

In general, ectodomains of different human TLRs are less conserved than their retrospective cytoplasmic Toll/IL-1 receptor (TIR) domains. The ectodomain of human TLR8 is most similar to human TLR7, with which it shows 40% identity (Table 2). Binding site residues for the small-molecule agonists are fairly conserved between human TLR7, TLR8 and TLR9 (Figure S 1). As already mentioned in the introduction (section 1.6), some reported human TLR8 agonists can also activate human TLR9 or TLR7 [100-107]. Conservation score is a numerical index that reflects the conservation of physicochemical properties in the alignment [164]; higher scores implicate better conservation of residues. In general, the loop regions involved in the dimerisation interfaces of TLR8 show high conservation scores across

Results

TLR7, TLR8 and TLR9 (Figure S 1). The exception is the Z-loop region, which is highly diverse among all four receptors (Figure S 1).

Table 2. Protein sequence similarity between ectodomains and TIR domains in human TLR8 and TLR3, TLR7 and TLR9.

	Ectodomain	TIR
TLR3	24%	29%
TLR7	40%	52%
TLR9	35%	35%

TLR8 is conserved across different species. The TIR domain of TLR8 from other animals shows 90% identity with the TIR domain of the human TLR8. Ectodomains are less conserved. For example, ectodomains of horse and human TLR8 are most conserved and show 75% identity. In comparison, ectodomains of mouse and rat TLR8 have 67% residues identical to the human variant (Table 3). Both binding pocket residues and the residues implicated in the dimerisation show high sequence conservation (Figure S 2), except residues in LRR5 and LRR20. The differences in specific amino acid residues in the binding site implicated in the interactions with ligands are discussed in the next chapters (section 4.2.2 and 4.2.9).

Table 3. Protein sequence similarity between ectodomains and TIR domains in human TLR8 and TLR8s from animals.

	Ectodomain	TIR
Mouse TLR8	67%	87%
Rat TLR8	67%	88%
Pig TLR8	70%	89%
Cow TLR8	71%	89%

Results

Sheep TLR8	70%	89%
Horse TLR8	74%	90%
Cat TLR8	74%	90%

4.2 Computationally-assisted identification of novel Toll-like receptor 8 modulators

In this part of the study, we aimed to identify novel modulators of TLR8. Since only small-molecule agonists, but not antagonists have been characterised at the beginning of this study, we focused our initial modelling efforts on understanding agonist. However, we hypothesised that agonists and antagonists might partially share interaction patterns. Therefore, our modelling approach would be able to identify both agonists and antagonists of TLR8.

The overview of the project is represented in Figure 20. First, we used the information on previously reported agonists of TLR8 and available structures of the TLR8 (section 4.1.1) to derive 3D pharmacophore models for TLR8 modulators. The derived models were subsequently employed in virtual screening. The experimental validation of the most promising compounds led to identifying the potent pyrimidine-based inhibitor of the TLR8 response. In the next step, we employed additional shape-based screening to find analogues of the initial hit. Further experimental characterisation of the subset of pyrimidine-based analogues confirmed the selective and potent inhibition of TLR8-mediated response. Finally, we used molecular modelling to predict the binding of the newly identified inhibitors to TLR8.

Most of the experimental work, including the compounds' pharmacological characterisation, was performed in cooperation by Dr. Maria Grabowski under Prof. Dr. Günther Weindl.

Results

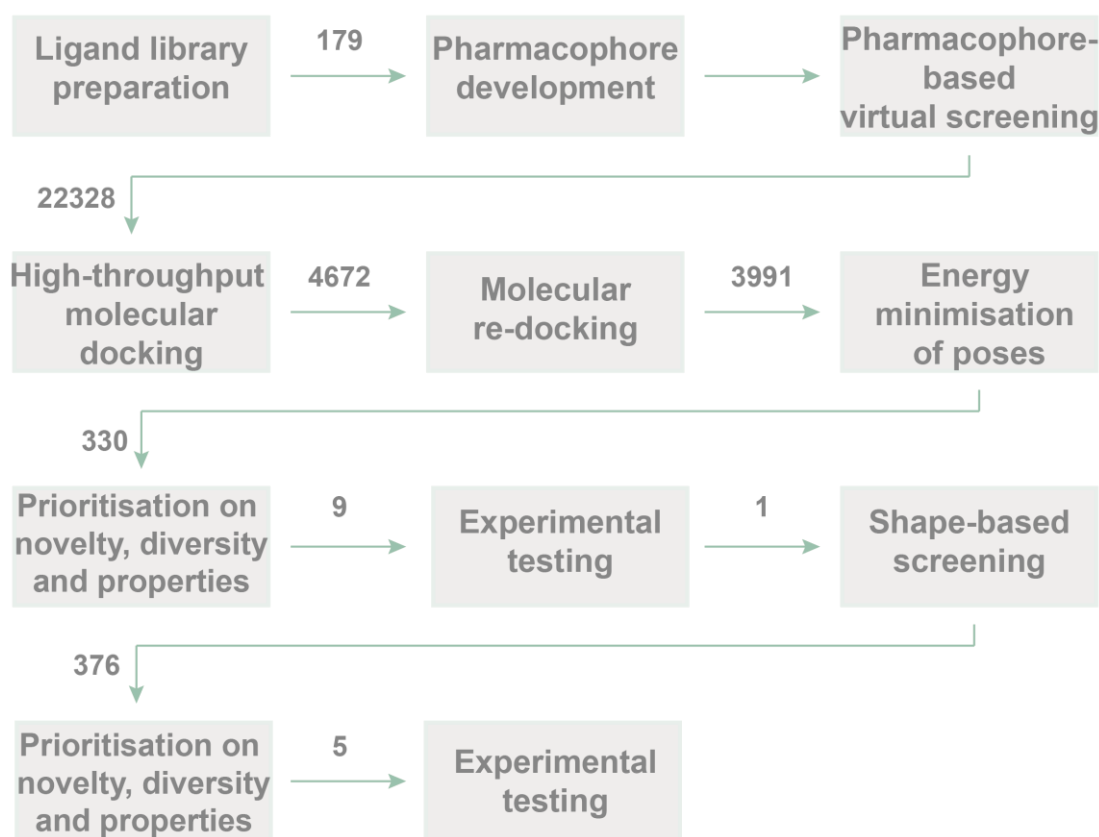


Figure 20. Overview of the workflow for computationally-assisted identification of novel TLR8 modulators. The number of compounds after each step is represented on the arrows.

4.2.1 Overview of previously reported TLR8 modulators

In the first step, we created a library and analysed physicochemical properties of previously reported TLR8 modulators. A total number of 179 TLR8 agonists and 63 TLR8 antagonists was collected from previous publications (Table S 3 and Table S 4). Agonists include structurally related series: 4-amino-fluro[2,3-c]quinolones [165], 4-amino-imidazo[4,5-c]quinolines [103], 4-amino-thiazolo[4,5-c]quinolines [102], 2-aminoquinolines [96, 161], 2-aminobenzimidazoles [97], 2-aminoimidazoles [98] and 2,4-diaminopyrimidines [99, 106]. Antagonists include derivatives of pyrazolo[1,5-a]pyrimidines and 4-phenyl-1-(2H)-phthalazinones [49, 109]. Series for which plausible binding mechanisms could not be established because of either lack of structural analogues or detailed experimental characterisation, were excluded from the library [94, 107, 108].

Most ligands are relatively small molecules with SlogP in the range –of two to five (Figure 21). Since TLR8 ligands have to reach the site of action in the endosomes, smaller

Results

molecules without charged groups or larger bulky moieties can efficiently pass both cellular and endosomal membranes.

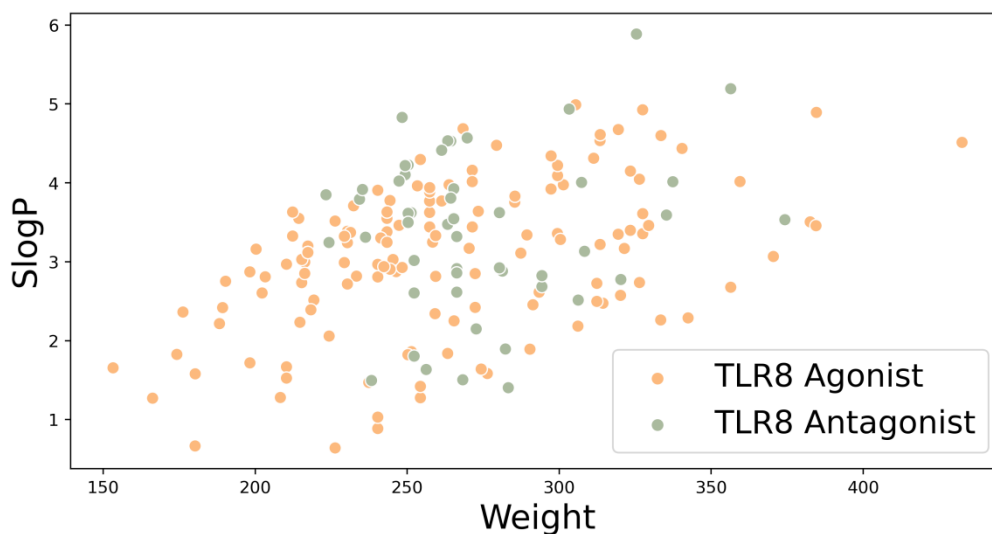


Figure 21. Scatter Plot of SlogP and Weight for the reported TLR8 agonists and antagonists.

Agonists and antagonists in general exhibit similar molecular properties and have similar structural features. However, the reported antagonists are limited to only a few reported scaffolds. Therefore, chemical space is still not sufficiently explored (Figure 21). Nonetheless, agonists show a tendency to be more flexible. They also tend to have more hydrogen bond donor moieties in the structure than antagonists (Figure 22 and Figure S 3).

Results

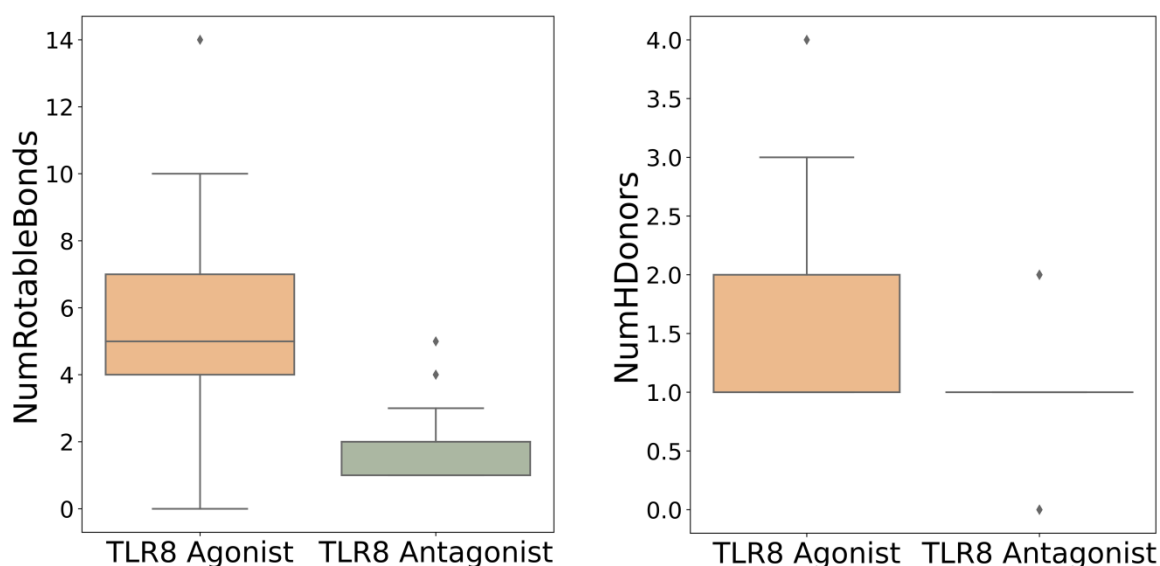


Figure 22. Distribution of the number of rotatable bonds (left) and the number of hydrogen bond donors (right) for TLR8 agonists and antagonists.

4.2.2 Binding of small-molecule agonists

At the beginning of the project, the binding of agonists to TLR8 has been already experimentally clarified. Accordingly, we focused our modelling on the activated form of TLR8. Crystal structures have confirmed that different synthetic small-molecule agonists bind in a very similar way to the pocket on the dimerisation interface (Table S 1 and Figure 23). The endogenous ligand uridine binds to the same pocket but only partially shares interaction patterns with the synthetic small molecule agonists (Figure 23). Since TLR8 activation by uridine also requires allosteric binding of short dinucleotides [31], we focused on the binding of the synthetic small-molecule agonists.

Results



Figure 23. Overlay of binding poses of synthetic small-molecule agonists (grey and white sticks) in the left panel and uridine (orange sticks) in the right panel from the superimposed crystal structures. For the sake of clarity, only following structures of TLR8 bound to selected ligands are depicted: DS-802 (PDB ID: 4QBZ), IMDQ (PDB ID: 5AWD), MB-564 (PDB ID: 5AWC), MB-343 (PDB ID: 5AZ5), dinucleotide and uridine (PDB ID:4R07).

In addition to available binding poses from crystal structures, molecular docking was used to predict binding poses of previously reported TLR8 agonists, for which no structural data was available [96, 97, 99, 102-104, 106, 141] (Table S 3).

Most of the studied ligands show hydrogen bonds between the amidine group of the ligand and Asp543 (Figure 24). N1 of the amidine group presumably becomes protonated in the acidic endosomal environment. It thereby enables the formation of strong bidentate hydrogen bonds with Asp543. Some of the ligands, such as 4-amino-furo[2,3-*c*]quinolines, 4-amino-imidazo[4,5-*c*]quinolines, 4-amino-thiazolo[4,5-*c*]quinolines and 2,4-diaminopyrimidines additionally form hydrogen bonds with the sidechain or backbone of Thr574. Both Asp543 and Thr574 are highly conserved across TLR7, TLR8 and TLR8s from different species (Figure S 1 and Figure S 2). The aromatic rings in all ligands exhibit aromatic π - π stacking with Phe405* and Tyr353*. Phe405* and Tyr353* are also well conserved across different TLRs (Figure S 1 and Figure S 2). The hydrophobic aliphatic side chain in all agonists protrudes in the hydrophobic sub-pocket, which is surrounded by Phe405*, Val378*, Tyr348*, Ile403*, Phe346* and Val573. Val378* is entirely conserved. Val573, Tyr348*, Phe346* and Ile403* are less conserved and may contribute to the observed differences in affinity for different ligands between different TLRs (Figure S 1 and Figure S 2). Several ligands, such as analogues of 2-amino-quinolines and 4-amino-imidazoquinolines, possess further amino groups which

Results

can form ionic or hydrogen bond interactions with Asp545 and Gly351*, respectively (Figure 23 and Figure 24). Interestingly, both residues show low conservation in the evolutionary related TLRs (Figure S 1 and Figure S 2).

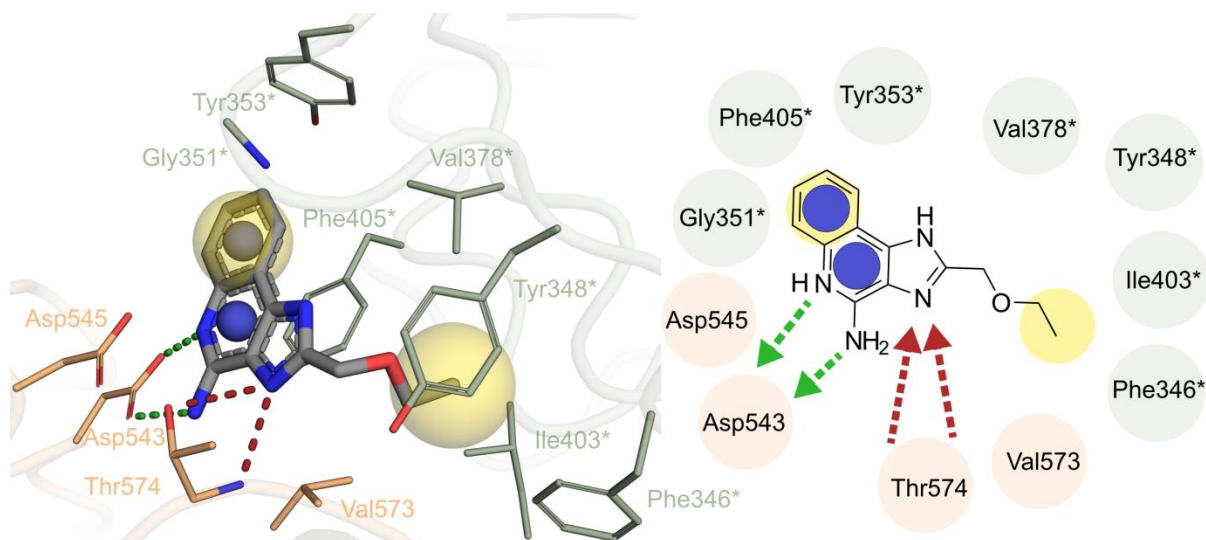


Figure 24. A binding pose of small-molecule agonist CL097 (grey sticks) with interacting TLR8 residues (orange and green sticks for each monomer) (PDB ID: 3W3J) in 3D (left) and 2D representation (right). Hydrophobic and aromatic interactions are represented as yellow and blue spheres/circles. Hydrogen bond acceptor and donor interactions are represented as red and green arrows, respectively.

4.2.3 Systematic development of the three-dimensional pharmacophore for TLR8 agonist binding

We wanted to derive an interaction pattern necessary for the binding of the agonists to the activated TLR8. Therefore, a 3D pharmacophore was developed starting from the binding poses of TLR8 agonists described above. The final 3D pharmacophore includes one hydrogen bond donor feature representing hydrogen bonds with Asp543* (HBD1) (Figure 25 A). It is still unclear if the bidentate hydrogen bond is mandatory for the binding. Studies showed that TLR8 is activated in an acidic environment [166]. However, this is more likely due to the necessity of proteolytic cleavage of the receptor for activation [47]. Therefore, we included only one hydrogen bond to Asp543 in the final pharmacophore.

Hydrogen bonds formed between the agonists and Thr574 are crucial for binding; this has been confirmed by mutational studies [22]. The Thr574Ala mutation completely abolished the binding of the imidazoquinoline derivatives. However, some high-affinity agonists lack

Results

hydrogen bonds, such as 2-aminoquinolines, 2-aminobenzimidazoles and 2-aminoimidazoles. Nonetheless, we included these hydrogen bonds (HBA1, 2) in the final pharmacophore to cover all potential binders. The pharmacophore model also describes the parallel pi-pi stacking between the aromatic ring system in the ligand and Phe405*, represented as an aromatic feature (AR1). The aromatic interaction with Tyr353* is not mandatory, as it is not formed by the agonists with a 2,4-diaminopyrimidine scaffold. The hydrophobic moiety is included in the model since it is preferred in the position close to Phe405* and Tyr353* (HYD1). The crucial hydrophobic substituent, surrounded by Phe405*, Val378*, Tyr348*, Ile403*, Phe346* and Val573 is depicted as the second hydrophobic feature in the model (HYD2).

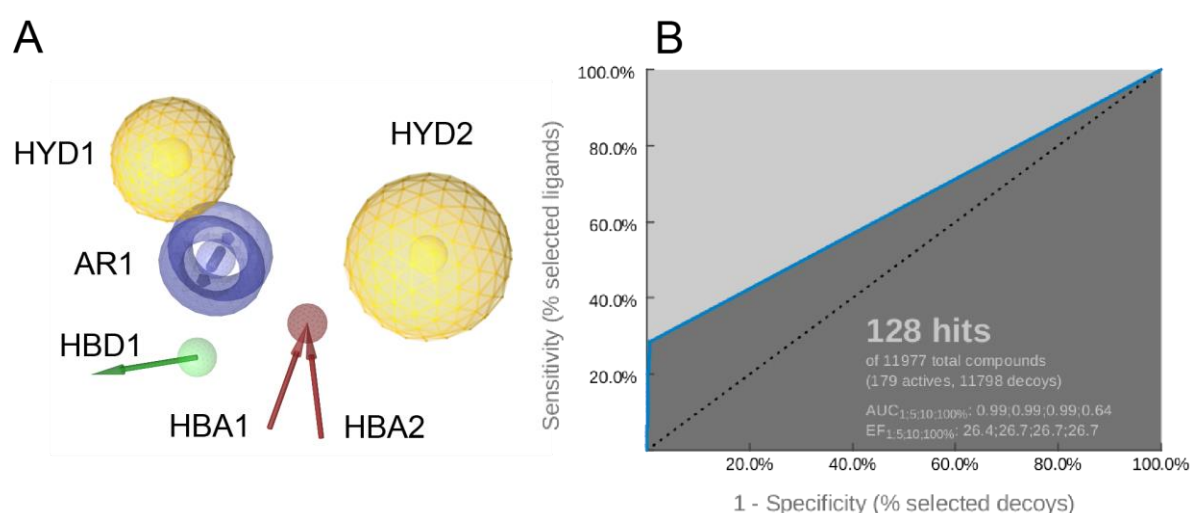


Figure 25. Final structure-based pharmacophore based on interaction pattern of TLR8 agonists (A) and associated ROC curve on the validation set (B). AR1 - aromatic interaction, HBD1 - hydrogen bond donor, HBA1, 2 - hydrogen bond acceptor 1 and 2, HYD1, 2 - hydrophobic feature 1 and 2.

Additional exclusion volume spheres were added on binding site residues to reflect the steric volume of the binding pocket. The derived pharmacophore was further iteratively optimised. Each iteration consisted of small modifications of selected feature tolerances and subsequent assessment of the pharmacophore on the previously generated validation set of 179 active ligands and 11798 decoy ligands. The ability of the pharmacophore to discriminate between active ligands and decoy ligands was assessed with the receiver operating characteristic curve (ROC) shown in Figure 25 B. The final pharmacophore shows a high degree of discriminative power: It recognised 51 of the active ligands and 77 of the decoy ligands.

4.2.4 Pharmacophore-based virtual screening

Results

Virtual screening of more than five million commercially available compounds using the developed 3D pharmacophore identified 22 328 hits. Next, a filtering pipeline was applied to reduce the large number of initial virtual screening hits (Figure 20). In the first stage, "fast" molecular docking with lower binding poses prediction accuracy was used to discard compounds that cannot generate reasonable binding poses efficiently. In the second stage, we used "slow" molecular docking with higher binding poses prediction accuracy. The second stage aimed to refine the predicted poses for the remaining compounds. The most plausible poses from both stages were filtered in the automated fashion - the resulting poses were rescored based on their ability to satisfy interaction from the initial 3D pharmacophore. The poses that fit the interaction pattern best were kept. The first and second docking round resulted in 4672 and 3991 molecules, respectively. Poses of the remaining 3991 compounds were energy-minimised and visually examined, with particular emphasis on the intermolecular interactions described earlier. This led to a selection of 330 molecules with optimal predicted binding poses. For a final prioritisation, we considered the number of intermolecular interactions, the novelty of the chemical scaffold compared to known ligands and the structural diversity among the selection. Because TLR8 is located in endosomes, potential modulators have to pass both the cell and the endosomal membrane. Therefore, smaller and less polar molecules are more probable to reach the site of action. The Lipinski's rule of five properties and number of rotatable bonds of the molecules were considered in the final selection. In the end, we selected and ordered nine compounds for experimental testing (Figure 26).

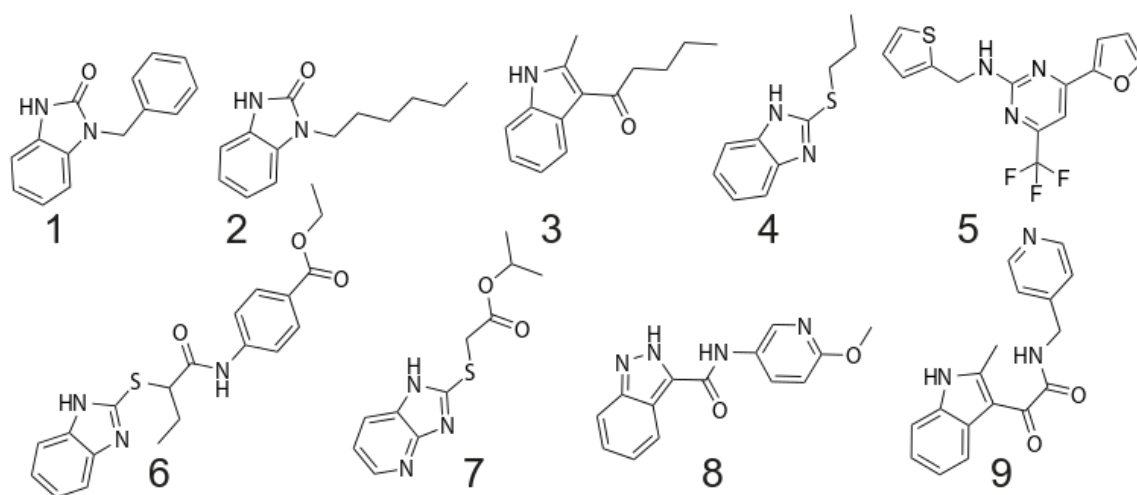


Figure 26. Selected virtual screening hits from the pharmacophore-based virtual screening.

4.2.5 Experimental validation of the hits from pharmacophore-based virtual screening

Before any further experimental characterisation, purity of the ordered commercial compounds was evaluated using High-Performance Liquid Chromatography (HPLC). All compounds showed one peak with > 95% purity.

Next, we aimed to validate the modulation of TLR8-mediated response of the compounds in cells. Our collaboration partner Dr. Maria Grabowski working in the group of Prof. Weindl used human embryonic kidney (HEK) cell line overexpressing hTLR8. The TLR8-mediated response was validated by measuring the activation of transcription factor NF- κ B and activator protein 1 (AP-1), which control the expression of an array of inflammatory cytokine genes (section 1.4). Activation of NF- κ B and AP-1 results in secreted embryonic alkaline phosphatase (SEAP) production that can be determined with the colourimetric substrate QuantiBlue by reading the optical density (OD). We used TLR7/TLR8 agonist CL075 [167] to trigger a potent NF- κ B/AP-1 activation in hTLR8 reporter cells when testing for the antagonistic activity. As a control for the antagonistic activity we used TLR7/8/9 antagonist ODN [168], which is a short single-stranded oligodeoxynucleotide.

None of the nine tested compounds induced TLR8-dependent NF- κ B/AP-1 activation (Figure 27 A). Three compounds, **5**, **6** and **9**, reduced the CL075-induced TLR8-dependent NF- κ B/AP-1 activation in HEK-Blue hTLR8 cells. **5** and **9** decreased the response to around 50 % and 40% at 25 μ M and 10 μ M, respectively (Figure 27 B). **6** reduced the response to approximately 40 % at 25 μ M. None of the tested compounds interfered with cell viability in the tested concentration range of the activity study. Details are shown in our joint publication [169].

Results

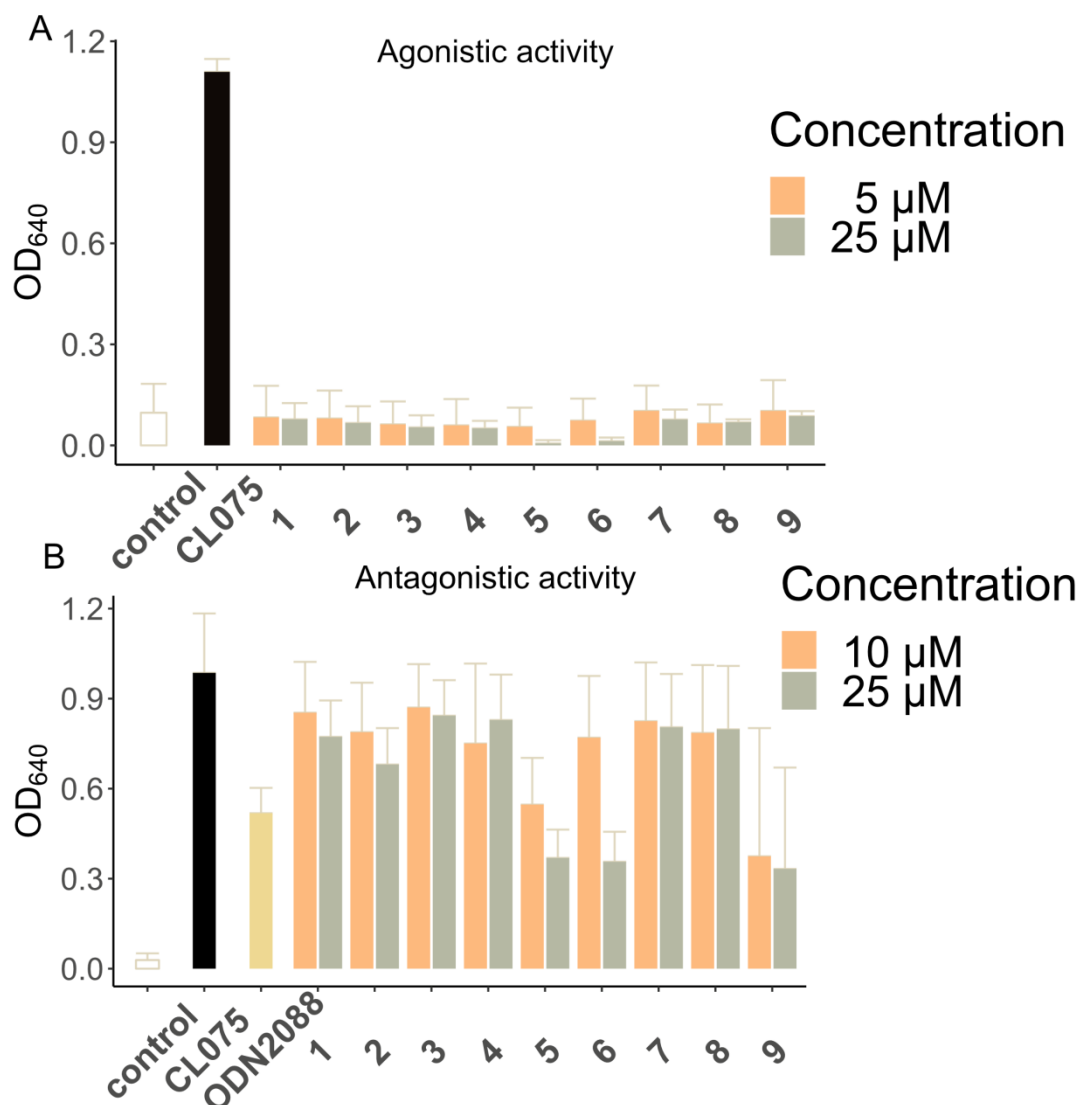


Figure 27. Modulation of hTLR8-mediated NF- κ B/AP-1 activation for virtual screening hits. (A) HEK-Blue hTLR8 cells were stimulated with CL075 or the compounds (5 and 25 μ M) for 24 h. Mean + SD (n=3). (B) HEK-Blue hTLR8 cells were preincubated with ODN2088 (1 μ M) or the compounds (10 and 25 μ M) for 1 h and afterwards stimulated with CL075 (8 μ M) for 24 h. Supernatants were analysed for TLR8-mediated NF- κ B/AP-1 activation by secreted embryonic alkaline phosphatase (SEAP) reporter assay using QuantiBlue (OD₆₄₀). Mean + SD (n=4).

After the primary screening, concentration-response curves for **5**, **6** and **9** were obtained in hTLR8 HEK-Blue cells, and IC₅₀ values were calculated. Only **5** strongly decreased the CL075-induced hTLR8-dependent NF- κ B/AP-1 activation in a concentration-dependent manner, with an IC₅₀ of 9.2 μ M (Figure 28). Interestingly, **5** did not completely abolish CL075-induced hTLR8-dependent NF- κ B/AP-1 response and showed partial inhibition by up to 50%. The molecular basis of this effect is currently unknown, yet, partial inhibition of exaggerated

Results

inflammatory responses may be advantageous over complete inhibition for potential therapeutic applications. Unfortunately, neither **6** nor **9** showed concentration-dependent inhibition as observed with **5**. Notably, activity measurements for **9** have a rather significant standard deviation.

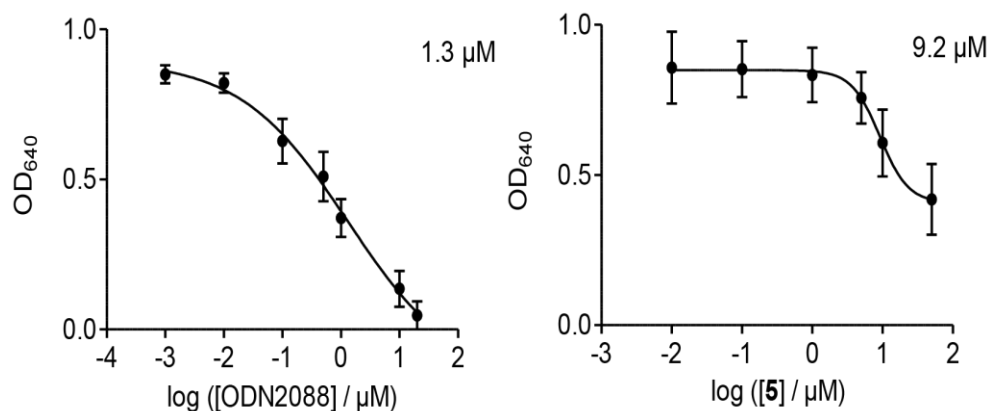


Figure 28. Concentration-response curves of the ODN2088 and **5**. HEK-Blue hTLR8 cells were incubated with increasing concentrations of ODN2088 or **5** for 1 h and stimulated with CL075 for 24 h. SEAP production was detected by QUANTI-Blue and OD was measured at 640 nm. Mean \pm SD ($n = 3$). Nonlinear regression with variable slope (four parameters) was used to fit the curve.

4.2.6 Virtual screening based on shape- and atom-based similarity search

Next, we aimed to identify analogues of **5** that could exhibit similar or better inhibitory activity on TLR8-mediated responses. Since neither binding site nor binding pose of small-molecule inhibitors were known at the time of the first experimental screening, we aimed to apply an alternative approach based on ligand-based information. In this case, we decided to use shape-based similarity implemented with rapid overlays of 3D chemical structures (ROCS). ROCS enables the identification of molecules with similar shape and potential interacting atoms to the query molecule [170] as describes in section 3.4. Therefore, more structurally diverse molecules can be identified with ROCS than with standard 2D and 3D molecular fingerprints based similarity searches [171]. Also, ROCS search can be performed with a single query molecule. In contrast, most of the ligand-based pharmacophore approaches require at least two molecules to generate a query.

Compounds with the highest shape- and pharmacophoric-similarity to **5** were selected. This resulted in 376 virtual hits, which were further prioritised based on their chemical diversity

Results

and physicochemical properties (Figure 20). In the end, we selected and ordered four compounds with a pyrimidine scaffold to get insights in structure-activity relationships (SAR), and an additional compound **13**, which is structurally distinct from **5**, but shares similar shape (Figure 29).

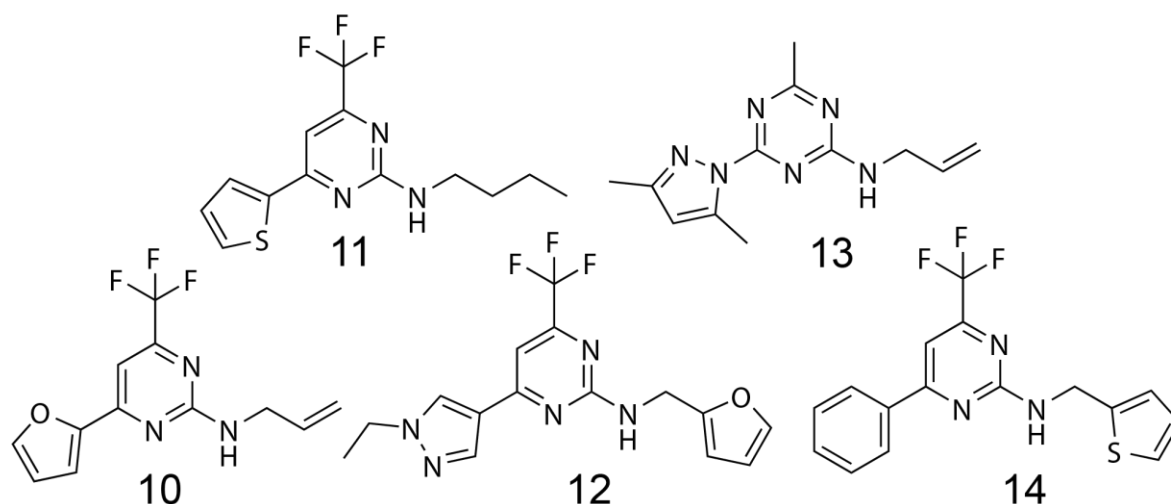


Figure 29. Selected virtual screening hits from shape- and atom-based similarity search.

4.2.7 Experimental validation of the hits from shape- and atom-based similarity search

The purity of the five compounds ordered from commercial vendors was confirmed to be >95% by HPLC. Afterwards, compounds were tested for modulation of the TLR8-mediated response in HEK-Blue hTLR8 cells by Dr Maria Grabowski (Figure 30 A). None of the five tested compounds appeared to activate TLR8, nor affected cell viability in the studied concentration range, which is shown in detail in our previous publication [169]. Compounds **11** and **14** presented a 50% and 60% reduction of hTLR8 response at 25 μ M and 10 μ M (Figure 30 B).

Results

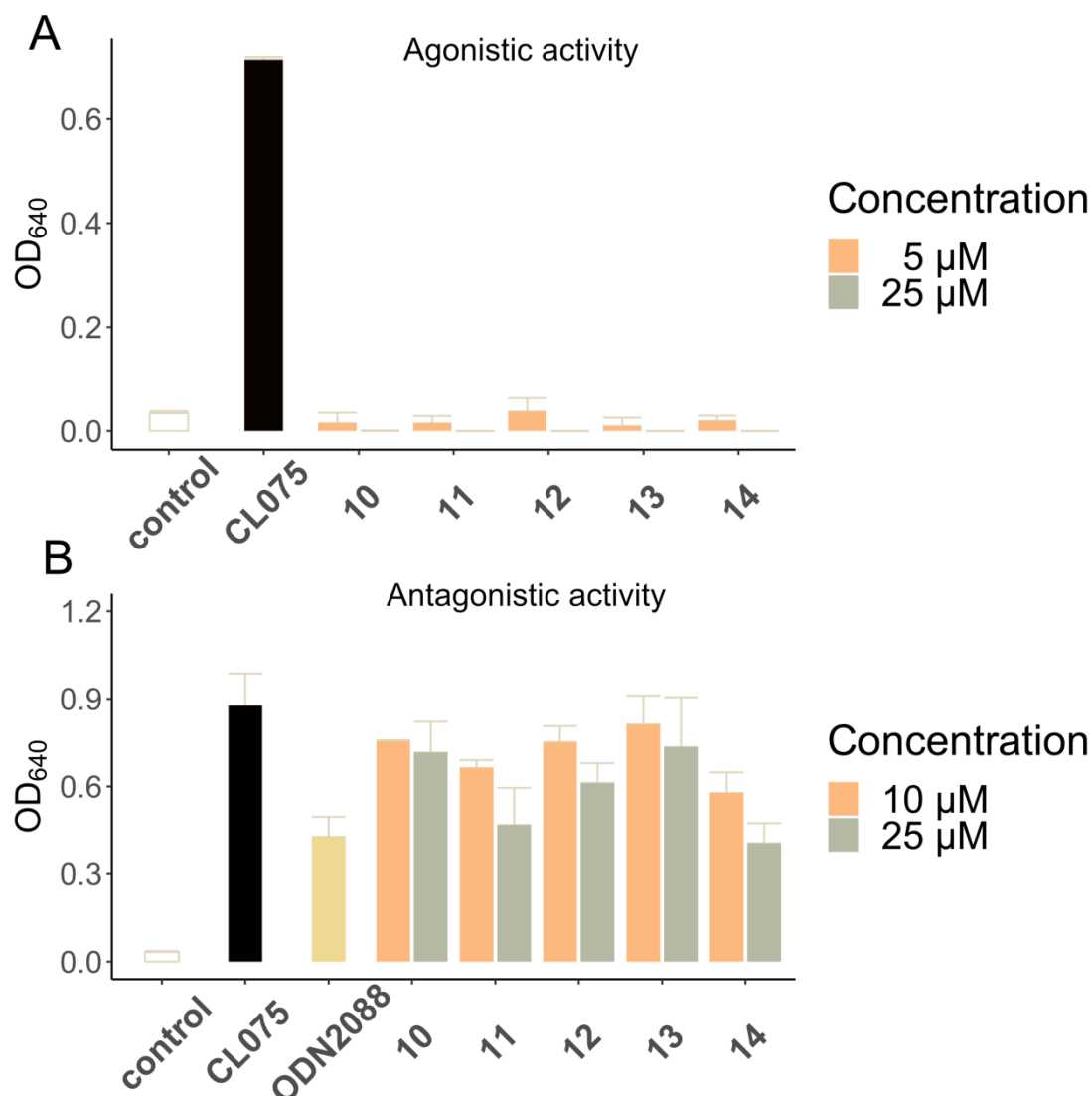


Figure 30. Modulation of hTLR8-mediated NF- κ B/AP-1 activation for the selected hits from the shape- and atom-based similarity search. (A) HEK-Blue hTLR8 cells were stimulated with CL075 or the compounds (5 and 25 μ M) for 24 h. Mean \pm SD (n=3). (B) HEK-Blue hTLR8 cells were preincubated with ODN2088 (1 μ M) or the compounds (10 and 25 μ M) for 1 h and afterwards stimulated with CL075 (8 μ M) for 24 h. Supernatants were analysed for TLR8-mediated NF- κ B/AP-1 activation by SEAP reporter assay using QuantiBlue (OD₆₄₀). Mean \pm SD (n=3).

Concentration-response curves were obtained for **11** and **14**. **5** was the most potent candidate (IC_{50} = 9.2 μ M) (Figure 28). However, as previously mentioned, **5** did not completely abolish the CL075-induced hTLR8-dependent NF- κ B/AP-1 response and showed partial inhibition by up to 50%. On the other hand, compounds **11** (IC_{50} = 35.5 μ M) and **14** (IC_{50} = 20 μ M) had a slightly higher IC_{50} value but completely blocked the hTLR8 response at the highest concentrations tested, similar to ODN2088 (Figure 31).

Results

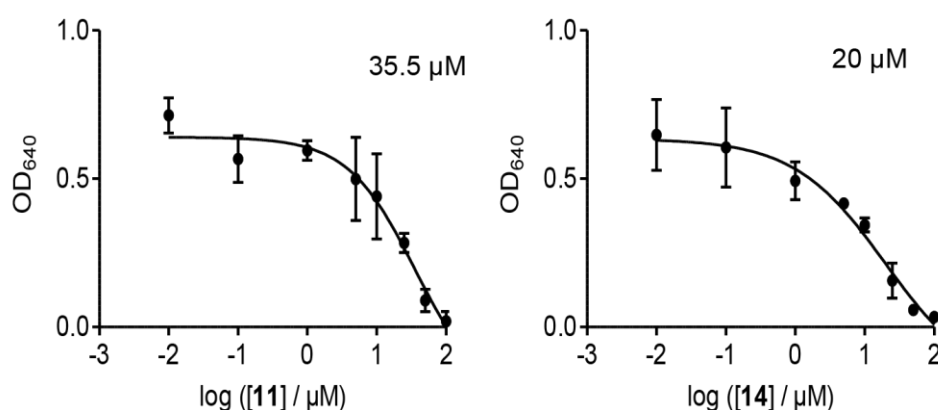


Figure 31. Concentration-response curves of the **11** and **14**. HEK-Blue hTLR8 cells were incubated with increasing concentrations of **11** or **14** for 1 h and additionally stimulated with CL075 for 24 h. SEAP production was detected by QUANTI-Blue and OD was measured at 640 nm. Mean \pm SD ($n = 3$). Nonlinear regression with variable slope (four parameters) was used to fit the curve.

4.2.8 Experimental assessment of the anti-inflammatory activity for the active compounds

Next, we aimed to characterise the impact of the compounds on the inflammatory response in a human monocytic leukaemia cell line (THP-1). THP-1 cells resemble macrophages in morphological and functional properties and are, therefore, more suitable for cytokine characterisation than HEK cells [172].

The selectivity of the compounds for TLR8 was assessed in the counter-screen against additional endosomal and cell-surface TLRs to eliminate nonspecific pathway inhibitors or compounds with assay interference (collaboration with Dr Maria Grabowski in the group of Prof. Weindl). For this purpose, THP-1 cells were stimulated with different TLR agonists. **5**, **11** and **14** did not affect TLR2-, TLR3-, TLR4-, TLR5- or TLR9-dependent IL-8 secretion in THP-1 cells. THP-1 cells express both TLR7 and TLR8. We could not use CL075-induced IL-8 secretion to distinguish selectivity towards TLR7 or TLR8 in THP-1 cells because CL075 activates both TLR7- and TLR8-mediated signalling. Therefore, we used HEK-Blue hTLR7 cells to estimate whether the three compounds also interact with hTLR7. Compounds did not affect CL075-induced NF- κ B activity in HEK-Blue hTLR7 cells. Details are shown in our joint publication [169].

Results

In order to characterise the immunomodulatory effects of **5**, **11** and **14**, Dr Maria Grabowski analysed cytokine production by THP-1. All three compounds reduced CL075-induced IL-8 and TNF- α secretion (Figure 32). **5**, **11**, and **14** were able to reduce CL075-induced IL-8 secretion to more than a half, comparable to ODN2088, which is TLR7, TLR8 and TLR9 antagonist. Compounds also reduced CL075-induced TNF- α secretion to around half. In comparison, ODN2088 almost completely abrogated TNF- α secretion.

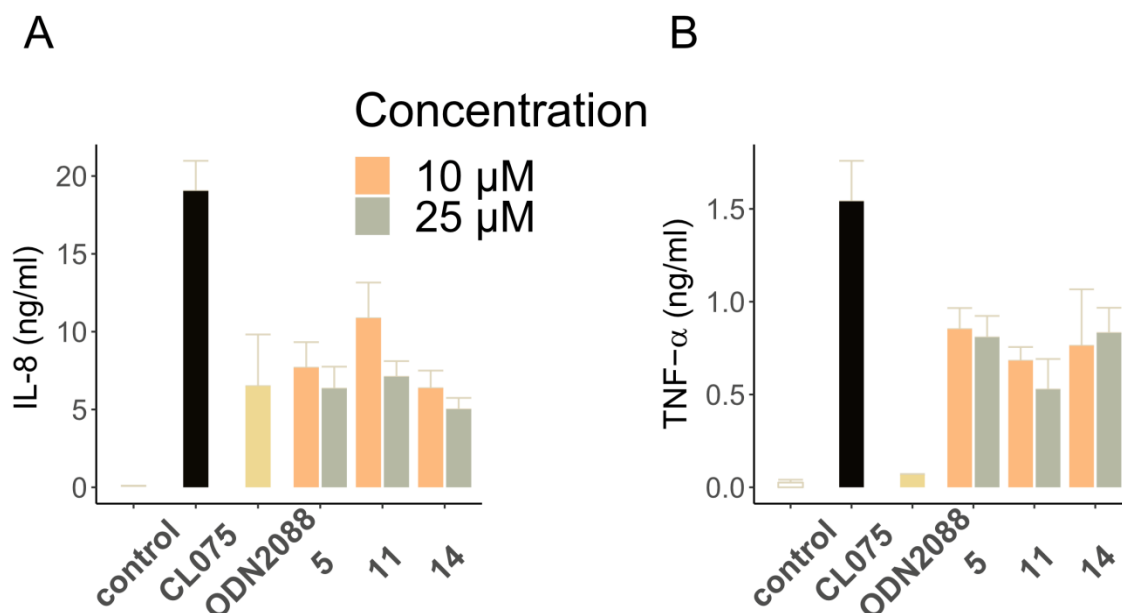


Figure 32. Modulation of hTLR8-mediated cytokine secretion in THP-1 cells. THP-1 cells were pre-incubated with ODN2088 (1 μ M) or the compounds **5**, **11** and **14** for 1 h and then additionally incubated with CL075 (8 μ M) for 24 h (A) or 4 h (B). Cytokine secretion into the culture medium was assessed by enzyme-linked immunosorbent assay (ELISA). Mean + SD (n=3).

4.2.9 Binding of small-molecule antagonists

During our study, Hang Yin's group published the work on the first selective and highly potent TLR8 antagonists [49, 109]. Additionally, the group solved the protein's crystal structures with the four active compounds from the starting pyrazolo[1,5-*a*]pyrimidine and 1(2*H*)-phthalazinone series. We used this information and studied the interaction patterns of TLR8 antagonists. In addition to available binding poses from crystal structures, we used molecular docking to predict binding poses of the rest of the reported TLR8 antagonists (Figure 33 and Table S 4).

Results

The hydrogen bond with Gly351* is crucial for the binding of the antagonists. Interestingly, Gly351* does not show high conservancy across evolutionary related TLRs (Figure S 1 and Figure S 2). An additional hydrogen bond with Val520, as in case of CU-CPT9b, led to improved potency of the analogues. For example, the presence of a hydroxyl, amide, or ester group at position 7 of the quinoline scaffold improves biological activity. Carboxylic acid derivatives are inactive, although the binding pose suggests an ideal orientation to Val520. Therefore, the inactivity of a carboxylic derivative may be a consequence of its inability to reach the endosomes rather than its inability to bind to the receptor. Val520 is conserved across different species, however, is replaced with threonine and alanine in TLR7 and TLR9. The core aromatic rings in the analogues exhibit aromatic pi-pi stacking with the conserved Phe495 and Tyr348*. Additional small hydrophobic substituents are surrounded with Phe495 and Val378* and are well tolerated. As in the case of 4-phenyl in CU-CPT9b, the aromatic substituent is surrounded by hydrophobic residues: Phe494, Val378*, Tyr348*, Tyr567 and Ala518. Except for Ala518, the hydrophobic residues are evolutionarily conserved (Figure S 1 and Figure S 2). Additional small hydrophobic substituents, such as methyl and trifluoromethyl groups, in *meta*- and *ortho*- position on the phenyl ring, fit perfectly and are surrounded by the hydrophobic residues. However, *meta*- substituents seem to be preferred over *ortho*-substituents as they lead to improved potency.

Results

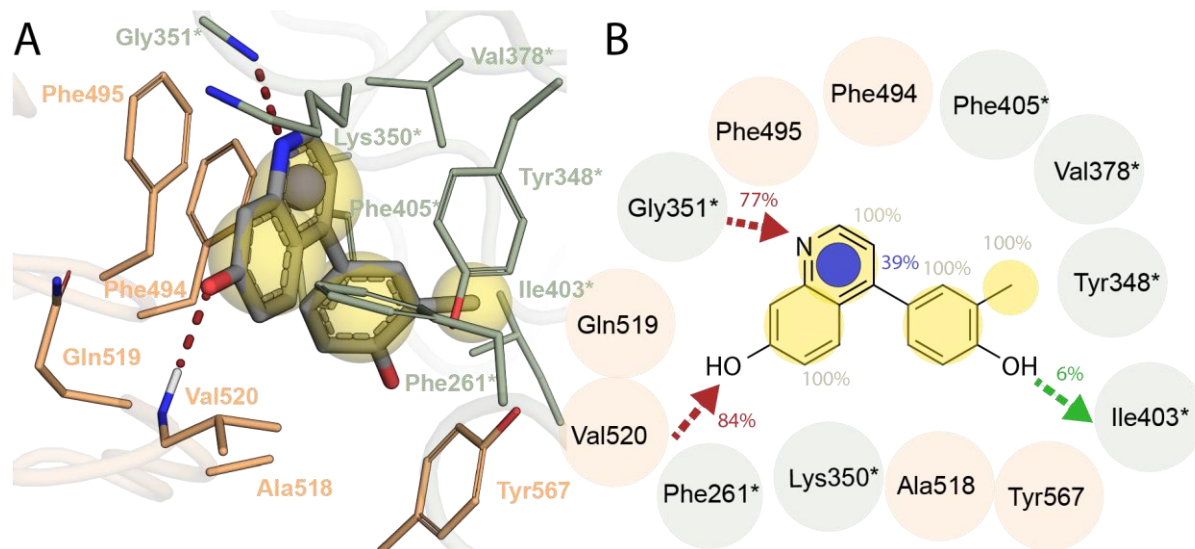


Figure 33. A binding pose of small-molecule antagonist CU-CPT9b (grey sticks) with interacting TLR8 residues (orange and green sticks for each monomer) (PDB ID: 5WYZ) in 3D (A) and 2D representation with the frequency of the formed interactions across triplicates of molecular dynamics simulation (B). Hydrophobic and aromatic interactions are represented as yellow and blue spheres/circles. Hydrogen bond acceptor and donor interactions are represented as red and green arrows, respectively.

Finally, we used MD simulations and subsequent dynophore analyses to study time-dependent interaction patterns between CU-CPT9b and TLR8 (Figure S 4). We observed that the above-described interactions show high frequencies throughout the 20 ns of all triplicates of MD simulations (Figure 33 B). We observed the additional hydrogen bond between the para-hydroxyl group on the phenyl ring and Ile403* during the MD simulations. However, this interaction does not seem to be frequent through the simulation time and occurs in only 6% of the frames.

4.2.10 Prediction of binding poses for discovered antagonists with the pyrimidine scaffold

We wanted to elucidate plausible mechanisms of binding to TLR8 for newly discovered antagonists with pyrimidine scaffold. We could establish a simple structure-activity relationship in the pyrimidine analogues since we had a small subset of the structurally related compounds with the corresponding activity and knowledge about previously elucidated binding poses. We docked pyrimidine analogues in a discovered antagonistic binding site (section 4.2.9) [49].

Results

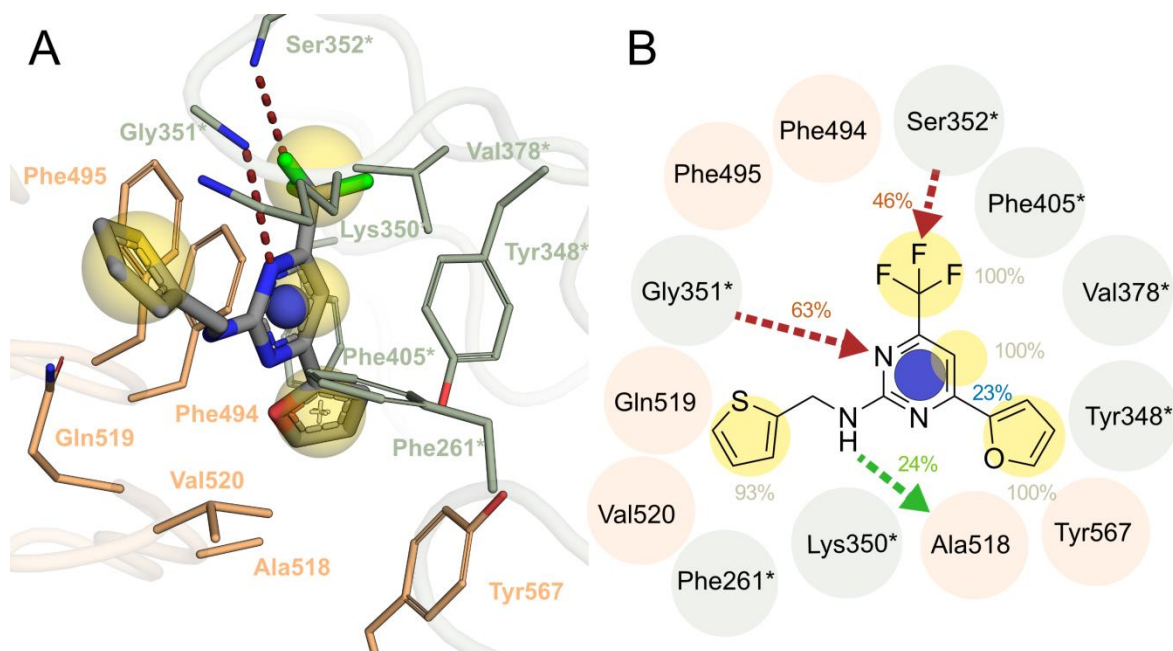


Figure 34. A predicted binding pose of **5** (grey sticks) with interacting TLR8 residues (orange and green sticks for each monomer) (PDB ID: 5WYZ) in 3D (A) and 2D representation with the frequency of the formed interactions during the molecular dynamics simulation (B). Hydrophobic and aromatic interactions are represented as yellow and blue spheres/circles. Hydrogen bond acceptor and donor interactions are represented as red and green arrows, respectively.

The proposed binding poses of pyrimidine analogues are similar to those observed with CU-CPT9b and its analogues (Figure 33 and Figure 34). The furan ring in **5**, thiophene ring in **11**, and phenyl ring in **14** are surrounded by hydrophobic residues: Phe494, Val378*, Tyr348*, Tyr567 and Ala518, analogously to the phenyl ring in CU-CPT9b. The pyrimidine ring in **5**, **11** and **14** exhibits aromatic pi-pi stacking with Phe495 and Tyr348*. Furthermore, compounds interact with TLR8 through hydrogen bond between the pyrimidine nitrogen in position 1 and the backbone of Gly351*. The trifluoromethyl group is near to the hydrophobic residues Phe495 and Val378*. Additionally, fluorine atoms act as hydrogen bond donor acceptors to Ser352*. The thiophene moiety in **5** and **14**, and butyl moiety in **11** are surrounded by hydrophilic residues (Gln519 and Lys350*) and hydrophobic residues Phe261* and Val520.

Table 4. Average interaction frequencies for **10**, **11**, **12**, and **14** through MD simulations triplicates. AR - aromatic interaction, HBD - hydrogen bond donor, HBA - hydrogen bond acceptor, HYD - hydrophobic feature.

Interaction (interaction partner)	10	11	12	14
-----------------------------------	----	----	----	----

Results

HBA1 (Gly351*)	23%	35%	82%	32%
HBA1(Ser352*)	26%	38%	24%	50%
HDB (Ala518)	19%	54%	8%	45%
AR (Phe495 and Tyr348*)	22%	41%	31%	30%
HYD1 (Phe494, Val378*, Tyr348*, Tyr567, Ala518)	67%	100%	100%	100%
HYD2 (Tyr348*, Val378*)	67%	100%	100%	100%
HYD3 (Phe495, Val378*)	67%	100%	100%	100%
HYD4 (Phe261*, Val520)	66%	83%	93%	97%

Next, we used MD simulations and subsequent dynophore analyses to study protein-ligand interaction patterns through time. All protein-ligands complexes reached the RMSD plateau during the first few ns of 20 ns molecular dynamics simulation (Figure S 4). Interestingly, we observed additional hydrogen bonds between the secondary amine and backbone of Ala518 throughout MD simulations (Figure 34 and Table 4). The thiophene, furan and butyl side chain in the active compounds **5**, **11** and **14** make hydrophobic contacts with Phe261* and Val520 through the whole MD simulation (Figure 35 A). On the other hand, **10** is inactive. During the MD simulation, shorter and smaller allyl side chain on the substituted nitrogen in **10** cannot optimally reorient itself towards Phe261* and Val520, which results in higher ligand flexibility with varying interaction partners (Figure 35 B). This may explain why **10** is inactive.

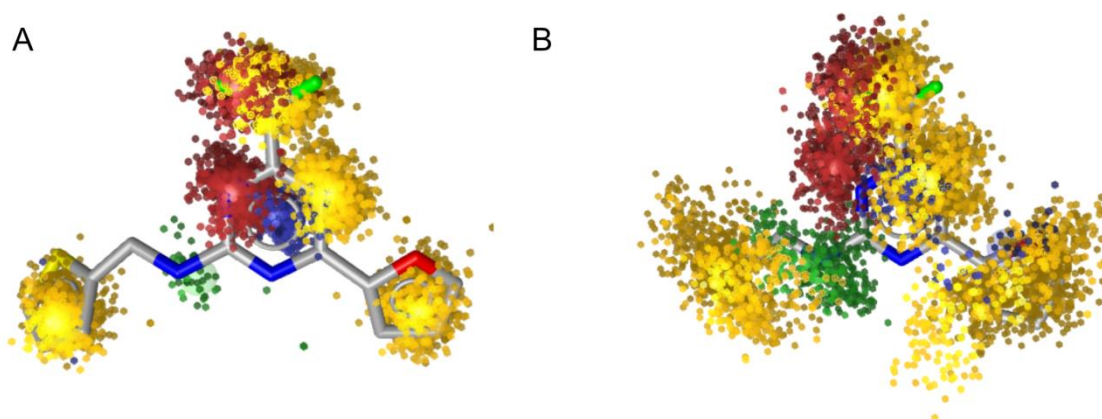


Figure 35. The 3D representation of the dynamic 3D pharmacophore derived from the MD simulations of **5** (A) and **10** (B) (grey sticks). Hydrophobic and aromatic interactions are represented as yellow and blue clouds of points. Hydrogen bond acceptor and donor interactions are represented as red and green clouds of points.

Results

The pyrazole ring's reduced hydrophobicity might explain the inactivity of compound **12** in position 4. This contrasts to furan, thiophene and phenyl rings in **5**, **11**, **14**, where a hydrophobic substituent allows the optimal interactions with Ala518, Tyr348* and Tyr567 (Figure 34). On the other hand, flexible ethyl substituent on the pyrazole ring of **12** cannot accommodate itself optimally towards Ala518 and Tyr348* (Figure 36).

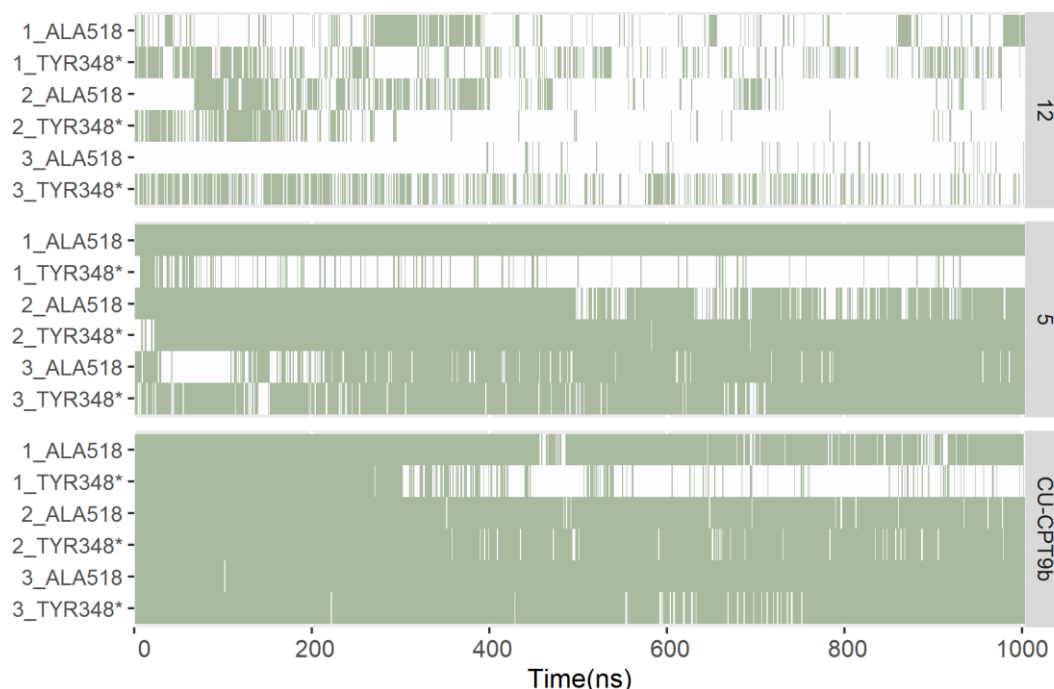


Figure 36. Bar code series representing hydrophobic interaction occurrence sequence of CU-CPT9b, **5** and **12** with Ala518 and Tyr348* during MD simulation. Simulation with each ligand was performed in triplicates.

4.3 Optimisation of novel Toll-like receptor 8 antagonists

In the most recent project, we aimed to optimise the molecules identified by the virtual screening described in the previous section. The project was a joint work consisting of cycles of molecular modelling, organic synthesis and the pharmacological characterisation of the analogues. From the molecular modelling perspective, the main goal was to establish a structure-activity relationship based on the tested molecules and incorporate this information to plan the next rounds of the synthesis. Ana Dolšak, under the supervision of Dr. Matej Sova, prepared the compounds. Dr Maria Grabowski, under the supervision of Prof. Dr. Günther Weindl, performed the pharmacological characterisation.

Results

4.3.1 Optimisation strategy

We incorporated results from the molecular modelling of the binding of the antagonists (sections 4.2.9 and 4.2.10) and proposed a general optimisation strategy (Figure 37).

First, we wanted to evaluate the importance of the trifluoromethyl group (R1). We planned the removal of the group from the pyrimidine core or replacement by a methyl group. Second, we have focused on the modifications of the part with the furan ring (R2). We wanted to explore the importance of the aromatic rings by preparing analogues in which different ring systems replace the furan ring. We hypothesised that additional small hydrophobic substituents on the ring, such as the methyl group, could be sterically beneficial. Additionally, extensions of this part of the molecule, e.g. on position 4 and 5, could enable favourable interactions with Glu427* or Ser516. Finally, we wanted to explore the importance of the N-[(thiophene-2-yl)-methyl] moiety (R3) and replace it with different aliphatic and aromatic moieties. The part of the pocket occupied by N-[(thiophene-2-yl)-methyl] moiety is not occupied by the previously reported antagonists. Thiophene is surrounded by hydrophilic residues, such as Gln519, Glu525 and Ser522, and we hypothesised that the incorporation of groups capable of hydrogen bonding with the surrounding residues might lead to enhanced activity.

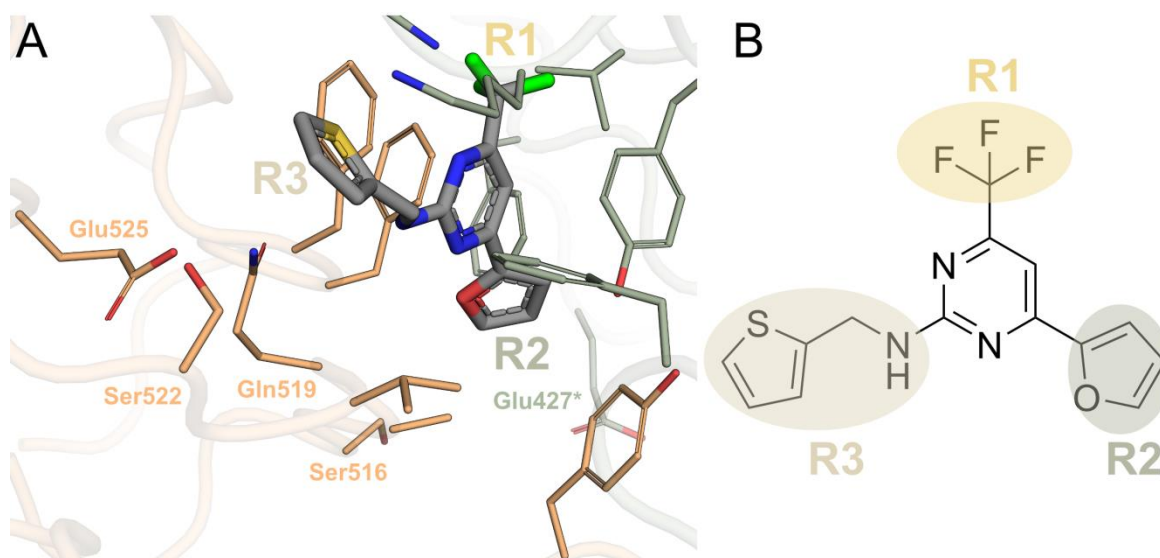


Figure 37. General optimisation strategy for **5** (grey sticks) with three main parts of the interest depicted in the 3D view of the binding site (left) and 2D depiction of **5** (right).

4.3.2 Synthesis and pharmacological evaluation of the analogues

Results

The set of the compounds was synthesised by Ana Dolšak (section 7.11.3) according to the proposed modifications from molecular modelling and subsequently experimentally validated in HEK-Blue hTLR8 cells by Dr Maria Grabowski. We decided to use the selective TLR8 agonist TL8-506 (EC₅₀ 0.59 μ M) for the activation of TLR8-mediated response, in contrast to the previously used CL075, which activates both TLR7- and TLR8-mediated response.

None of the tested compounds induces TLR8-dependent NF- κ B/AP-1 activation (Figure 38).

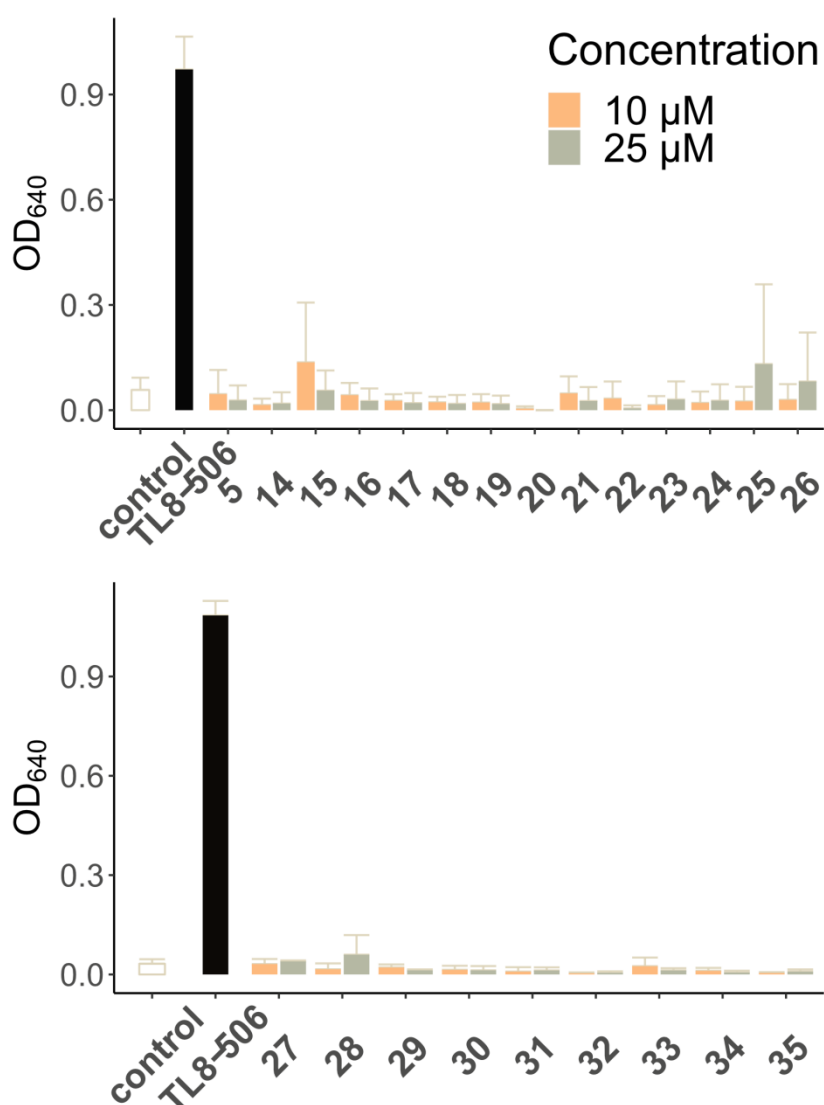


Figure 38. Induction of hTLR8-mediated NF- κ B/AP-1 activation of the synthesised analogues. HEK-Blue hTLR8 cells were stimulated with TL8-506 or the compounds (10 and 25 μ M) for 24 h. Mean +SD (n=3).

Results

On the other hand, most of the synthesised compounds reduce at least slightly the TL8-506-induced TLR8-dependent NF- κ B/AP-1 activation (Figure 39). **15**, **20** and **22** inhibit the TL8-506-induced TLR8-dependent NF- κ B/AP-1 activation almost completely at 25 μ M. They show similar or more potent TLR8 inhibition compared to ODN2088 (1 μ M) and previously characterised **5** and **14** (section 4.2.5 and 4.2.7). At 10 μ M, they reduce TL8-506-induced TLR8-dependent NF- κ B/AP-1 activation to less than 50%. However, all three compounds interfere with cell viability at 50 μ M. Unfortunately, the most active analogue **15** already shows a slight reduction of cell viability at 25 μ M. Compounds **32**, **33**, **34** and **35** inhibit TLR8-dependent NF- κ B/AP-1 activation to the same extent as the starting compound **5**, with 40% and 50% inhibition at 10 and 25 μ M, respectively.

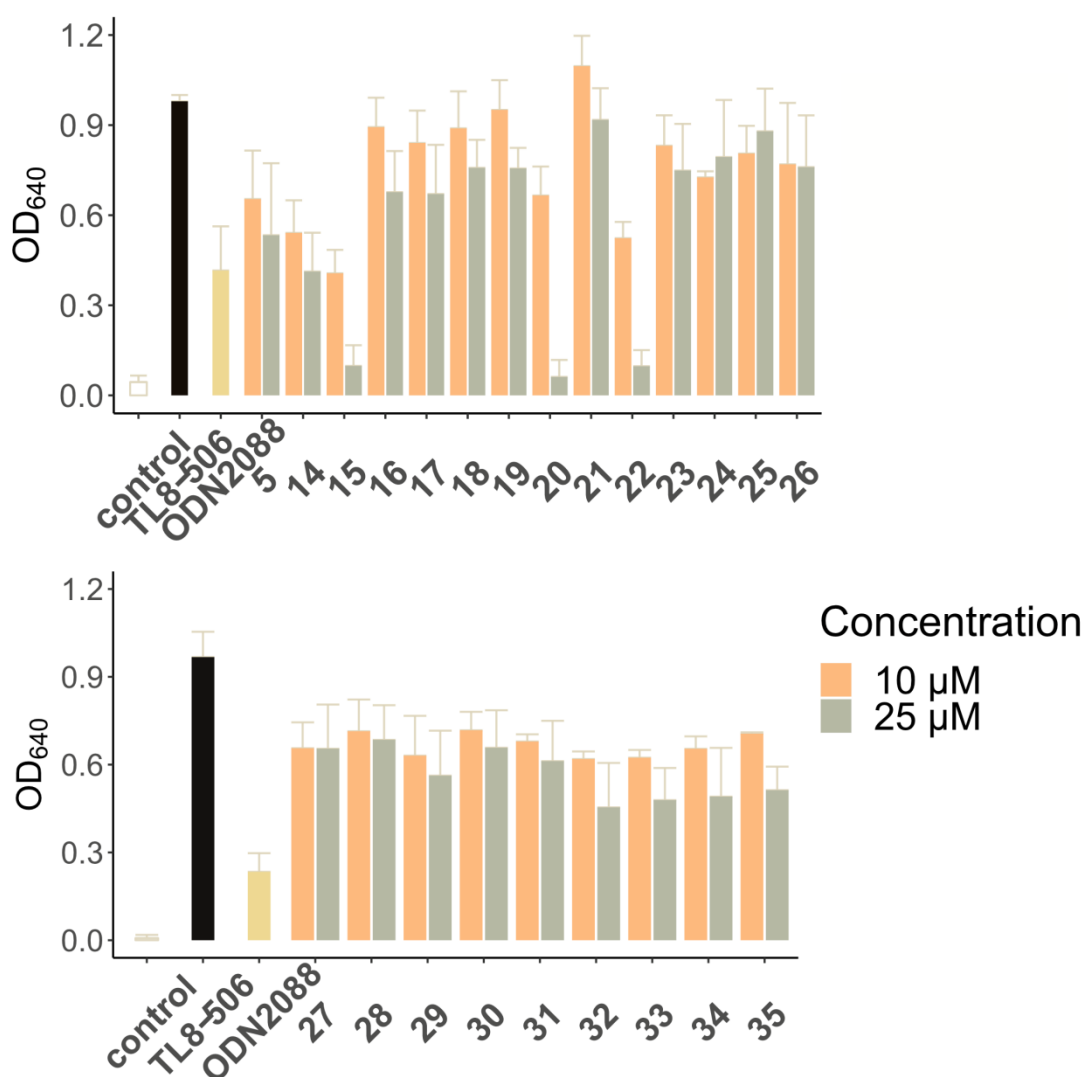


Figure 39. Inhibition of hTLR8-mediated NF- κ B/AP-1 activation of the synthesised analogues. HEK-Blue hTLR8 cells were preincubated with ODN2088 (1 μ M) or the compounds (10 and 25 μ M) for 1 h

Results

and afterwards stimulated with TL8-506 (0.6 μ M) for 24 h. Supernatants were analysed for TLR8-mediated NF- κ B/AP-1 activation by SEAP reporter assay using QuantiBlue (OD640). Mean \pm SD (n=3).

4.3.3 Prediction of the binding poses for the synthesised compounds

We wanted to study plausible binding mechanisms of the reported active compounds and explain observed differences in the synthesised compounds' activity. Using similar methodology as in the previous section (section 4.2.10), we first docked all synthesised compounds into the antagonistic binding site. In the next steps, we used MD simulations and subsequent dynophore analyses of the active compounds to study protein-ligand interaction patterns through time. All simulated protein-ligands complexes reached the RMSD plateau during the first few ns of 20 ns molecular dynamics simulation (Figure S 4).

Both replacements with methyl group and removal of the trifluoromethyl group diminished the activity of analogues **26** and **27**, which indicates the essential role of the group. Fluorine atoms could act as hydrogen bond acceptor to Ser352*. **15**, which shows the highest inhibitory activity in the series, exhibits the highly similar interaction pattern to the previously described **5**, **11** and **14** (section 4.2.10) (Figure 40 A). **15** lacks hydrophobic substituent in place of N-[(thiophene-2-yl)-methyl] moiety in **5**. Instead, the sulfonyl group in **15** can form hydrogen bonds with the surrounding Ans262* and Val520 throughout the trajectory (Figure 40B). The observed hydrogens bonds with Gly351* and Val520 in **15** are not stable as the hydrogen bonds in **5** and CU-CPT9b (sections 4.2.9 and 4.2.10), and occur through 18% and 21% of frames, respectively.

Results

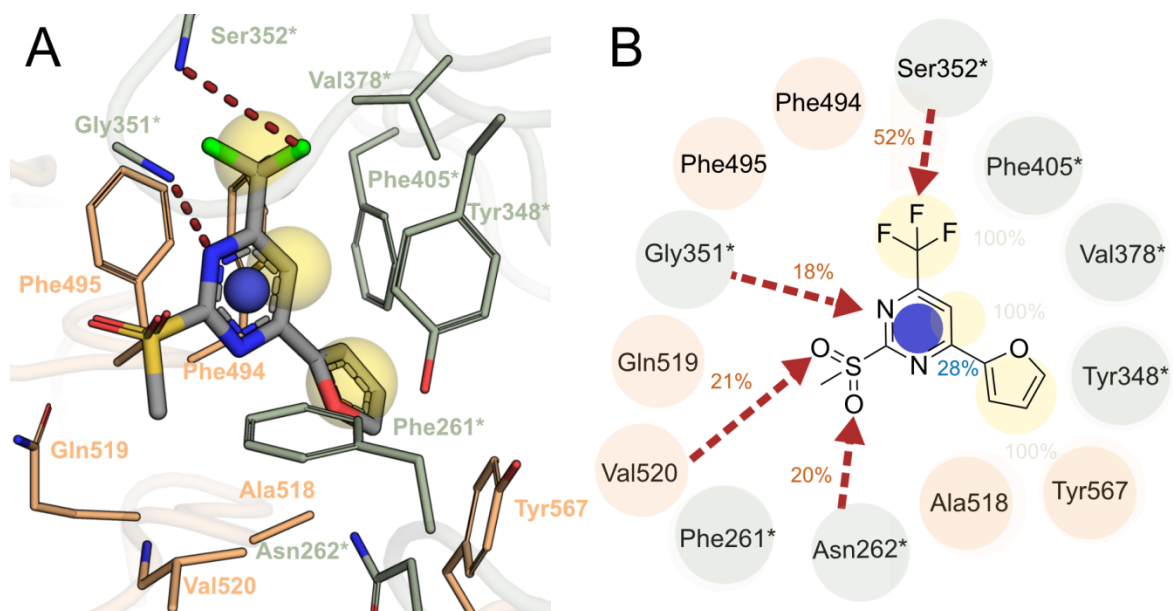


Figure 40. A predicted binding pose of **15** (grey sticks) with interacting TLR8 residues (orange and green sticks for each monomer) (PDB ID: 5WYZ) in 3D (A) and 2D representation with the frequency of the formed interactions during the molecular dynamics simulation (B). Hydrophobic and aromatic interactions are represented as yellow and blue spheres/circles. Hydrogen bond acceptor and donor interactions are represented as red and green arrows, respectively.

20 and **22**, which have a *N*-[(3-hydroxyphenyl)methyl] and *N*-[(4-hydroxyphenyl)methyl] on a place of *N*-[(thiophene-2-yl)-methyl moiety, also show potent inhibition on TLR8-mediated signalling (Figure 41A-C). In comparison, **16** lacks a hydroxyl group on the phenyl ring and does not significantly inhibit TLR8-mediated signalling (Figure 41 D). **20** and **22** exhibit additional hydrogen bonds between the hydroxyl group and Val520 and Ser522, explaining their higher inhibitory activity. However, the observed hydrogen bonds with Val520 are not as stable as those observed in CU-CPT9b (Figure 33). **32**, **33**, **34** and **35** have modest inhibitory activity. Their activity indicates the general preference of the ring systems over alkyl substituents on the position of *N*-[(thiophene-2-yl)-methyl moiety.

Results

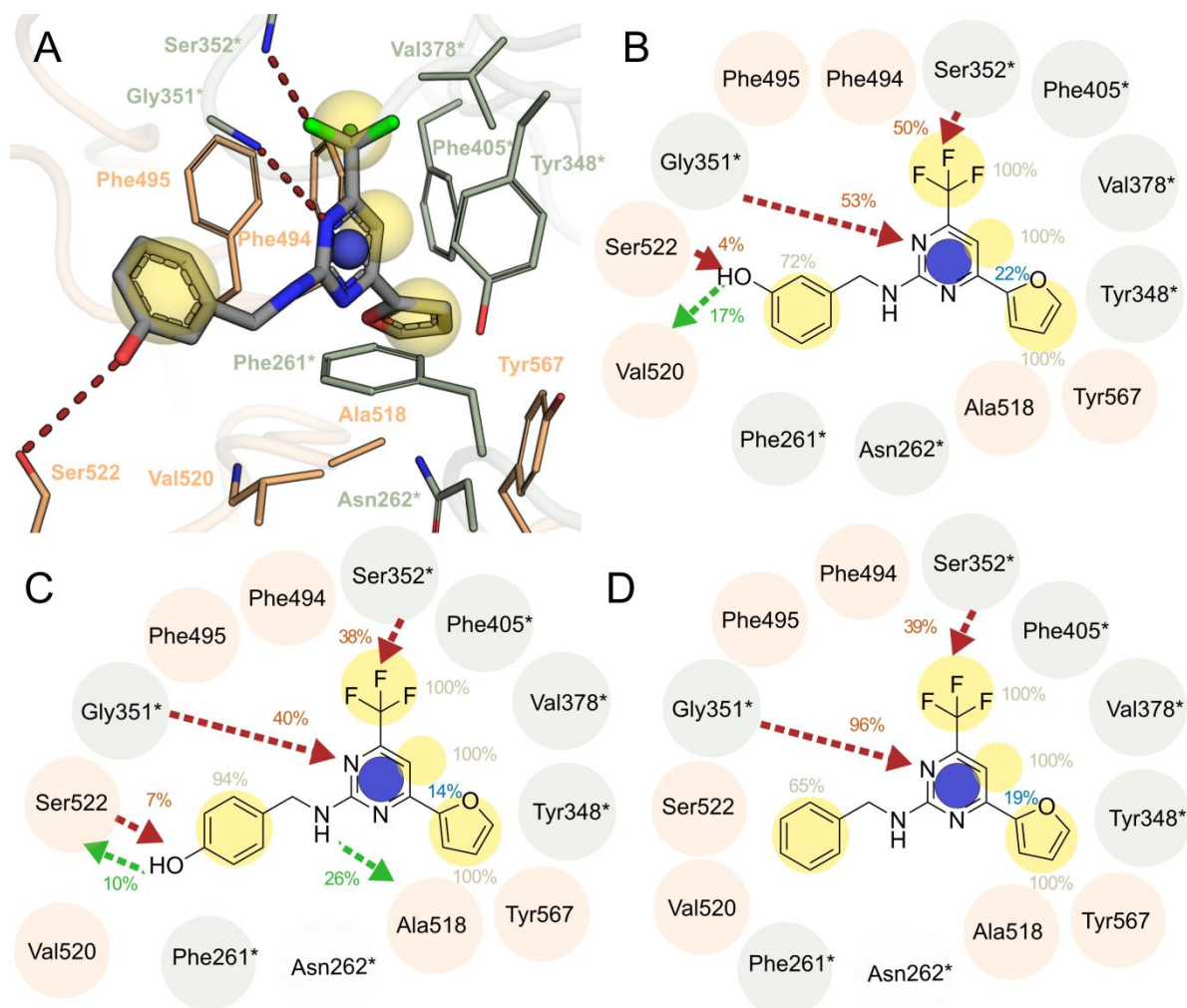


Figure 41. Predicted binding pose of **20** (grey sticks) with interacting TLR8 residues (orange and green sticks for each monomer) (PDB ID: 5WYZ) in 3D (A) and 2D representation with the frequency of the formed interactions during the molecular dynamics simulation for **20** (B), **22** (C) and **16** (D). Hydrophobic and aromatic interactions are represented as yellow and blue spheres/circles. Hydrogen bond acceptor and donor interactions are represented as red and green arrows, respectively.

5 Discussion

Throughout the project, we focused on the computer-aided development of novel modulators of Toll-like receptor 8 (TLR8). The previously solved crystal structures represent an excellent starting point to understand both activation and inhibition of the Toll-like receptor 8 by different ligands (section 5.1). The dimerisation interface between two monomers of TLR8 ectodomains is vital for the function of the receptor. Ligands binding leads to rearrangement of the dimerisation interface, which drives the large structural change that modulates the receptor. Therefore, we wanted to understand, how the dimerisation interface rearranges in the receptor's different forms. Next, we used the structural information, together with known ligands, to derive plausible binding patterns for the modulators of TLR8 (section 5.2). In this context, subtle differences in the agonist and antagonist structures and physicochemical properties are fascinating because they lead to opposite functional effects in the cells (section 5.3). We also discuss the experimental results for the tested compounds that partly confirm modelling hypotheses, but also contain new information for further development rounds (section 5.4). Finally, the compounds' optimisation has enabled an in-depth description of structure-activity relationship (SAR) and more precise elucidation of the binding mode (section 5.5), which is discussed in the final part of the chapter.

5.1 Overview of the structure of Toll-like receptor 8

TLR8 shows high structural similarity to TLR7 and TLR9 (section 4.1.3), which may be primarily attributed to the similar function that endosomal TLRs exhibit in recognition of nucleic acids [173-175]. Furthermore, we observed that the residues implicated in the interaction on the two TLR8 monomers' dimerisation interface are conserved across the three TLRs. The exception is the Z-loop region, whose sequence is diverse across the three receptors (section 4.1.3). Surprisingly, despite the high conservation of residue implicated in the dimerisation of TLR8 in TLR7 and TLR9, current evidence suggests that TLR7 and TLR9 form monomers in their inactive state [22, 176, 177]. Most notably, TLR7 and TLR9 presumably dimerise only after the binding of the ligand. How can we explain the observed difference in the dimerisation pattern between TLR8, and TLR7 and TLR9? The assumptions about the full-length receptors' dimerisation are based on the experimental data that includes only TLRs' ectodomains because structural information for any of the full-length TLRs is not

Discussion

available. However, membrane portions and TIR domains of the TLRs may also contribute to the dimerisation, and TLR7 and TLR9 may form pre-existing dimers in cells as well. For example, an earlier study of full-length TLR9 in cells suggested that TLR9 also forms inactive dimers in the absence of the bound nucleic acid [50].

Both TLR7 and TLR9 have the same conserved binding site on the dimerisation interface as TLR8. However, TLR7 and TLR9 primarily recognise guanosine and 5'-xCx DNA [178, 179]. Understanding the structural differences that affect the receptor selectivity towards specific ligands is necessary, because it may enable the fine-tuning of the receptor's selectivity towards ligands, and subsequent immune response modulation. Interestingly, guanosine in TLR7 and 5'-xCx motif in TLR9 in DNA occupy the same position as uridine in TLR8 [177, 179]. Both ligands interact with the residues analogous to Asp543 and Phe405* in TLR8, which underlines the functional importance of the residues for the receptors' activation. On the other hand, less conserved residues may be responsible for the selectivity for nucleosides and include Lys350*, Gly351*, Ser352*, Ile403*, Arg429*, Val520, Asp345 and Val573 [177, 179]. For example, the double mutation of Arg429Lys and Val573Ile lead to enhanced activation of the TLR8 by guanosine [180].

We also investigated different forms of TLR8. Monomers do not show substantial conformational differences (section 4.1.1). For example, only uridine-bound TLR8 shows an average difference of 1 Å to other agonist-bound activated forms, with the most significant difference near the ectodomain's C-terminal. Interestingly, although it is structurally similar to the activated forms of TLR8, the uridine-bound TLR8 does not activate the intracellular signalling pathways [31]. The conformational change near the C-terminal may affect membrane portions and TIR domains of the receptor, hindering the receptor's activation. However, a more plausible explanation is that conformational changes in Z-loop play an essential role in the receptor's function. Both allosteric and small-ligand binding sites are near the Z-loop; therefore, the binding of both types of ligands may affect the Z-loop's conformation. Unfortunately, Z-loop's role in the activation of the receptor upon ligand binding is currently unknown because the Z-loop does not show clear electron density in the solved crystal structures. The Z-loop region may contribute both to the already discussed differences in the dimerisation of TLR7, TLR8 and TLR9, and activation of the receptor upon the ligand binding.

Discussion

Both activation and inhibition of TLR8 are connected to the dimerisation interface changes (section 4.1.2). Binding of the antagonist, which stabilises the resting state, leads to an increase in hydrophobic contacts between the two monomers. Our observations are in line with the previous research, which has shown that homodimers manifest more hydrophobic interfaces than heterodimers [181-183]. The buriedness of hydrophobic patches results in higher entropy gain, thereby stabilising the resulting complex. On the other hand, the activated form of the TLR8 is characterised by the increased number of hydrogen bonds and salt-bridges between the two monomers. The interfaces that include transient protein-protein interactions are reported to involve more salt-bridges and hydrogen bonds [184]. Interestingly, loop regions of LRR8 and LRR18 contribute to the dimerisation in both active and inactive forms, which once more indicates their functional importance.

5.2 Computationally-assisted identification of novel Toll-like receptor 8 modulators

Traditionally, Toll-like receptors have been considered as “hard to drug” targets. Two major factors contribute to this opinion. First, natural ligands for the TLRs are various biopolymers (Table 1). Therefore, mimicking or disrupting the interactions between the receptor and the natural ligand by small molecules presents a challenging task. Second, as in TLR8, the binding site for ligands is located on the protein-protein interface (PPIs). The targeting of PPIs with small molecules is generally considered difficult [185]. Nonetheless, several small molecules that target TLR8 have been reported (section 1.6). The relatively large number of the ligands for TLR8 and TLR7, compared to other TLRs, can be accounted to the unconventional binding pocket for the small nucleosides on the dimerisation interface [22, 177]. The binding pocket represents a promising target binding site for small molecules in the ectodomain of TLR8. Small-molecule modulators offer several advantages over the oligonucleotide-based drugs: they have superior stability, lower molecular weight, oral administration, lower price, non-immunogenicity, and better accessibility to intracellular targets.

In addition to the ectodomains of TLR8, TIR domains may also be targeted by small molecules. For example, TAK-242 binds to the cytoplasmic TIR domain of TLR4 [186]. Targeting of evolutionarily conserved TIR domains may enable simultaneous modulation of

Discussion

the multiple receptor pathways. However, targeting of TIR domains has been underdeveloped compared to the targeting of the ectodomains of TLRs [186].

We are aware of two studies that previously used molecular modelling to design the novel ligands of TLR8. Deng and colleagues [187] employed 3D quantitative structure-activity relationship (QSAR), molecular docking and MD simulations on the small subset of the known agonists to study the features essential for the agonistic activity. The study does not include experimental validation of molecular modelling findings and includes three available chemotypes, focusing on furo[2,3-*c*]pyridines. Our study excluded furo[2,3-*c*]pyridine scaffold because the reliable binding to TLR8 has not been confirmed [94]. Therefore, it is hard to compare the results of the two studies. The second study by Pei and colleagues was a retrospective study to assess different pipelines for identification of TLR8 agonists. The best pipeline included structure-based pharmacophore-based screen, shape-based screen and molecular docking [188]. The derived structure-based pharmacophore is highly similar to the pharmacophore employed in our virtual screening campaign and includes aromatic feature, hydrogen bond donor feature and hydrophobic feature. However, Pei and colleagues included substantially smaller datasets for the generation and validation of the pharmacophore. Furthermore, although they provide valuable insight into different approaches for the modelling of TLR8 agonists, they do not provide experimental validation of their modelling results.

In our approach, we focused on the reported small-molecule agonist binding site in the activated receptor. We systematically derived a three-dimensional pharmacophore model to represent the interaction pattern of the synthetic small-molecule agonists. Natural agonist uridine binds to the same pocket, however, exhibits slightly different interaction patterns in the binding site than the reported synthetic agonists. Since the uridine binding alone is not sufficient to activate the receptor, and it requires binding of the additional allosteric oligonucleotides, we excluded uridine from the pharmacophore generation [31].

In addition to the binding poses from the crystal structures, we subsequently used the library of previously reported ligands to evaluate and further refine the pharmacophoric model. Previously reported ligands represent valuable information. However, the reported activity data from the literature should be considered with caution. The activity of most of the compounds has been assessed in cell-based assays. The main limitation of the cell-based assays is that the assessed activity does not entirely reflect the ligands' binding affinity to the receptor. Instead,

Discussion

it also includes additional factors such as metabolism of the compound and compound permeability in cells. In the case of endosomal TLRs, this means that some of the reported inactive compounds are simply not reaching the site of action in endosomes. Therefore, in our pharmacophore validation set, we included artificially generated decoys rather than reported inactive compounds.

Several reported active compounds show activity on several TLRs, which typically represents a red flag. For example, one of the compounds reported by Beesu and colleagues [98] has been rejected as a pan-TLR inhibitor after additional experiments that confirmed that the compound inhibits one of the downstream kinases. However, for most of the compounds from the literature, only activity against TLR8 was reported.

Finally, we cannot directly compare the activity values across different publications because they include different experimental conditions. Therefore, quantitative activity data cannot be used to assess the importance of specific pharmacophoric features. Rather, we relied on the extraction of the common features to the active ligands' set. The points discussed above lead to additional noise in the agonist data set and may reflect the ROC curve's underperformance in assessing the quality of the final pharmacophore.

Interestingly, we successfully identified compounds with a novel scaffold that inhibit TLR8 function, while starting with an agonist-bound TLR8 complex, discussed in more detail in the next section (section 5.3). This underlines a significant advantage of virtual screening: finding novel chemical entities for a specific target independent of their functionality. At the same time, this is a shortcoming since it is exceptionally challenging to specifically screen for a distinct functional outcome.

5.3 The paradigm of the agonist binding

The derived pharmacophore model for virtual screening partially reflects binding interactions for the later reported antagonists (sections 4.2.2 and 4.2.9) [49, 109]. The TLR8 agonists and antagonists share the binding site on one of the TLR8 monomers. While the antagonist's binding stabilises inactive conformation, the agonists' binding introduces a substantial movement of the monomers. For the agonists' binding, the starting inactive conformation and the final activated conformation are known. However, we still do not know how the agonists bind to the inactive TLR8 and how it introduces a conformational change to

Discussion

the observed active state. Interestingly, both antagonists in the stabilised inactive state and agonist in the receptor's activated state interact with the residues Phe346*, Tyr348*, Val378*, Ile403*, Tyr353* and Phe405* and Gly351* (sections 4.2.2, 4.2.9 and 4.2.10). In case of the binding of the antagonist, hydrophobic interactions between two monomers are undisturbed. The interactions include hydrophobic contacts between Phe494 and Phe495 on the first monomer and Tyr353*, Val378* and Phe405* on the second monomer. These residues are conserved across TLR8 and TLR7 (Figure S 1 and Figure S 2). Binding of the antagonists introduces a conformational change that enables additional hydrophobic interactions, e.g. between Phe346 and Phe348, and Tyr567* and Tyr568* (Table S 2), which may further contribute to the stabilisation of the inactive state.

We hypothesise that the agonists' binding disturbs the hydrophobic contacts between two chains in the binding site's proximity, leading to the chains' movement. Moreover, when looking at the physicochemical properties of the previously confirmed ligands, we notice the apparent difference in flexibility of the agonists and antagonists (Figure 22). This may reflect the fact that agonists may need to accommodate two different conformations upon the binding to the receptor: the initial conformation bound to the inactive receptor and subsequently the conformation in the activated receptor. Recently, Huang and colleagues identified key features for distinguishing the TLR8 agonists from antagonists using an emerging chemical pattern (ECP) [189, 190]. They concluded that the agonists have stronger specific hydrogen bond properties, while antagonists exhibit stronger non-specific hydrophobic properties. In the future, it may be possible to address the phenomenon using, e.g. cryogenic electron microscopy (cryo-EM). Cryo-EM has been used recently to elucidate the binding mechanism of TLR7 antagonists [191]. In the study, cryo-EM explained that the complex between TLR7 and antagonist in solution adopted both the inactive- and active conformation. Interestingly, TLR7 antagonists exhibited analogous interactions to the ones observed between TLR8 antagonists and receptor.

5.4 Pharmacological characterisation of the compounds

Many of the currently available immunomodulating drugs target cytokines and act in later inflammatory response stages [192]. In contrast, TLRs are central upstream mediators in the inflammatory responses and modulate pathway activation at an early point. In some pathological conditions, the aberrant recognition of TLRs' ligands may be the first step in initiating the disease [18]. Therefore, they are more likely to manipulate the immune system to reduce disease severity effectively.

We identified several compounds with the pyrimidine scaffold that showed potent concentration-dependent inhibition of hTLR8-dependent NF- κ B/AP-1 activation. Initial hit **5** is the most potent compound. **6** and **9** inhibit TLR8-mediated signalling in the primary screen; however, do not inhibit the signalling in the concentration-dependent manner. We hypothesised that **6** inhibits TLR8-mediated signalling at higher concentrations, while the observed activity of **9** in the primary screen may result from non-specific binding. **9** contains α -ketoamide that is able to covalently bind to serine or cysteine residues in proteins [193, 194], and therefore potentially result in off-target reactivity. Interestingly, **5** indicates only partial inhibition of hTLR8-dependent NF- κ B/AP-1 activation, compared to less potent, but fully inhibiting **11** and **14** (section 4.2.7). Partial inhibition may be an artefact of toxicity of **5** in higher concentration ranges. All three compounds exhibit selective inhibition of hTLR8-dependent NF- κ B/AP-1 activation over other TLRs. Although inhibition of multiple TLR-mediated pathways may provide an improved pharmacological profile, the selective inhibition of hTLR8-dependent NF- κ B/AP-1 was preferred in our case because it excluded non-specific binding or the interference with the assay. Selective inhibition of TLR8 without affecting TLR7 is still a challenge for small molecule drug development. TLR7 and TLR8 are structurally similar and recognise similar ligands, such as ssRNA, guanosine analogues, and nonselective imidazoquinoline agonists and inhibitors [22, 178]. Therefore, most of the reported potent TLR8 antagonists also inhibit TLR7 [195-198]. Currently, the most potent selective TLR8 antagonist inhibits the TLR8-mediated signalling in the picomolar range [109]. As already discussed in section 5.2, we cannot directly compare the activity data because of differences in the experimental conditions. However, we concluded that it might be possible to optimise the initial hit **5** by utilising additional interactions in the binding site. We went further intending to improve the potency and synthesised analogues of **5**. Results showed that several compounds show improved potency compared to **5**.

Discussion

We also assessed potency of **5**, **11**, and **14** by analysing the production of downstream molecules IL-8 and TNF- α (section 4.2.8). The analysis of the cytokines has the advantage that it can be easier correlated with the response in primary cells. **5**, **11**, and **14** reduced CL075-induced cytokine secretion to around half. Interestingly, the inhibition of IL-8 secretion was comparable to the reference ODN2088. On the other hand, ODN2088 reduced TNF- α much more dramatically than our compounds. The observed difference in inhibition of IL-8 and TNF- α secretion by ODN2088 and compounds could be attributed to the fact that CL075 activated both TLR7 and TLR8 but **5**, **11** and **14** only inhibited the TLR8 activation. TLR8 activation induces more pronounced IL-8 secretion than TLR7 activation, while TNF- α secretion is induced by both TLR7 and TLR8 [167, 199, 200].

5.5 Elucidation of the binding mode for antagonists

We proposed a plausible binding mode for the discovered pyrimidine compounds (sections 4.2.10 and 4.3.3). We used dynophores to study binding interactions through MD simulation. Dynophores enabled identifying the interactions that were not apparent from the static ligand conformations derived from molecular docking.

The hydrogen bond with Gly351* seems crucial for the binding of the identified antagonists and the previously reported antagonists from the literature [49, 109, 196-198, 201]. Interestingly, Gly351* is not evolutionary conserved, which is expected, since antagonists' binding is not under evolutionary pressure as the agonist binding. However, this enables easier selective targeting of TLR8 over other TLRs. Furthermore, generated docking poses of the pyrimidine compounds and previously reported crystal structures with TLR8 antagonists indicate the importance of the hydrophobic moiety surrounded by Phe494, Val378*, Tyr348*, Tyr567, Ala518 and the aromatic feature for the stacking with Phe495 and Tyr348*. Recently reported antagonist utilised salt bridges with Glu427* [196-198]. In contrast, we focused on the interactions with Ser522 and Val520.

6 Conclusion and outlook

Toll-like receptors (TLRs) play a pivotal role in innate immunity by recognising invading pathogens and host-derived danger signals and starting the inflammatory response. Consequently, altered TLR response contributes to the pathogenesis of a multitude of severe diseases. TLRs, therefore, represent attractive targets for novel therapeutic agents. In particular, TLR8 is a promising target for rational computer development of new drug candidates because its crystal structure is solved, and several modulators are known from high throughput screenings. TLR8 agonists show potential therapeutic applications in diseases like cancer, allergic rhinitis or as vaccine adjuvants. Unfortunately, many TLR8 agonists failed in clinical trials, mostly because of the receptor and tissue-specific immune responses. On the other hand, TLR8 antagonists could be beneficial in autoimmune diseases, e.g. systemic lupus and rheumatoid arthritis. Despite significant efforts being devoted to find a TLR8 antagonist, there are currently no clinically approved drugs.

In this specific PhD project, the main goal was to discover novel small molecule TLR8 modulators and understand their mechanism of action on the molecular level using computational approaches.

In the initial phase of the project, we studied relevant structural features in available crystal structures of TLR8. Although TLR8 has high structural similarity to closely related TLR7 and TLR9, it also exhibits some unique features such as dimerisation in the inactivated form and affinity to specific ligands. Furthermore, monomers in different forms of the receptor do not show substantial conformational differences. The most significant conformational differences are associated with the loop region in the dimerisation interface. Most notably, the binding of the ligands leads to rearrangement of the interface. The resulting rearrangement drives the large structural change that activates or inhibits the receptor. Furthermore, we have used available crystal structures of TLR8 ectodomains and available ligands to systematically develop structure-based 3D pharmacophores. The most promising pharmacophore model was employed in a virtual screening campaign, which allows for rational compound prioritisation for experimental testing. One of the nine experimentally tested compounds shows dose-dependent inhibitory activity on TLR8-signalling with an IC_{50} value in the low micromolar range. Therefore, the identified compound represents a promising lead compound. As a

Conclusion and outlook

subsequent step, a shape-based virtual screening was implemented to identify analogues of the initial hit. Two of five virtual hits showed inhibition of TLR8 signalling in a dose-dependent manner, comparable to the initial compound. Furthermore, the identified pyrimidine-based compounds selectively inhibit TLR8 response with potent reduction of IL-8 and TNF- α secretion in macrophages. All experimental data derived in collaboration with Maria Grabowski in the group of Prof. Weindl suggest that tested compounds bind exclusively to TLR8. Therefore, they represented a good starting point for further optimisation by directed synthesis. To understand the structure-activity relationship, we have used molecular docking and molecular dynamics simulations to investigate possible binding modes. We integrated the identified TLR8 antagonist from our study and the reported TLR8 antagonists from the literature to understand the structural features necessary for TLR8 antagonism. Finally, we incorporated the molecular modelling results to propose novel compounds for the synthesis with optimised binding interactions and improved activity.

Conclusively, we have identified novel and promising TLR8 antagonists in *silico* and confirmed biological activity, selectivity and low cytotoxicity in vitro. In this project, we successfully combined computational methods with pharmacological characterisation and organic synthesis.

We hope that results from a study on TLR8 will help us understand the means necessary for successful drug design of other TLR and facilitate the future design of small molecule TLR modulators.

7 Experimental section

7.1 Data collection and preparation

7.1.1 Ligand data

Structural and activity information on the reported TLR8 agonists and antagonists was gathered from the scientific publications [49, 96-99, 102-104, 106, 109, 160, 161, 165]. Simplified molecular-input line-entry system representations of molecules (SMILES) were extracted from the structural representation in MarvinSketch 5.8.0 (Chemaxon, Budapest, Hungary), and subsequently transformed into 3D representation in corina 3.0.0 (Molecular networks, Nürnberg, Germany).

7.1.2 Protein data

Published crystal structures of TLR8 ectodomains were retrieved from the Protein Data Bank (PDB) [202]. All water and sugar molecules were removed from the crystal structures in Molecular Operating Environment 2015.10 (MOE, Chemical Computing Group, Montreal, QC, Canada). Hydrogen atoms were added to the protein with pH = 5.5 and T=310 K using the MOE Protonate 3D module [203].

7.2 Analysis of the protein structure

Multiple sequence alignment for TLR8 from various species and human TLR3, TLR7, TLR9 were performed with a Clustal Omega (<https://www.ebi.ac.uk/Tools/msa/clustalo/>) [204]. The protein sequences were downloaded from UniProt (<https://www.uniprot.org/>) [205].

3D protein structures were superimposed and alpha carbon root-mean-square deviation (RMSD) was calculated using R (R: A language and environment for statistical computing, R Foundation for Statistical Computing, Vienna, Austria) package Bio3D [206, 207].

7.3 Analysis of the ligand properties

Molecular descriptors were calculated from the SMILES of the collected agonists and antagonists using RDKit (RDKit: Open-source cheminformatics; <http://www.rdkit.org>) in

Experimental section

Python 3.6. Analysed descriptors include molecular weight, SlogP, number of hydrogen bond donors, number of hydrogen bond acceptors, number of rings, number of rotatable bonds and topological polar surface area (TPSA). Calculated properties were analysed in Python 3.6.

7.4 Molecular docking for binding pose prediction

The crystal structure of TLR8 ectodomain with CL097 (PDB ID:3W3J) [22] was used for docking studies of the agonists. For studies on antagonists, the crystal structure of TLR8 ectodomain with CU-CPT9b (PDB ID:5WYZ) [49] was used.

Molecular docking of the ligands in the binding site was performed using the genetic algorithm (GA), which is implemented in GOLD 5.2 (Genetic Optimization for Ligand Docking, CCDC Software, Cambridge, UK) [116]. The binding site was composed of all amino acid residues in a protein that were within 6 Å of the bound ligand. All protein residues were kept rigid during the docking. The search efficiency of the genetic algorithm was set to default. Fifteen diverse poses were generated for each ligand and evaluated with GoldScore [116]. After the docking, generated docking poses were minimised using MMFF9453 force field implemented in LigandScout 4.09 (Inte:ligand, Vienna, Austria) [144, 208].

7.5 Three-dimensional pharmacophore modelling

First, DUD•E Decoys free online system [209] was used to generate decoy ligands from the previously collected TLR8 agonists. The library of the reported TLR8 agonists and decoy ligands was transformed into an appropriate multi-conformer library with idbgen (Inte:ligand, Vienna, Austria) and used afterwards as a validation set for the pharmacophore generation and refinement.

The structure-based pharmacophore model was generated from the small-molecule agonist bound crystal structure of TLR8 in LigandScout (PDB ID: 3W3J) [144, 208]. Additional exclusion volumes were added on binding site residues. The pharmacophore was further refined in the iterative fashion; feature tolerance spheres and exclusion volumes were adjusted in respect to the optimal discriminative ability of the pharmacophore, assessed as receiver operating characteristic curve (ROC).

7.6 Virtual screening workflow

Experimental section

Libraries of commercially available compounds were prepared before the virtual screening. First, molecular fragments and salts were removed using an in-house workflow implemented in KNIME (KNIME AG, Zurich, Switzerland). Next, molecules were protonated and standardised using ChemAxon Standardizer for structure canonicalisation and transformation (ChemAxon Ltd., Budapest, Hungary). Finally, a multi-conformer library was generated using the command-line tool idbgen (Inte:ligand, Vienna, Austria). The screened library consisted of 5 554 482 compounds from the following vendors: Asinex (Moscow, Russia), Chembridge (San Diego, CA, USA), ChemDiv (San Diego, CA, USA), KeyOrganics (Camelford, UK), LifeChemicals (Niagara on the Lake, ON, Canada), Maybridge (Waltham, MA, USA), Specs (Delft, Netherlands) and Vitas-M (Hong Kong, China). Virtual screening was conducted using the command-line tool iscreen (Inte:ligand, Vienna, Austria).

Virtual screening hits were docked into the crystal structure of the activated TLR8 (PDB ID:3W3J) in two rounds. In the first docking round, the docking algorithm was specified to find five poses per molecule with the search efficiency of virtual screening. The generated poses that fulfilled initial pharmacophore interactions the best, were filtered based on the calculated “unaligned pharmacophore score without exclusion volumes” in LigandScout. The threshold was set to 50. After that, selected molecules were docked using more efficient genetic algorithm options, as already described in the docking section. The best poses with the threshold for “unaligned pharmacophore score without exclusion volume” above 50, were selected. The poses further were energy minimised based on MMFF94 force field in LigandScout to eliminate steric clashes of the final selection of molecules. Remaining poses were visually examined and the best ones selected based on the observed interactions in the binding site. Prioritisation based on calculated Lipinski’s rule of five properties and number of rotatable bonds, structural novelty, structural diversity and commercial availability, led to the final selection of compounds for experimental testing.

7.7 Shape- and atom-based similarity search

The same commercial databases used for pharmacophore-based virtual screening were processed with the conformer generator OMEGA (Openeye, Santa Fe, USA) [210] with the flipper option set to True.

Experimental section

Low-energy conformer of compound **5** was used as a query for shape- and atom-based similarity search using rapid overlays of 3D chemical structures (ROCS, Openeye, Santa Fe, USA) [211]. Default options were used for query generation. The query was used for the screening of the database of commercially available compounds. 500 hits with the best score were retrieved from each database. The molecules with ShapeTanimoto above 0.70, ColorTanimoto above 0.6, and TanimotoCombo above 1.45 were kept.

7.8 Molecular dynamics simulations

Protein structures of the unliganded TLR8 (PDB ID: 3W3G), TLR8 with CL097 (PDB ID: 3W3J), TLR8 with CU-CPT9b (PDB ID: 5WYZ), and complexes of previously docked compounds of interest were used for molecular dynamics (MD) simulations. Crystal structures were preprocessed with Structure Preparation Module in Molecular Operating Environment 2015.10 (MOE, Chemical Computing Group, Montreal, QC, Canada) by adding missing atoms and capping the terminal residues and larger chain breaks. Afterwards, the structures were prepared for molecular dynamics simulation in Maestro (D. E. Shaw Research, New York, USA). The hydrogen-bonding network was optimised. The system was placed in a cubic box filled with SPC water [212]. Chloride ions were added to neutralise the charge of the system. The system was parameterised with the OPLS force field [213]. The default protocol for energy minimisation and consecutive short simulations were used to minimise and equilibrate the system, followed by 20 ns production simulation under constant temperature of 310 K and pressure of 1 bar. The system was simulated in triplicates with Desmond 2018-3 (D. E. Shaw Research, New York, USA) [141]. After the MD simulation, the trajectory was processed in VMD [214]. The protein was centred in the periodic boundary condition (PBC) box, and every frame of the trajectory was aligned to the first frame.

7.9 Analysis of protein dimerisation interface

Protein-protein interactions throughout a MD trajectory were analyzed with PyContact. PyContact screens MD trajectories for noncovalent interactions, also referred to as “contacts,” based on interatomic distances, geometries, and the type of molecules involved [215]. The trajectory was first transformed into a suitable format for PyContact using library MDAnalysis in Python 2.7 [216]. The chain IDs, which were lost after the MD simulation, were added. Additionally, water molecules were removed from the system. For PyContact, the maximal

Experimental section

atom-atom distance for contact scoring was set to 5 Å, cut-off angle for hydrogen bonds was set to 120°, and distance cut-off between the hydrogen bond acceptor and the hydrogen atom was set to 3.5 Å. Only contacts which occur in all three replicates in more than 30% trajectory frames were kept.

7.10 Dynophore analysis

Throughout complete MD trajectory, protein-ligand interactions were analysed using dynamic three-dimensional feature-based interaction patterns, a novel MD analysis approach termed dynophores [153-155]. Dynophores were analysed in triplicates. For the specific interaction occurrences, the mean value from triplicates was calculated.

7.11 Experimental methods

The project's experimental part was conducted in collaboration with researchers from the Freie University Berlin, Germany and University of Ljubljana, Slovenia. Dora Šribar assessed the purity of the commercial compounds. Dr. Maria Grabowski conducted the pharmacological characterisation under Prof. Dr. Günther Weindl (Freie University Berlin/University of Bonn). Ana Dolšak performed the organic synthesis under the coordination of Dr. Matej Sova (University of Ljubljana). Since collaborators mainly did pharmacological characterisation and organic synthesis, only general procedures are described in the following section. For more specific information, please refer to Šribar and colleagues [169].

7.11.1 The purity of commercial compounds

The compounds from the virtual screening campaigns were ordered from Vitas-M Laboratory (Hong Kong, China); **1**: STK387502; **2**: STL482042; **3**: STK059773; **4**: STK387443; **5**: STK341649; **6**: STK209079; **7**: STK657805; **8**: STL309252; **9**: STK710838; **10**: STL180818; **11**: STL180707; **12**: STL412660; **13**: STK711655, and from ChemDiv (San Diego, USA); **14**: C130-0049. Prior to the further experimental characterization, compound purity was assessed with High Performance Liquid Chromatography (HPLC).

Samples were prepared by dissolving small amounts (<1mg) of the compound in pure methanol. The compounds' purity was determined with an Agilent (Santa Clara, USA) 1100

Experimental section

HPLC system using RP18 column and 100 % methanol as a fluxing agent. The flowrate was set to 0,9ml/min.

7.11.2 Pharmacological characterisation

Compounds were pharmacologically characterised in human embryonic kidney (HEK) cell line overexpressing either hTLR8 or hTLR7 (InvivoGen, Toulouse, France), and THP-1 cell line (DSMZ, Braunschweig, Germany). To determine agonistic effects of the compound of interest, the hTLR8 HEK cells were incubated with the compound. Stimulation of hTLR8 reporter cells with TLR8 agonists activates nuclear factor kappa-light-chain-enhancer of activated B cells (NF- κ B). Activation of NF- κ B results in secreted embryonic alkaline phosphatase (SEAP) production determined with the colourimetric substrate QuantiBlue by reading the optical density (OD). For the inhibitory studies, hTLR8 cells were first preincubated with the compound of interest or ODN2088 and afterwards incubated with the respective TLR agonist. Besides, to analyse the concentration-response curves and obtain IC₅₀ values, nonlinear regression with variable slope (four parameters) was used. THP-1 and hTLR7 cells were first preincubated with the compound of interest to assess the compounds' selectivity and, afterwards, incubated with the agonist for the respective TLR. To quantify cytokines, cell culture supernatants from pre-incubated THP-1 cells were collected, and amounts of IL-8 and TNF- α were measured with the commercially available ELISA kits (ELISA-Ready Set Go; Thermo Fisher Scientific, Waltham, United States).

Cell viability was analysed by MTT assay in HEK and THP-1 cells. 10% (v/v) DMSO was used as toxic control, and the viability of the unstimulated cells (vehicle control) was set at 100%.

7.11.3 General synthetic procedure

A focused library of analogues of the hit compound **5** was prepared. Two different synthetic routes implemented changes in the primary scaffold.

In the first route, trifluoromethyl- β -diketones were prepared by Claisen condensation from aryl/alkyl methyl ketones and ethyl trifluoromethylacetate. The cyclisation of trifluoromethyl- β -diketones and S-methylisothiourea hemisulfate in glacial acetic acid led to methylthio-(trifluoromethyl)pyrimidine scaffold. Next, oxidation of methylthio-(trifluoromethyl)pyrimidine to methyl sulfone was accomplished with the addition of Oxone®.

Experimental section

In the last step, the nucleophilic substitution of methyl sulfone with primary/secondary amine was performed to obtain the final compounds.

In the second route, substituents were introduced by Suzuki coupling and subsequent nucleophilic aromatic substitution, respectively, to yield the final compounds.

8 Summary

Toll-like receptors (TLRs) play a central role in innate immunity by recognising invading pathogens and host-derived danger signals and initiating the inflammatory response. Aberrant TLR response is involved in the pathogenesis of cancers, infections, autoimmune disorders and allergic diseases. Therefore, TLRs represent attractive targets for novel therapeutic agents.

The PhD project's main research aim is to discover novel small molecule modulators of Toll-like receptor 8 (TLR8) and understand their mechanisms of action using computational approaches. TLR8 crystal structure is solved, and several modulators are known from previous drug screens. Therefore, TLR8 is a promising target for rational computer-aided development of novel drug candidates.

In the initial phase of the project, the main goal was to study relevant structural features in available crystal structures of TLR8. The focus was on the dimerisation interface because of its role in the binding of ligands and subsequent activation of the receptor. Additionally, we studied the conservation of the relevant structural features across the closely related TLRs. The second part shifts the focus to the binding of the small molecules to TLR8. We investigated interactions between the known ligands and TLR8 and used it to develop the most plausible 3D pharmacophore model. Subsequently, we employed the developed 3D pharmacophore model in virtual screening to identify novel modulators of TLR8. We identified a pyrimidine-based compound that inhibits TLR8-mediated signalling in the micromolar concentration range. The potent anti-inflammatory and dose-dependent response has been confirmed in a series of derivatives of this initial virtual hit, which allowed for a detailed elucidation of structure-activity relationships (SAR) and more precise description of the binding mode.

Conclusively, we have developed a novel and promising pyrimidine-based TLR8 inhibitors *in silico* and confirmed their biological activity, selectivity and low cytotoxicity *in vitro*. Results from the study on TLR8 represent a solid basis for the future design of small molecule TLR modulators as novel therapeutic agents for modulating immune response and inflammation.

9 Zusammenfassung

Toll-like Rezeptoren (TLRs) spielen eine zentrale Rolle in angeborenem Immunsystem, indem sie eindringende Pathogene sowie endogene Gefahrensignale erkennen und Entzündungsreaktionen einleiten. TLRs sind an der Pathogenese von Krebserkrankungen, Infektionen, Autoimmunerkrankungen und allergischen Erkrankungen beteiligt. Aus diesem Grund stellen TLRs attraktive Ziele für neue, niedermolekulare Wirkstoffe dar.

Das Hauptziel dieses Promotionsprojekts ist die Entdeckung neuer niedermolekularer Modulatoren des Toll-like-Rezeptors 8 (TLR8) und das Verständnis ihrer Wirkmechanismen mit Hilfe computergestützter Ansätze. Die Kristallstruktur von TLR8 ist verfügbar und mehrere Modulatoren sind aus früheren Wirkstoffscreens bekannt. Daher ist TLR8 ein vielversprechendes Ziel für die rationale computergestützte Entwicklung neuer Wirkstoffkandidaten.

Am Beginn des Projekts bestand das Hauptziel darin, relevante strukturelle Merkmale in den verfügbaren Kristallstrukturen von TLR8 zu untersuchen. Der Fokus lag dabei auf dem Dimerisierungsbereich, da dieser eine wichtige Rolle bei der Bindung von Liganden und der anschließenden Aktivierung des Rezeptors spielt. Zusätzlich untersuchten wir die Konservierung der relevanten Strukturmerkmale über die eng verwandten TLRs hinweg. Der zweite Teil verlagert den Fokus auf die Bindung kleiner Moleküle an TLR8. Wir untersuchten die Interaktionen zwischen den bekannten Liganden und TLR8 und entwickelten daraus systemtisch ein 3D-Pharmakophormodell. Anschließend setzten wir das entwickelte 3D-Pharmakophormodell im virtuellen Screening ein, um neuartige Modulatoren des TLR8 zu identifizieren. Wir identifizierten ein Pyrimidin-Analogon, das die TLR8-vermittelte Signalweiterleitung im mikromolaren Konzentrationsbereich hemmt. Die potente entzündungshemmende und dosisabhängige Wirkung wurde in einer kleinen Serie von Analoga bestätigt. Schließlich optimierten wir die identifizierten Pyrimidinverbindungen weiter, was eine detailliertere Struktur-Aktivitäts-Analyse und eine genauere Aufklärung des Bindungsmodus ermöglichte.

Zusammenfassend haben wir neuartige und vielversprechende TLR8-Inhibitoren auf Pyrimidinbasis *in silico* entwickelt und ihre *in vitro* biologische Aktivität, Selektivität und geringe Zytotoxizität bestätigt. Die Ergebnisse der Studie zu TLR8 helfen uns, die Prozesse zu

Zusammenfassung

verstehen, die für ein erfolgreiches Wirkstoffdesign auch bei anderen TLR notwendig sind und stellen eine gute Ausgangsbasis dar, um in Zukunft optimierte, niedermolekulare TLR-Modulatoren zu entwickeln und damit Entzündung und die Immunreaktion effizient zu modulieren.

10 List of publications

10.1 Publications

D. Šribar, M. Grabowski, M.S. Murgueitio, M. Bermudez, G. Weindl, G. Wolber, Identification and characterization of a novel chemotype for human TLR8 inhibitors, *Eur J Med Chem*, 179 (2019) 744-752

D. Schaller, D. Šribar, T. Noonan, L. Deng, T.N. Nguyen, S. Pach, D. Machalz, M. Bermudez, G. Wolber, Next generation 3D pharmacophore modeling, *WIREs Comput Mol Sci*, 10 (2020)

M. Grabowski, M. Bermudez, T. Rudolf, D. Šribar, P. Varga, M.S. Murgueitio, G. Wolber, J. Rademann, G. Weindl, Identification and validation of a novel dual small-molecule TLR2/8 antagonist, *Biochem Pharmacol*, 177 (2020) 113957

C. Omieczynski, T.N. Nguyen, D. Šribar, L. Deng, D. Stepanov, D. Schaller, G. Wolber, M. Bermudez, BiasDB: A Comprehensive Database for Biased GPCR Ligands, *bioRxiv*

10.2 Conference posters

D. Šribar, M. Grabowski, M.S. Murgueitio, M. Bermudez, G. Weindl, G. Wolber, Tailoring Toll-like receptor 8 ligands for balancing immune response and inflammation, *EUROPIN Summer School Drug Design 2017*, September 17-22, 2017, Vienna, Austria

D. Šribar, M. Grabowski, M.S. Murgueitio, M. Bermudez, G. Weindl, G. Wolber, Tailoring Toll-like receptor 8 ligands for balancing immune response and inflammation, *Learning from the Yins and Yangs in Cancer*, May 24-25, 2019, Berlin, Germany

D. Šribar, M. Grabowski, M.S. Murgueitio, M. Bermudez, G. Weindl, G. Wolber, Tailoring Toll-like receptor 8 ligands for balancing immune response and inflammation, *Tag der Pharmazie*, July 6th, 2018, Berlin, Germany

D. Šribar, M. Grabowski, M.S. Murgueitio, M. Bermudez, G. Weindl, G. Wolber, Rational design of novel Toll-like receptor 8 ligands, *EFMC International Symposium on Advances in Synthetic and Medicinal Chemistry*, September 1-5, 2019, Athens, Greece

11 Bibliography

- [1] J.A. Hoffmann, F.C. Kafatos, C.A. Janeway, R.A. Ezekowitz, Phylogenetic perspectives in innate immunity, *Science*, 284 (1999) 1313-1318, doi:10.1126/science.284.5418.1313.
- [2] R. Medzhitov, C.A. Janeway, Innate Immunity: The Virtues of a Nonclonal System of Recognition, *Cell*, 91 (1997) 295-298, doi:10.1016/s0092-8674(00)80412-2.
- [3] G.P. Amarante-Mendes, S. Adjemian, L.M. Branco, L.C. Zanetti, R. Weinlich, K.R. Bortoluci, Pattern Recognition Receptors and the Host Cell Death Molecular Machinery, *Front Immunol*, 9 (2018) 2379, doi:10.3389/fimmu.2018.02379.
- [4] P. Matzinger, Tolerance, danger, and the extended family, *Annu Rev Immunol*, 12 (1994) 991-1045, doi:10.1146/annurev.iy.12.040194.005015.
- [5] T. Kawai, S. Akira, The role of pattern-recognition receptors in innate immunity: update on Toll-like receptors, *Nat Immunol*, 11 (2010) 373-384, doi:10.1038/ni.1863.
- [6] R. Medzhitov, C.A. Janeway, Jr., Innate immunity: impact on the adaptive immune response, *Curr Opin Immunol*, 9 (1997) 4-9, doi:10.1016/s0952-7915(97)80152-5.
- [7] T.H. Mogensen, Pathogen recognition and inflammatory signaling in innate immune defenses, *Clin Microbiol Rev*, 22 (2009) 240-273, doi:10.1128/CMR.00046-08.
- [8] S. Akira, K. Takeda, Toll-like receptor signalling, *Nat Rev Immunol*, 4 (2004) 499-511, doi:10.1038/nri1391.
- [9] K. Takeda, S. Akira, Toll-like receptors, *Curr Protoc Immunol*, 109 (2015) 14 12 11-14 12 10, doi:10.1002/0471142735.im1412s109.
- [10] T. Kawasaki, T. Kawai, Toll-like receptor signaling pathways, *Front Immunol*, 5 (2014) 461, doi:10.3389/fimmu.2014.00461.
- [11] M.P. Schon, M. Schon, TLR7 and TLR8 as targets in cancer therapy, *Oncogene*, 27 (2008) 190-199, doi:10.1038/sj.onc.1210913.
- [12] T. Kawai, S. Akira, Innate immune recognition of viral infection, *Nat Immunol*, 7 (2006) 131-137, doi:10.1038/ni1303.
- [13] M. Farrugia, B. Baron, The Role of Toll-Like Receptors in Autoimmune Diseases through Failure of the Self-Recognition Mechanism, *Int J Inflam*, 2017 (2017) 8391230, doi:10.1155/2017/8391230.
- [14] D.N. Cook, D.S. Pisetsky, D.A. Schwartz, Toll-like receptors in the pathogenesis of human disease, *Nat Immunol*, 5 (2004) 975-979, doi:10.1038/ni1116.
- [15] S.C. Gangloff, M. Guenounou, Toll-like receptors and immune response in allergic disease, *Clin Rev Allergy Immunol*, 26 (2004) 115-125, doi:10.1007/s12016-004-0006-0.
- [16] A. Savva, T. Roger, Targeting toll-like receptors: promising therapeutic strategies for the management of sepsis-associated pathology and infectious diseases, *Front Immunol*, 4 (2013) 387, doi:10.3389/fimmu.2013.00387.
- [17] E.J. Hennessy, A.E. Parker, L.A. O'Neill, Targeting Toll-like receptors: emerging therapeutics?, *Nat Rev Drug Discov*, 9 (2010) 293-307, doi:10.1038/nrd3203.

Bibliography

- [18] L.A. O'Neill, C.E. Bryant, S.L. Doyle, Therapeutic targeting of Toll-like receptors for infectious and inflammatory diseases and cancer, *Pharmacol Rev*, 61 (2009) 177-197, doi:10.1124/pr.109.001073.
- [19] H. Hemmi, T. Kaisho, O. Takeuchi, S. Sato, H. Sanjo, K. Hoshino, T. Horiuchi, H. Tomizawa, K. Takeda, S. Akira, Small anti-viral compounds activate immune cells via the TLR7 MyD88-dependent signaling pathway, *Nat Immunol*, 3 (2002) 196-200, doi:10.1038/ni758.
- [20] J.R. Baldrige, R.T. Crane, Monophosphoryl lipid A (MPL) formulations for the next generation of vaccines, *Methods*, 19 (1999) 103-107, doi:10.1006/meth.1999.0834.
- [21] R. Brunner, E. Jensen-Jarolim, I. Pali-Scholl, The ABC of clinical and experimental adjuvants--a brief overview, *Immunol Lett*, 128 (2010) 29-35, doi:10.1016/j.imlet.2009.10.005.
- [22] H. Tanji, U. Ohto, T. Shibata, K. Miyake, T. Shimizu, Structural reorganization of the Toll-like receptor 8 dimer induced by agonistic ligands, *Science*, 339 (2013) 1426-1429, doi:10.1126/science.1229159.
- [23] J.L. Cervantes, C.J. La Vake, B. Weinerman, S. Luu, C. O'Connell, P.H. Verardi, J.C. Salazar, Human TLR8 is activated upon recognition of *Borrelia burgdorferi* RNA in the phagosome of human monocytes, *J Leukoc Biol*, 94 (2013) 1231-1241, doi:10.1189/jlb.0413206.
- [24] S.H. Moen, B. Ehrnstrom, J.F. Kojen, M. Yurchenko, K.S. Beckwith, J.E. Afset, J.K. Damas, Z. Hu, H. Yin, T. Espevik, J. Stenvik, Human Toll-like Receptor 8 (TLR8) Is an Important Sensor of Pyogenic Bacteria, and Is Attenuated by Cell Surface TLR Signaling, *Front Immunol*, 10 (2019) 1209, doi:10.3389/fimmu.2019.01209.
- [25] A.L. Blasius, B. Beutler, Intracellular toll-like receptors, *Immunity*, 32 (2010) 305-315, doi:10.1016/j.immuni.2010.03.012.
- [26] P. Ranganathan, A. Ngankeu, N.C. Zitzer, P. Leoncini, X. Yu, L. Casadei, K. Challagundla, D.K. Reichenbach, S. Garman, A.S. Ruppert, S. Volinia, J. Hofstetter, Y.A. Efebera, S.M. Devine, B.R. Blazar, M. Fabbri, R. Garzon, Serum miR-29a Is Upregulated in Acute Graft-versus-Host Disease and Activates Dendritic Cells through TLR Binding, *J Immunol*, 198 (2017) 2500-2512, doi:10.4049/jimmunol.1601778.
- [27] F.J. Barrat, T. Meeker, J. Gregorio, J.H. Chan, S. Uematsu, S. Akira, B. Chang, O. Duramad, R.L. Coffman, Nucleic acids of mammalian origin can act as endogenous ligands for Toll-like receptors and may promote systemic lupus erythematosus, *J Exp Med*, 202 (2005) 1131-1139, doi:10.1084/jem.20050914.
- [28] M. Sioud, Single-stranded small interfering RNA are more immunostimulatory than their double-stranded counterparts: a central role for 2'-hydroxyl uridines in immune responses, *Eur J Immunol*, 36 (2006) 1222-1230, doi:10.1002/eji.200535708.
- [29] J.T. Marques, B.R. Williams, Activation of the mammalian immune system by siRNAs, *Nat Biotechnol*, 23 (2005) 1399-1405, doi:10.1038/nbt1161.
- [30] M. Sioud, Induction of inflammatory cytokines and interferon responses by double-stranded and single-stranded siRNAs is sequence-dependent and requires endosomal localization, *J Mol Biol*, 348 (2005) 1079-1090, doi:10.1016/j.jmb.2005.03.013.
- [31] H. Tanji, U. Ohto, T. Shibata, M. Taoka, Y. Yamauchi, T. Isobe, K. Miyake, T. Shimizu, Toll-like receptor 8 senses degradation products of single-stranded RNA, *Nat Struct Mol Biol*, 22 (2015) 109-115, doi:10.1038/nsmb.2943.

Bibliography

- [32] D. Ganguly, G. Chamilos, R. Lande, J. Gregorio, S. Meller, V. Facchinetti, B. Homey, F.J. Barrat, T. Zal, M. Gilliet, Self-RNA-antimicrobial peptide complexes activate human dendritic cells through TLR7 and TLR8, *J Exp Med*, 206 (2009) 1983-1994, doi:10.1084/jem.20090480.
- [33] T.H. Chuang, R.J. Ulevitch, Cloning and characterization of a sub-family of human toll-like receptors: hTLR7, hTLR8 and hTLR9, *Eur Cytokine Netw*, 11 (2000) 372-378.
- [34] X. Du, A. Poltorak, Y. Wei, B. Beutler, Three novel mammalian toll-like receptors: gene structure, expression, and evolution, *Eur Cytokine Netw*, 11 (2000) 362-371.
- [35] B.R. Umiker, S. Andersson, L. Fernandez, P. Korgaokar, A. Larbi, M. Pilichowska, C.C. Weinkauf, H.H. Wortis, J.F. Kearney, T. Imanishi-Kari, Dosage of X-linked Toll-like receptor 8 determines gender differences in the development of systemic lupus erythematosus, *Eur J Immunol*, 44 (2014) 1503-1516, doi:10.1002/eji.201344283.
- [36] G. McDonald, N. Cabal, A. Vannier, B. Umiker, R.H. Yin, A.V. Orjalo, Jr., H.E. Johansson, J.H. Han, T. Imanishi-Kari, Female Bias in Systemic Lupus Erythematosus is Associated with the Differential Expression of X-Linked Toll-Like Receptor 8, *Front Immunol*, 6 (2015) 457, doi:10.3389/fimmu.2015.00457.
- [37] N.G. de Groot, R.E. Bontrop, COVID-19 pandemic: is a gender-defined dosage effect responsible for the high mortality rate among males?, *Immunogenetics*, 72 (2020) 275-277, doi:10.1007/s00251-020-01165-7.
- [38] T. Umehara, N. Tsujita, M. Shimada, Activation of Toll-like receptor 7/8 encoded by the X chromosome alters sperm motility and provides a novel simple technology for sexing sperm, *PLoS Biol*, 17 (2019) e3000398, doi:10.1371/journal.pbio.3000398.
- [39] V. Hornung, S. Rothenfusser, S. Britsch, A. Krug, B. Jahrsdorfer, T. Giese, S. Endres, G. Hartmann, Quantitative expression of toll-like receptor 1-10 mRNA in cellular subsets of human peripheral blood mononuclear cells and sensitivity to CpG oligodeoxynucleotides, *J Immunol*, 168 (2002) 4531-4537, doi:10.4049/jimmunol.168.9.4531.
- [40] L. Alexopoulou, B. Desnues, O. Demaria, [Toll-like receptor 8: the awkward TLR], *Med Sci (Paris)*, 28 (2012) 96-102, doi:10.1051/medsci/2012281023.
- [41] M.G. Netea, C. van der Graaf, J.W. Van der Meer, B.J. Kullberg, Toll-like receptors and the host defense against microbial pathogens: bringing specificity to the innate-immune system, *J Leukoc Biol*, 75 (2004) 749-755, doi:10.1189/jlb.1103543.
- [42] A. Iwasaki, R. Medzhitov, Regulation of adaptive immunity by the innate immune system, *Science*, 327 (2010) 291-295, doi:10.1126/science.1183021.
- [43] G. Peng, Z. Guo, Y. Kiniwa, K.S. Voo, W. Peng, T. Fu, D.Y. Wang, Y. Li, H.Y. Wang, R.F. Wang, Toll-like receptor 8-mediated reversal of CD4+ regulatory T cell function, *Science*, 309 (2005) 1380-1384, doi:10.1126/science.1113401.
- [44] J. Lee, Y. Tian, S.T. Chan, J.Y. Kim, C. Cho, J.H. Ou, TNF-alpha Induced by Hepatitis C Virus via TLR7 and TLR8 in Hepatocytes Supports Interferon Signaling via an Autocrine Mechanism, *PLoS Pathog*, 11 (2015) e1004937, doi:10.1371/journal.ppat.1004937.
- [45] Y. Ma, J. Li, I. Chiu, Y. Wang, J.A. Sloane, J. Lu, B. Kosaras, R.L. Sidman, J.J. Volpe, T. Vartanian, Toll-like receptor 8 functions as a negative regulator of neurite outgrowth and inducer of neuronal apoptosis, *J Cell Biol*, 175 (2006) 209-215, doi:10.1083/jcb.200606016.
- [46] J.K. Bell, G.E.D. Mullen, C.A. Leifer, A. Mazzoni, D.R. Davies, D.M. Segal, Leucine-rich repeats and pathogen recognition in Toll-like receptors, *Trends Immunol*, 24 (2003) 528-533, doi:10.1016/s1471-4906(03)00242-4.

Bibliography

- [47] H. Tanji, U. Ohto, Y. Motoi, T. Shibata, K. Miyake, T. Shimizu, Autoinhibition and relief mechanism by the proteolytic processing of Toll-like receptor 8, *Proc Natl Acad Sci U S A*, 113 (2016) 3012-3017, doi:10.1073/pnas.1516000113.
- [48] W. Greulich, M. Wagner, M.M. Gaidt, C. Stafford, Y. Cheng, A. Linder, T. Carell, V. Hornung, TLR8 Is a Sensor of RNase T2 Degradation Products, *Cell*, 179 (2019) 1264-1275 e1213, doi:10.1016/j.cell.2019.11.001.
- [49] S. Zhang, Z. Hu, H. Tanji, S. Jiang, N. Das, J. Li, K. Sakaniwa, J. Jin, Y. Bian, U. Ohto, T. Shimizu, H. Yin, Small-molecule inhibition of TLR8 through stabilization of its resting state, *Nat Chem Biol*, 14 (2018) 58-64, doi:10.1038/nchembio.2518.
- [50] E. Latz, A. Verma, A. Visintin, M. Gong, C.M. Sirois, D.C. Klein, B.G. Monks, C.J. McKnight, M.S. Lamphier, W.P. Duprex, T. Espevik, D.T. Golenbock, Ligand-induced conformational changes allosterically activate Toll-like receptor 9, *Nat Immunol*, 8 (2007) 772-779, doi:10.1038/ni1479.
- [51] S. Janssens, R. Beyaert, Functional diversity and regulation of different interleukin-1 receptor-associated kinase (IRAK) family members, *Mol Cell*, 11 (2003) 293-302, doi:10.1016/s1097-2765(03)00053-4.
- [52] N. Suzuki, S. Suzuki, G.S. Duncan, D.G. Millar, T. Wada, C. Mirtsos, H. Takada, A. Wakeham, A. Itie, S. Li, J.M. Penninger, H. Wesche, P.S. Ohashi, T.W. Mak, W.C. Yeh, Severe impairment of interleukin-1 and Toll-like receptor signalling in mice lacking IRAK-4, *Nature*, 416 (2002) 750-756, doi:10.1038/nature736.
- [53] S.C. Lin, Y.C. Lo, H. Wu, Helical assembly in the MyD88-IRAK4-IRAK2 complex in TLR/IL-1R signalling, *Nature*, 465 (2010) 885-890, doi:10.1038/nature09121.
- [54] J.H. Shim, C. Xiao, A.E. Paschal, S.T. Bailey, P. Rao, M.S. Hayden, K.Y. Lee, C. Bussey, M. Steckel, N. Tanaka, G. Yamada, S. Akira, K. Matsumoto, S. Ghosh, TAK1, but not TAB1 or TAB2, plays an essential role in multiple signaling pathways in vivo, *Genes Dev*, 19 (2005) 2668-2681, doi:10.1101/gad.1360605.
- [55] C. Wang, L. Deng, M. Hong, G.R. Akkaraju, J. Inoue, Z.J. Chen, TAK1 is a ubiquitin-dependent kinase of MKK and IKK, *Nature*, 412 (2001) 346-351, doi:10.1038/35085597.
- [56] L. Deng, C. Wang, E. Spencer, L. Yang, A. Braun, J. You, C. Slaughter, C. Pickart, Z.J. Chen, Activation of the I κ B Kinase Complex by TRAF6 Requires a Dimeric Ubiquitin-Conjugating Enzyme Complex and a Unique Polyubiquitin Chain, *Cell*, 103 (2000) 351-361, doi:10.1016/s0092-8674(00)00126-4.
- [57] M.A. Lomaga, W.C. Yeh, I. Sarosi, G.S. Duncan, C. Furlonger, A. Ho, S. Morony, C. Capparelli, G. Van, S. Kaufman, A. van der Heiden, A. Itie, A. Wakeham, W. Khoo, T. Sasaki, Z. Cao, J.M. Penninger, C.J. Paige, D.L. Lacey, C.R. Dunstan, W.J. Boyle, D.V. Goeddel, T.W. Mak, TRAF6 deficiency results in osteopetrosis and defective interleukin-1, CD40, and LPS signaling, *Genes Dev*, 13 (1999) 1015-1024, doi:10.1101/gad.13.8.1015.
- [58] T. Kawai, S. Akira, Signaling to NF-kappaB by Toll-like receptors, *Trends Mol Med*, 13 (2007) 460-469, doi:10.1016/j.molmed.2007.09.002.
- [59] S. Akira, S. Uematsu, O. Takeuchi, Pathogen recognition and innate immunity, *Cell*, 124 (2006) 783-801, doi:10.1016/j.cell.2006.02.015.
- [60] J.L. Cervantes, B. Weinerman, C. Basole, J.C. Salazar, TLR8: the forgotten relative revindicated, *Cell Mol Immunol*, 9 (2012) 434-438, doi:10.1038/cmi.2012.38.

Bibliography

- [61] P.L. Cheng, H.L. Eng, M.H. Chou, H.L. You, T.M. Lin, Genetic polymorphisms of viral infection-associated Toll-like receptors in Chinese population, *Transl Res*, 150 (2007) 311-318, doi:10.1016/j.trsl.2007.03.010.
- [62] S. Davila, M.L. Hibberd, R. Hari Dass, H.E. Wong, E. Sahiratmadja, C. Bonnard, B. Alisjahbana, J.S. Szeszko, Y. Balabanova, F. Drobniowski, R. van Crevel, E. van de Vosse, S. Nejentsev, T.H. Ottenhoff, M. Seielstad, Genetic association and expression studies indicate a role of toll-like receptor 8 in pulmonary tuberculosis, *PLoS Genet*, 4 (2008) e1000218, doi:10.1371/journal.pgen.1000218.
- [63] N. Mikhalkovich, B. Becknell, M.A. Caligiuri, M.D. Bates, R. Harvey, W.P. Zheng, Responsiveness of naive CD4 T cells to polarizing cytokine determines the ratio of Th1 and Th2 cell differentiation, *J Immunol*, 176 (2006) 1553-1560, doi:10.4049/jimmunol.176.3.1553.
- [64] S. Moller-Larsen, M. Nyegaard, A. Haagerup, J. Vestbo, T.A. Kruse, A.D. Borglum, Association analysis identifies TLR7 and TLR8 as novel risk genes in asthma and related disorders, *Thorax*, 63 (2008) 1064-1069, doi:10.1136/thx.2007.094128.
- [65] F. Horak, VTX-1463, a novel TLR8 agonist for the treatment of allergic rhinitis, *Expert Opin Investig Drugs*, 20 (2011) 981-986, doi:10.1517/13543784.2011.583237.
- [66] H. Kanzler, F.J. Barrat, E.M. Hessel, R.L. Coffman, Therapeutic targeting of innate immunity with Toll-like receptor agonists and antagonists, *Nat Med*, 13 (2007) 552-559, doi:10.1038/nm1589.
- [67] M.J. Laska, A. Trolborg, B. Hansen, K. Stengaard-Pedersen, P. Junker, B.A. Nexø, A. Voss, Polymorphisms within Toll-like receptors are associated with systemic lupus erythematosus in a cohort of Danish females, *Rheumatology (Oxford)*, 53 (2014) 48-55, doi:10.1093/rheumatology/ket316.
- [68] J. Vollmer, S. Tluk, C. Schmitz, S. Hamm, M. Jurk, A. Forsbach, S. Akira, K.M. Kelly, W.H. Reeves, S. Bauer, A.M. Krieg, Immune stimulation mediated by autoantigen binding sites within small nuclear RNAs involves Toll-like receptors 7 and 8, *J Exp Med*, 202 (2005) 1575-1585, doi:10.1084/jem.20051696.
- [69] N.L. Tran, C. Manzin-Lorenzi, M.L. Santiago-Raber, Toll-like receptor 8 deletion accelerates autoimmunity in a mouse model of lupus through a Toll-like receptor 7-dependent mechanism, *Immunology*, 145 (2015) 60-70, doi:10.1111/imm.12426.
- [70] C. Guiducci, M. Gong, A.M. Cepika, Z. Xu, C. Tripodo, L. Bennett, C. Crain, P. Quartier, J.J. Cush, V. Pascual, R.L. Coffman, F.J. Barrat, RNA recognition by human TLR8 can lead to autoimmune inflammation, *J Exp Med*, 210 (2013) 2903-2919, doi:10.1084/jem.20131044.
- [71] S.M. Sacre, A. Lo, B. Gregory, R.E. Simmonds, L. Williams, M. Feldmann, F.M. Brennan, B.M. Foxwell, Inhibitors of TLR8 reduce TNF production from human rheumatoid synovial membrane cultures, *J Immunol*, 181 (2008) 8002-8009, doi:10.4049/jimmunol.181.11.8002.
- [72] N. Prinz, N. Clemens, D. Strand, I. Putz, M. Lorenz, A. Daiber, P. Stein, A. Degreif, M. Radsak, H. Schild, S. Bauer, P. von Landenberg, K.J. Lackner, Antiphospholipid antibodies induce translocation of TLR7 and TLR8 to the endosome in human monocytes and plasmacytoid dendritic cells, *Blood*, 118 (2011) 2322-2332, doi:10.1182/blood-2011-01-330639.
- [73] Y. Doring, J. Hurst, M. Lorenz, N. Prinz, N. Clemens, M.D. Drechsler, S. Bauer, J. Chapman, Y. Shoenfeld, M. Blank, K.J. Lackner, P. von Landenberg, Human antiphospholipid antibodies induce TNF α in monocytes via Toll-like receptor 8, *Immunobiology*, 215 (2010) 230-241, doi:10.1016/j.imbio.2009.03.002.

Bibliography

- [74] M. Saruta, S.R. Targan, L. Mei, A.F. Ippoliti, K.D. Taylor, J.I. Rotter, High-frequency haplotypes in the X chromosome locus TLR8 are associated with both CD and UC in females, *Inflamm Bowel Dis*, 15 (2009) 321-327, doi:10.1002/ibd.20754.
- [75] M. Ciechomska, C.A. Huigens, T. Hugle, T. Stanly, A. Gessner, B. Griffiths, T.R. Radstake, S. Hambleton, S. O'Reilly, J.M. van Laar, Toll-like receptor-mediated, enhanced production of profibrotic TIMP-1 in monocytes from patients with systemic sclerosis: role of serum factors, *Ann Rheum Dis*, 72 (2013) 1382-1389, doi:10.1136/annrheumdis-2012-201958.
- [76] B. Huang, J. Zhao, J.C. Unkeless, Z.H. Feng, H. Xiong, TLR signaling by tumor and immune cells: a double-edged sword, *Oncogene*, 27 (2008) 218-224, doi:10.1038/sj.onc.1210904.
- [77] R. Chen, A.B. Alvero, D.A. Silasi, G. Mor, Inflammation, cancer and chemoresistance: taking advantage of the toll-like receptor signaling pathway, *Am J Reprod Immunol*, 57 (2007) 93-107, doi:10.1111/j.1600-0897.2006.00441.x.
- [78] F. Balkwill, L.M. Coussens, Cancer: an inflammatory link, *Nature*, 431 (2004) 405-406, doi:10.1038/431405a.
- [79] Z.L. Chang, Important aspects of Toll-like receptors, ligands and their signaling pathways, *Inflamm Res*, 59 (2010) 791-808, doi:10.1007/s00011-010-0208-2.
- [80] B. Drobits, M. Holcman, N. Amberg, M. Swiecki, R. Grundtner, M. Hammer, M. Colonna, M. Sibilio, Imiquimod clears tumors in mice independent of adaptive immunity by converting pDCs into tumor-killing effector cells, *J Clin Invest*, 122 (2012) 575-585, doi:10.1172/JCI61034.
- [81] G. Stry, C. Bangert, M. Tauber, R. Strohal, T. Kopp, G. Stingl, Tumoricidal activity of TLR7/8-activated inflammatory dendritic cells, *J Exp Med*, 204 (2007) 1441-1451, doi:10.1084/jem.20070021.
- [82] T. Lan, E.R. Kandimalla, D. Yu, L. Bhagat, Y. Li, D. Wang, F. Zhu, J.X. Tang, M.R. Putta, Y. Cong, A.F. Trombino, T. Sullivan, S. Agrawal, Stabilized immune modulatory RNA compounds as agonists of Toll-like receptors 7 and 8, *Proc Natl Acad Sci U S A*, 104 (2007) 13750-13755, doi:10.1073/pnas.0706059104.
- [83] Y. Zhang, H. Yang, P.A. Barnie, P. Yang, Z. Su, J. Chen, Z. Jiao, L. Lu, S. Wang, H. Xu, The expression of Toll-like receptor 8 and its relationship with VEGF and Bcl-2 in cervical cancer, *Int J Med Sci*, 11 (2014) 608-613, doi:10.7150/ijms.8428.
- [84] J. Cherfils-Vicini, S. Platonova, M. Gillard, L. Laurans, P. Validire, R. Caliandro, P. Magdeleinat, F. Mami-Chouaib, M.C. Dieu-Nosjean, W.H. Fridman, D. Damotte, C. Sautes-Fridman, I. Cremer, Triggering of TLR7 and TLR8 expressed by human lung cancer cells induces cell survival and chemoresistance, *J Clin Invest*, 120 (2010) 1285-1297, doi:10.1172/JCI36551.
- [85] M.J. Szczepanski, M. Czystowska, M. Szajnik, M. Harasymczuk, M. Boyiadzis, A. Kruk-Zagajewska, W. Szyfter, J. Zeromski, T.L. Whiteside, Triggering of Toll-like receptor 4 expressed on human head and neck squamous cell carcinoma promotes tumor development and protects the tumor from immune attack, *Cancer Res*, 69 (2009) 3105-3113, doi:10.1158/0008-5472.CAN-08-3838.
- [86] J. Bohnhorst, T. Rasmussen, S.H. Moen, M. Flottum, L. Knudsen, M. Borset, T. Espevik, A. Sundan, Toll-like receptors mediate proliferation and survival of multiple myeloma cells, *Leukemia*, 20 (2006) 1138-1144, doi:10.1038/sj.leu.2404225.

Bibliography

- [87] T. Grimmig, N. Matthes, K. Hoeland, S. Tripathi, A. Chandraker, M. Grimm, R. Moench, E.M. Moll, H. Friess, I. Tsaour, R.A. Blaheta, C.T. Germer, A.M. Waaga-Gasser, M. Gasser, TLR7 and TLR8 expression increases tumor cell proliferation and promotes chemoresistance in human pancreatic cancer, *Int J Oncol*, 47 (2015) 857-866, doi:10.3892/ijo.2015.3069.
- [88] M. Fabbri, A. Paone, F. Calore, R. Galli, E. Gaudio, R. Santhanam, F. Lovat, P. Fadda, C. Mao, G.J. Nuovo, N. Zanesi, M. Crawford, G.H. Ozer, D. Wernicke, H. Alder, M.A. Caligiuri, P. Nana-Sinkam, D. Perrotti, C.M. Croce, MicroRNAs bind to Toll-like receptors to induce prometastatic inflammatory response, *Proc Natl Acad Sci U S A*, 109 (2012) E2110-2116, doi:10.1073/pnas.1209414109.
- [89] J.P. Pradere, D.H. Dapito, R.F. Schwabe, The Yin and Yang of Toll-like receptors in cancer, *Oncogene*, 33 (2014) 3485-3495, doi:10.1038/onc.2013.302.
- [90] S.C. Tang, S.J. Yeh, Y.I. Li, Y.C. Wang, S.H. Baik, T. Santro, A. Widiapradja, S. Manzanero, C.G. Sobey, D.G. Jo, T.V. Arumugam, J.S. Jeng, Evidence for a detrimental role of TLR8 in ischemic stroke, *Exp Neurol*, 250 (2013) 341-347, doi:10.1016/j.expneurol.2013.10.012.
- [91] Z.J. Zhang, J.S. Guo, S.S. Li, X.B. Wu, D.L. Cao, B.C. Jiang, P.B. Jing, X.Q. Bai, C.H. Li, Z.H. Wu, Y. Lu, Y.J. Gao, TLR8 and its endogenous ligand miR-21 contribute to neuropathic pain in murine DRG, *J Exp Med*, 215 (2018) 3019-3037, doi:10.1084/jem.20180800.
- [92] C.M. Royer, K. Rudolph, G.N. Dietsch, R.M. Hershberg, E.G. Barrett, VTX-1463, a novel TLR-8 agonist, attenuates nasal congestion after ragweed challenge in sensitized beagle dogs, *Immun Inflamm Dis*, 4 (2016) 45-51, doi:10.1002/iid3.91.
- [93] D.M. Balak, M.B. van Doorn, R.D. Arbeit, R. Rijneveld, E. Klaassen, T. Sullivan, J. Brevard, H.B. Thio, E.P. Prens, J. Burggraaf, R. Rissmann, IMO-8400, a toll-like receptor 7, 8, and 9 antagonist, demonstrates clinical activity in a phase 2a, randomized, placebo-controlled trial in patients with moderate-to-severe plaque psoriasis, *Clin Immunol*, 174 (2017) 63-72, doi:10.1016/j.clim.2016.09.015.
- [94] D.B. Salunke, E. Yoo, N.M. Shukla, R. Balakrishna, S.S. Malladi, K.J. Serafin, V.W. Day, X. Wang, S.A. David, Structure-activity relationships in human Toll-like receptor 8-active 2,3-diamino-furo[2,3-c]pyridines, *J Med Chem*, 55 (2012) 8137-8151, doi:10.1021/jm301066h.
- [95] D.J. Dowling, Z. Tan, Z.M. Prokopowicz, C.D. Palmer, M.A. Matthews, G.N. Dietsch, R.M. Hershberg, O. Levy, The ultra-potent and selective TLR8 agonist VTX-294 activates human newborn and adult leukocytes, *PLoS One*, 8 (2013) e58164, doi:10.1371/journal.pone.0058164.
- [96] H.P. Kokatla, D. Sil, H. Tanji, U. Ohto, S.S. Malladi, L.M. Fox, T. Shimizu, S.A. David, Structure-based design of novel human Toll-like receptor 8 agonists, *ChemMedChem*, 9 (2014) 719-723, doi:10.1002/cmdc.201300573.
- [97] M. Beesu, S.S. Malladi, L.M. Fox, C.D. Jones, A. Dixit, S.A. David, Human Toll-like receptor 8-selective agonistic activities in 1-alkyl-1H-benzimidazol-2-amines, *J Med Chem*, 57 (2014) 7325-7341, doi:10.1021/jm500701q.
- [98] M. Beesu, G. Caruso, A.C. Salyer, N.M. Shukla, K.K. Khetani, L.J. Smith, L.M. Fox, H. Tanji, U. Ohto, T. Shimizu, S.A. David, Identification of a Human Toll-Like Receptor (TLR) 8-Specific Agonist and a Functional Pan-TLR Inhibitor in 2-Aminoimidazoles, *J Med Chem*, 59 (2016) 3311-3330, doi:10.1021/acs.jmedchem.6b00023.
- [99] M. Beesu, A.C. Salyer, K.L. Trautman, J.K. Hill, S.A. David, Human Toll-like Receptor (TLR) 8-Specific Agonistic Activity in Substituted Pyrimidine-2,4-diamines, *J Med Chem*, 59 (2016) 8082-8093, doi:10.1021/acs.jmedchem.6b00872.

Bibliography

- [100] M. Beesu, A.C. Salyer, M.J. Brush, K.L. Trautman, J.K. Hill, S.A. David, Identification of High-Potency Human TLR8 and Dual TLR7/TLR8 Agonists in Pyrimidine-2,4-diamines, *J Med Chem*, 60 (2017) 2084-2098, doi:10.1021/acs.jmedchem.6b01860.
- [101] N.M. Shukla, C.A. Mutz, S.S. Malladi, H.J. Warshakoon, R. Balakrishna, S.A. David, Toll-like receptor (TLR)-7 and -8 modulatory activities of dimeric imidazoquinolines, *J Med Chem*, 55 (2012) 1106-1116, doi:10.1021/jm2010207.
- [102] H.P. Kokatla, E. Yoo, D.B. Salunke, D. Sil, C.F. Ng, R. Balakrishna, S.S. Malladi, L.M. Fox, S.A. David, Toll-like receptor-8 agonistic activities in C2, C4, and C8 modified thiazolo[4,5-c]quinolines, *Org Biomol Chem*, 11 (2013) 1179-1198, doi:10.1039/c2ob26705e.
- [103] C.E. Schiaffo, C. Shi, Z. Xiong, M. Olin, J.R. Ohlfest, C.C. Aldrich, D.M. Ferguson, Structure-activity relationship analysis of imidazoquinolines with Toll-like receptors 7 and 8 selectivity and enhanced cytokine induction, *J Med Chem*, 57 (2014) 339-347, doi:10.1021/jm4004957.
- [104] E. Yoo, D.B. Salunke, D. Sil, X. Guo, A.C. Salyer, A.R. Hermanson, M. Kumar, S.S. Malladi, R. Balakrishna, W.H. Thompson, H. Tanji, U. Ohto, T. Shimizu, S.A. David, Determinants of activity at human Toll-like receptors 7 and 8: quantitative structure-activity relationship (QSAR) of diverse heterocyclic scaffolds, *J Med Chem*, 57 (2014) 7955-7970, doi:10.1021/jm500744f.
- [105] W. Embrechts, F. Herschke, F. Pauwels, B. Stoops, S. Last, S. Pieters, V. Pande, G. Pille, K. Amssoms, I. Smyej, D. Dhuyvetter, A. Scholliers, W. Mostmans, K. Van Dijck, B. Van Schoubroeck, T. Thone, D. De Pooter, G. Fanning, T.H.M. Jonckers, H. Horton, P. Raboisson, D. McGowan, 2,4-Diaminoquinazolines as Dual Toll-like Receptor (TLR) 7/8 Modulators for the Treatment of Hepatitis B Virus, *J Med Chem*, 61 (2018) 6236-6246, doi:10.1021/acs.jmedchem.8b00643.
- [106] D. McGowan, F. Herschke, F. Pauwels, B. Stoops, S. Last, S. Pieters, A. Scholliers, T. Thone, B. Van Schoubroeck, D. De Pooter, W. Mostmans, M.D. Khamlichi, W. Embrechts, D. Dhuyvetter, I. Smyej, E. Arnoult, S. Demin, H. Borghys, G. Fanning, J. Vlach, P. Raboisson, Novel Pyrimidine Toll-like Receptor 7 and 8 Dual Agonists to Treat Hepatitis B Virus, *J Med Chem*, 59 (2016) 7936-7949, doi:10.1021/acs.jmedchem.6b00747.
- [107] L. Zhang, V. Dewan, H. Yin, Discovery of Small Molecules as Multi-Toll-like Receptor Agonists with Proinflammatory and Anticancer Activities, *J Med Chem*, 60 (2017) 5029-5044, doi:10.1021/acs.jmedchem.7b00419.
- [108] N.M. Shukla, S.S. Malladi, V. Day, S.A. David, Preliminary evaluation of a 3H imidazoquinoline library as dual TLR7/TLR8 antagonists, *Bioorg Med Chem*, 19 (2011) 3801-3811, doi:10.1016/j.bmc.2011.04.052.
- [109] Z. Hu, H. Tanji, S. Jiang, S. Zhang, K. Koo, J. Chan, K. Sakaniwa, U. Ohto, A. Candia, T. Shimizu, H. Yin, Small-Molecule TLR8 Antagonists via Structure-Based Rational Design, *Cell Chem Biol*, 25 (2018) 1286-1291 e1283, doi:10.1016/j.chembiol.2018.07.004.
- [110] G. Sliwoski, S. Kothiwale, J. Meiler, E.W. Lowe, Jr., Computational methods in drug discovery, *Pharmacol Rev*, 66 (2014) 334-395, doi:10.1124/pr.112.007336.
- [111] T. Zhu, S. Cao, P.C. Su, R. Patel, D. Shah, H.B. Chokshi, R. Szukala, M.E. Johnson, K.E. Hevener, Hit identification and optimization in virtual screening: practical recommendations based on a critical literature analysis, *J Med Chem*, 56 (2013) 6560-6572, doi:10.1021/jm301916b.

Bibliography

- [112] D.B. Kitchen, H. Decornez, J.R. Furr, J. Bajorath, Docking and scoring in virtual screening for drug discovery: methods and applications, *Nat Rev Drug Discov*, 3 (2004) 935-949, doi:10.1038/nrd1549.
- [113] D.T. Moustakas, P.T. Lang, S. Pegg, E. Pettersen, I.D. Kuntz, N. Brooijmans, R.C. Rizzo, Development and validation of a modular, extensible docking program: DOCK 5, *J Comput Aided Mol Des*, 20 (2006) 601-619, doi:10.1007/s10822-006-9060-4.
- [114] D.S. Goodsell, M.F. Sanner, A.J. Olson, S. Forli, The AutoDock suite at 30, *Protein Sci*, 30 (2021) 31-43, doi:10.1002/pro.3934.
- [115] R.A. Friesner, J.L. Banks, R.B. Murphy, T.A. Halgren, J.J. Klicic, D.T. Mainz, M.P. Repasky, E.H. Knoll, M. Shelley, J.K. Perry, D.E. Shaw, P. Francis, P.S. Shenkin, Glide: a new approach for rapid, accurate docking and scoring. 1. Method and assessment of docking accuracy, *J Med Chem*, 47 (2004) 1739-1749, doi:10.1021/jm0306430.
- [116] G. Jones, P. Willett, R.C. Glen, A.R. Leach, R. Taylor, Development and validation of a genetic algorithm for flexible docking, *J Mol Biol*, 267 (1997) 727-748, doi:10.1006/jmbi.1996.0897.
- [117] O. Trott, A.J. Olson, AutoDock Vina: improving the speed and accuracy of docking with a new scoring function, efficient optimization, and multithreading, *J Comput Chem*, 31 (2010) 455-461, doi:10.1002/jcc.21334.
- [118] M. Rarey, B. Kramer, T. Lengauer, G. Klebe, A fast flexible docking method using an incremental construction algorithm, *J Mol Biol*, 261 (1996) 470-489, doi:10.1006/jmbi.1996.0477.
- [119] L.G. Ferreira, R.N. Dos Santos, G. Oliva, A.D. Andricopulo, Molecular docking and structure-based drug design strategies, *Molecules*, 20 (2015) 13384-13421, doi:10.3390/molecules200713384.
- [120] M.L. Verdonk, J.C. Cole, M.J. Hartshorn, C.W. Murray, R.D. Taylor, Improved protein-ligand docking using GOLD, *Proteins*, 52 (2003) 609-623, doi:10.1002/prot.10465.
- [121] N. Huang, C. Kalyanaraman, K. Bernacki, M.P. Jacobson, Molecular mechanics methods for predicting protein-ligand binding, *Phys Chem Chem Phys*, 8 (2006) 5166-5177, doi:10.1039/b608269f.
- [122] M.D. Eldridge, C.W. Murray, T.R. Auton, G.V. Paolini, R.P. Mee, Empirical scoring functions: I. The development of a fast empirical scoring function to estimate the binding affinity of ligands in receptor complexes, *J Comput Aided Mol Des*, 11 (1997) 425-445, doi:10.1023/a:1007996124545.
- [123] W.T. Mooij, M.L. Verdonk, General and targeted statistical potentials for protein-ligand interactions, *Proteins*, 61 (2005) 272-287, doi:10.1002/prot.20588.
- [124] T. Cheng, Q. Li, Z. Zhou, Y. Wang, S.H. Bryant, Structure-based virtual screening for drug discovery: a problem-centric review, *AAPS J*, 14 (2012) 133-141, doi:10.1208/s12248-012-9322-0.
- [125] T. Cheng, X. Li, Y. Li, Z. Liu, R. Wang, Comparative assessment of scoring functions on a diverse test set, *J Chem Inf Model*, 49 (2009) 1079-1093, doi:10.1021/ci9000053.
- [126] G.L. Warren, C.W. Andrews, A.M. Capelli, B. Clarke, J. LaLonde, M.H. Lambert, M. Lindvall, N. Nevins, S.F. Semus, S. Senger, G. Tedesco, I.D. Wall, J.M. Woolven, C.E. Peishoff, M.S. Head, A critical assessment of docking programs and scoring functions, *J Med Chem*, 49 (2006) 5912-5931, doi:10.1021/jm050362n.

Bibliography

- [127] R. Brandman, Y. Brandman, V.S. Pande, A-site residues move independently from P-site residues in all-atom molecular dynamics simulations of the 70S bacterial ribosome, *PLoS One*, 7 (2012) e29377, doi:10.1371/journal.pone.0029377.
- [128] I. Tinoco, Jr., J.D. Wen, Simulation and analysis of single-ribosome translation, *Phys Biol*, 6 (2009) 025006, doi:10.1088/1478-3975/6/2/025006.
- [129] J.A. McCammon, B.R. Gelin, M. Karplus, Dynamics of folded proteins, *Nature*, 267 (1977) 585-590, doi:10.1038/267585a0.
- [130] K. Goossens, H. De Winter, Molecular Dynamics Simulations of Membrane Proteins: An Overview, *J Chem Inf Model*, 58 (2018) 2193-2202, doi:10.1021/acs.jcim.8b00639.
- [131] S.A. Hollingsworth, R.O. Dror, Molecular Dynamics Simulation for All, *Neuron*, 99 (2018) 1129-1143, doi:10.1016/j.neuron.2018.08.011.
- [132] W.D. Cornell, P. Cieplak, C.I. Bayly, I.R. Gould, K.M. Merz, D.M. Ferguson, D.C. Spellmeyer, T. Fox, J.W. Caldwell, P.A. Kollman, A Second Generation Force Field for the Simulation of Proteins, Nucleic Acids, and Organic Molecules, *J Am Chem Soc*, 117 (1995) 5179-5197, doi:10.1021/ja00124a002.
- [133] P.E. Lopes, O. Guvench, A.D. Mackerell, Jr., Current status of protein force fields for molecular dynamics simulations, *Methods Mol Biol*, 1215 (2015) 47-71, doi:10.1007/978-1-4939-1465-4_3.
- [134] W.L. Jorgensen, J. Tirado-Rives, Potential energy functions for atomic-level simulations of water and organic and biomolecular systems, *Proc Natl Acad Sci U S A*, 102 (2005) 6665-6670, doi:10.1073/pnas.0408037102.
- [135] A. Hospital, J.R. Goni, M. Orozco, J.L. Gelpi, Molecular dynamics simulations: advances and applications, *Adv Appl Bioinform Chem*, 8 (2015) 37-47, doi:10.2147/AABC.S70333.
- [136] X. Cheng, I. Ivanov, Molecular dynamics, *Methods Mol Biol*, 929 (2012) 243-285, doi:10.1007/978-1-62703-050-2_11.
- [137] D.A. Case, T.E. Cheatham, 3rd, T. Darden, H. Gohlke, R. Luo, K.M. Merz, Jr., A. Onufriev, C. Simmerling, B. Wang, R.J. Woods, The Amber biomolecular simulation programs, *J Comput Chem*, 26 (2005) 1668-1688, doi:10.1002/jcc.20290.
- [138] B.R. Brooks, C.L. Brooks, 3rd, A.D. Mackerell, Jr., L. Nilsson, R.J. Petrella, B. Roux, Y. Won, G. Archontis, C. Bartels, S. Boresch, A. Caflisch, L. Caves, Q. Cui, A.R. Dinner, M. Feig, S. Fischer, J. Gao, M. Hodoscek, W. Im, K. Kuczera, T. Lazaridis, J. Ma, V. Ovchinnikov, E. Paci, R.W. Pastor, C.B. Post, J.Z. Pu, M. Schaefer, B. Tidor, R.M. Venable, H.L. Woodcock, X. Wu, W. Yang, D.M. York, M. Karplus, CHARMM: the biomolecular simulation program, *J Comput Chem*, 30 (2009) 1545-1614, doi:10.1002/jcc.21287.
- [139] B. Hess, C. Kutzner, D. van der Spoel, E. Lindahl, GROMACS 4: Algorithms for Highly Efficient, Load-Balanced, and Scalable Molecular Simulation, *J Chem Theory Comput*, 4 (2008) 435-447, doi:10.1021/ct700301q.
- [140] M.T. Nelson, W. Humphrey, A. Gursoy, A. Dalke, L.V. Kalé, R.D. Skeel, K. Schulten, NAMD: a Parallel, Object-Oriented Molecular Dynamics Program, *Int J High Perform Comput Appl*, 10 (2016) 251-268, doi:10.1177/109434209601000401.
- [141] K.J. Bowers, F.D. Sacerdoti, J.K. Salmon, Y. Shan, D.E. Shaw, E. Chow, H. Xu, R.O. Dror, M.P. Eastwood, B.A. Gregersen, J.L. Klepeis, I. Kolossvary, M.A. Moraes, Molecular dynamics---Scalable algorithms for molecular dynamics simulations on commodity clusters, *Proceedings of the 2006 ACM/IEEE conference on Supercomputing*, (2006) 84, doi:10.1145/1188455.1188544.

Bibliography

- [142] J.H. Van Drie, Generation of three-dimensional pharmacophore models, *WIREs Comput Mol Sci*, 3 (2013) 449-464, doi:10.1002/wcms.1129.
- [143] A.R. Leach, V.J. Gillet, R.A. Lewis, R. Taylor, Three-dimensional pharmacophore methods in drug discovery, *J Med Chem*, 53 (2010) 539-558, doi:10.1021/jm900817u.
- [144] G. Wolber, T. Langer, LigandScout: 3-D pharmacophores derived from protein-bound ligands and their use as virtual screening filters, *J Chem Inf Model*, 45 (2005) 160-169, doi:10.1021/ci049885e.
- [145] M. Baroni, G. Cruciani, S. Sciabola, F. Perruccio, J.S. Mason, A common reference framework for analyzing/comparing proteins and ligands. Fingerprints for Ligands and Proteins (FLAP): theory and application, *J Chem Inf Model*, 47 (2007) 279-294, doi:10.1021/ci600253e.
- [146] D. Barnum, J. Greene, A. Smellie, P. Sprague, Identification of common functional configurations among molecules, *J Chem Inf Comput Sci*, 36 (1996) 563-571, doi:10.1021/ci950273r.
- [147] Strategies for 3D pharmacophore-based virtual screening, *Drug Discov Today Technol*, 7 (2010) e203-270, doi:10.1016/j.ddtec.2010.11.004.
- [148] S.L. Dixon, A.M. Smondyrev, E.H. Knoll, S.N. Rao, D.E. Shaw, R.A. Friesner, PHASE: a new engine for pharmacophore perception, 3D QSAR model development, and 3D database screening: 1. Methodology and preliminary results, *J Comput Aided Mol Des*, 20 (2006) 647-671, doi:10.1007/s10822-006-9087-6.
- [149] J. Taminiau, G. Thijs, H. De Winter, Pharao: pharmacophore alignment and optimization, *J Mol Graph Model*, 27 (2008) 161-169, doi:10.1016/j.jmgm.2008.04.003.
- [150] T. Langer, G. Wolber, Pharmacophore definition and 3D searches, *Drug Discov Today Technol*, 1 (2004) 203-207, doi:10.1016/j.ddtec.2004.11.015.
- [151] D. Schaller, D. Šribar, T. Noonan, L. Deng, T.N. Nguyen, S. Pach, D. Machalz, M. Bermudez, G. Wolber, Next generation 3D pharmacophore modeling, *WIREs Comput Mol Sci*, 10 (2020) doi:10.1002/wcms.1468.
- [152] N. Triballeau, F. Acher, I. Brabet, J.P. Pin, H.O. Bertrand, Virtual screening workflow development guided by the "receiver operating characteristic" curve approach. Application to high-throughput docking on metabotropic glutamate receptor subtype 4, *J Med Chem*, 48 (2005) 2534-2547, doi:10.1021/jm049092j.
- [153] J. Mortier, J.R.C. Prevost, D. Sydow, S. Teuchert, C. Omieczynski, M. Bermudez, R. Frederick, G. Wolber, Arginase Structure and Inhibition: Catalytic Site Plasticity Reveals New Modulation Possibilities, *Sci Rep*, 7 (2017) 13616, doi:10.1038/s41598-017-13366-4.
- [154] A. Bock, M. Bermudez, F. Krebs, C. Matera, B. Chirinda, D. Sydow, C. Dallanocce, U. Holzgrabe, M. De Amici, M.J. Lohse, G. Wolber, K. Mohr, Ligand Binding Ensembles Determine Graded Agonist Efficacies at a G Protein-coupled Receptor, *J Biol Chem*, 291 (2016) 16375-16389, doi:10.1074/jbc.M116.735431.
- [155] B. Nizami, D. Sydow, G. Wolber, B. Honarparvar, Molecular insight on the binding of NNRTI to K103N mutated HIV-1 RT: molecular dynamics simulations and dynamic pharmacophore analysis, *Mol Biosyst*, 12 (2016) 3385-3395, doi:10.1039/c6mb00428h.
- [156] A. Kumar, K.Y.J. Zhang, Advances in the Development of Shape Similarity Methods and Their Application in Drug Discovery, *Front Chem*, 6 (2018) 315, doi:10.3389/fchem.2018.00315.

Bibliography

- [157] P.C. Hawkins, A.G. Skillman, A. Nicholls, Comparison of shape-matching and docking as virtual screening tools, *J Med Chem*, 50 (2007) 74-82, doi:10.1021/jm0603365.
- [158] T.S. Rush, 3rd, J.A. Grant, L. Mosyak, A. Nicholls, A shape-based 3-D scaffold hopping method and its application to a bacterial protein-protein interaction, *J Med Chem*, 48 (2005) 1489-1495, doi:10.1021/jm040163o.
- [159] J.A. Grant, B.T. Pickup, A Gaussian Description of Molecular Shape, *J Phys Chem*, 99 (1995) 3503-3510, doi:10.1021/j100011a016.
- [160] L. Ganapathi, S. Van Haren, D.J. Dowling, I. Bergelson, N.M. Shukla, S.S. Malladi, R. Balakrishna, H. Tanji, U. Ohto, T. Shimizu, S.A. David, O. Levy, The Imidazoquinoline Toll-Like Receptor-7/8 Agonist Hybrid-2 Potently Induces Cytokine Production by Human Newborn and Adult Leukocytes, *PLoS One*, 10 (2015) e0134640, doi:10.1371/journal.pone.0134640.
- [161] M. Beesu, G. Caruso, A.C. Salyer, K.K. Khetani, D. Sil, M. Weerasinghe, H. Tanji, U. Ohto, T. Shimizu, S.A. David, Structure-Based Design of Human TLR8-Specific Agonists with Augmented Potency and Adjuvanticity, *J Med Chem*, 58 (2015) 7833-7849, doi:10.1021/acs.jmedchem.5b01087.
- [162] J. Liu, C. Xu, L.C. Hsu, Y. Luo, R. Xiang, T.H. Chuang, A five-amino-acid motif in the undefined region of the TLR8 ectodomain is required for species-specific ligand recognition, *Mol Immunol*, 47 (2010) 1083-1090, doi:10.1016/j.molimm.2009.11.003.
- [163] J. Zhu, K. Lai, R. Brownile, L.A. Babiuk, G.K. Mutwiri, Porcine TLR8 and TLR7 are both activated by a selective TLR7 ligand, imiquimod, *Mol Immunol*, 45 (2008) 3238-3243, doi:10.1016/j.molimm.2008.02.028.
- [164] C.D. Livingstone, G.J. Barton, Protein sequence alignments: a strategy for the hierarchical analysis of residue conservation, *Comput Appl Biosci*, 9 (1993) 745-756, doi:10.1093/bioinformatics/9.6.745.
- [165] H.P. Kokatla, D. Sil, S.S. Malladi, R. Balakrishna, A.R. Hermanson, L.M. Fox, X. Wang, A. Dixit, S.A. David, Exquisite selectivity for human toll-like receptor 8 in substituted furo[2,3-c]quinolines, *J Med Chem*, 56 (2013) 6871-6885, doi:10.1021/jm400694d.
- [166] R.J. Gibbard, P.J. Morley, N.J. Gay, Conserved features in the extracellular domain of human toll-like receptor 8 are essential for pH-dependent signaling, *J Biol Chem*, 281 (2006) 27503-27511, doi:10.1074/jbc.M605003200.
- [167] K.B. Gorden, K.S. Gorski, S.J. Gibson, R.M. Kedl, W.C. Kieper, X. Qiu, M.A. Tomai, S.S. Alkan, J.P. Vasilakos, Synthetic TLR agonists reveal functional differences between human TLR7 and TLR8, *J Immunol*, 174 (2005) 1259-1268, doi:10.4049/jimmunol.174.3.1259.
- [168] L.L. Stunz, P. Lenert, D. Peckham, A.K. Yi, S. Haxhinasto, M. Chang, A.M. Krieg, R.F. Ashman, Inhibitory oligonucleotides specifically block effects of stimulatory CpG oligonucleotides in B cells, *Eur J Immunol*, 32 (2002) 1212-1222, doi:10.1002/1521-4141(200205)32:5<1212::AID-IMMU1212>3.0.CO;2-D.
- [169] D. Srihar, M. Grabowski, M.S. Murgueitio, M. Bermudez, G. Weindl, G. Wolber, Identification and characterization of a novel chemotype for human TLR8 inhibitors, *Eur J Med Chem*, 179 (2019) 744-752, doi:10.1016/j.ejmech.2019.06.084.
- [170] G.B. McGaughey, R.P. Sheridan, C.I. Bayly, J.C. Culberson, C. Kretsoulas, S. Lindsley, V. Maiorov, J.F. Truchon, W.D. Cornell, Comparison of topological, shape, and docking methods in virtual screening, *J Chem Inf Model*, 47 (2007) 1504-1519, doi:10.1021/ci700052x.

Bibliography

- [171] A.C. Good, M.A. Hermsmeier, S.A. Hindle, Measuring CAMD technique performance: a virtual screening case study in the design of validation experiments, *J Comput Aided Mol Des*, 18 (2004) 529-536, doi:10.1007/s10822-004-4067-1.
- [172] W. Chanput, J.J. Mes, H.J. Wichers, THP-1 cell line: an in vitro cell model for immune modulation approach, *Int Immunopharmacol*, 23 (2014) 37-45, doi:10.1016/j.intimp.2014.08.002.
- [173] F. Heil, H. Hemmi, H. Hochrein, F. Ampenberger, C. Kirschning, S. Akira, G. Lipford, H. Wagner, S. Bauer, Species-specific recognition of single-stranded RNA via toll-like receptor 7 and 8, *Science*, 303 (2004) 1526-1529, doi:10.1126/science.1093620.
- [174] S.S. Diebold, T. Kaisho, H. Hemmi, S. Akira, C. Reis e Sousa, Innate antiviral responses by means of TLR7-mediated recognition of single-stranded RNA, *Science*, 303 (2004) 1529-1531, doi:10.1126/science.1093616.
- [175] S. Bauer, C.J. Kirschning, H. Hacker, V. Redecke, S. Hausmann, S. Akira, H. Wagner, G.B. Lipford, Human TLR9 confers responsiveness to bacterial DNA via species-specific CpG motif recognition, *Proc Natl Acad Sci U S A*, 98 (2001) 9237-9242, doi:10.1073/pnas.161293498.
- [176] U. Ohto, T. Shibata, H. Tanji, H. Ishida, E. Krayukhina, S. Uchiyama, K. Miyake, T. Shimizu, Structural basis of CpG and inhibitory DNA recognition by Toll-like receptor 9, *Nature*, 520 (2015) 702-705, doi:10.1038/nature14138.
- [177] Z. Zhang, U. Ohto, T. Shibata, E. Krayukhina, M. Taoka, Y. Yamauchi, H. Tanji, T. Isobe, S. Uchiyama, K. Miyake, T. Shimizu, Structural Analysis Reveals that Toll-like Receptor 7 Is a Dual Receptor for Guanosine and Single-Stranded RNA, *Immunity*, 45 (2016) 737-748, doi:10.1016/j.immuni.2016.09.011.
- [178] T. Shibata, U. Ohto, S. Nomura, K. Kibata, Y. Motoi, Y. Zhang, Y. Murakami, R. Fukui, T. Ishimoto, S. Sano, T. Ito, T. Shimizu, K. Miyake, Guanosine and its modified derivatives are endogenous ligands for TLR7, *Int Immunol*, 28 (2016) 211-222, doi:10.1093/intimm/dxv062.
- [179] U. Ohto, H. Ishida, T. Shibata, R. Sato, K. Miyake, T. Shimizu, Toll-like Receptor 9 Contains Two DNA Binding Sites that Function Cooperatively to Promote Receptor Dimerization and Activation, *Immunity*, 48 (2018) 649-658 e644, doi:10.1016/j.immuni.2018.03.013.
- [180] Z. Zhang, U. Ohto, T. Shibata, M. Taoka, Y. Yamauchi, R. Sato, N.M. Shukla, S.A. David, T. Isobe, K. Miyake, T. Shimizu, Structural Analyses of Toll-like Receptor 7 Reveal Detailed RNA Sequence Specificity and Recognition Mechanism of Agonistic Ligands, *Cell Rep*, 25 (2018) 3371-3381 e3375, doi:10.1016/j.celrep.2018.11.081.
- [181] S. Jones, J.M. Thornton, Analysis of protein-protein interaction sites using surface patches, *J Mol Biol*, 272 (1997) 121-132, doi:10.1006/jmbi.1997.1234.
- [182] C. Yan, F. Wu, R.L. Jernigan, D. Dobbs, V. Honavar, Characterization of protein-protein interfaces, *Protein J*, 27 (2008) 59-70, doi:10.1007/s10930-007-9108-x.
- [183] R.P. Bahadur, P. Chakrabarti, F. Rodier, J. Janin, Dissecting subunit interfaces in homodimeric proteins, *Proteins*, 53 (2003) 708-719, doi:10.1002/prot.10461.
- [184] S.E. Acuner Ozbabacan, H.B. Engin, A. Gursoy, O. Keskin, Transient protein-protein interactions, *Protein Eng Des Sel*, 24 (2011) 635-648, doi:10.1093/protein/gzr025.
- [185] H. Lu, Q. Zhou, J. He, Z. Jiang, C. Peng, R. Tong, J. Shi, Recent advances in the development of protein-protein interactions modulators: mechanisms and clinical trials, *Signal Transduct Target Ther*, 5 (2020) 213, doi:10.1038/s41392-020-00315-3.

Bibliography

- [186] K.A. Shirey, W. Lai, L.J. Brown, J.C.G. Blanco, R. Beadenkopf, Y. Wang, S.N. Vogel, G.A. Snyder, Select targeting of intracellular Toll-interleukin-1 receptor resistance domains for protection against influenza-induced disease, *Innate Immun*, 26 (2020) 26-34, doi:10.1177/1753425919846281.
- [187] F. Deng, S. Ma, M. Xie, X. Zhang, P. Li, H. Zhai, Study on the agonists for the human Toll-like receptor-8 by molecular modeling, *Mol Biosyst*, 10 (2014) 2202-2214, doi:10.1039/c4mb00183d.
- [188] F. Pei, H. Jin, X. Zhou, J. Xia, L. Sun, Z. Liu, L. Zhang, Enrichment assessment of multiple virtual screening strategies for Toll-like receptor 8 agonists based on a maximal unbiased benchmarking data set, *Chem Biol Drug Des*, 86 (2015) 1226-1241, doi:10.1111/cbdd.12590.
- [189] J. Auer, J. Bajorath, Emerging chemical patterns: a new methodology for molecular classification and compound selection, *J Chem Inf Model*, 46 (2006) 2502-2514, doi:10.1021/ci600301t.
- [190] S. Huang, H. Mei, D. Zhang, T. Shi, L. Chen, Z. Kuang, Y. Heng, X. Pan, L. Lu, Subtle differences in chemical pattern between human toll-like receptor 8 agonists and antagonists: Emerging chemical patterns analysis, *Chem Biol Drug Des*, 94 (2019) 1824-1834, doi:10.1111/cbdd.13590.
- [191] S. Tojo, Z. Zhang, H. Matsui, M. Tahara, M. Ikeguchi, M. Kochi, M. Kamada, H. Shigematsu, A. Tsutsumi, N. Adachi, T. Shibata, M. Yamamoto, M. Kikkawa, T. Senda, Y. Isobe, U. Ohto, T. Shimizu, Structural analysis reveals TLR7 dynamics underlying antagonism, *Nat Commun*, 11 (2020) 5204, doi:10.1038/s41467-020-19025-z.
- [192] A. Jezierska, I.A. Kolosova, A.D. Verin, Toll Like Receptors Signaling Pathways as a Target for Therapeutic Interventions, *Curr Signal Transduct Ther*, 6 (2011) 428-440, doi:10.2174/157436211797483930.
- [193] S. Banerjee, An insight into the interaction between alpha-ketoamide- based inhibitor and coronavirus main protease: A detailed in silico study, *Biophys Chem*, 269 (2021) 106510, doi:10.1016/j.bpc.2020.106510.
- [194] J. Zhou, E.D. Mock, A. Martella, V. Kantae, X. Di, L. Burggraaff, M.P. Baggelaar, K. Al-Ayed, A. Bakker, B.I. Florea, S.H. Grimm, H. den Dulk, C.T. Li, L. Mulder, H.S. Overkleeft, T. Hankemeier, G.J.P. van Westen, M. van der Stelt, Activity-Based Protein Profiling Identifies alpha-Ketoamides as Inhibitors for Phospholipase A2 Group XVI, *ACS Chem Biol*, 14 (2019) 164-169, doi:10.1021/acscchembio.8b00969.
- [195] R. Padilla-Salinas, R. Anderson, K. Sakaniwa, S. Zhang, P. Nordeen, C. Lu, T. Shimizu, H. Yin, Discovery of Novel Small Molecule Dual Inhibitors Targeting Toll-Like Receptors 7 and 8, *J Med Chem*, 62 (2019) 10221-10244, doi:10.1021/acs.jmedchem.9b01201.
- [196] T. Knoepfel, P. Nimsgern, S. Jacquier, M. Bourrel, E. Vangrevelinghe, R. Glatthar, D. Behnke, P.B. Alper, P.Y. Michellys, J. Deane, T. Junt, G. Zipfel, S. Limonta, S. Hawtin, C. Andre, T. Boulay, P. Loetscher, M. Faller, J. Blank, R. Feifel, C. Betschart, Target-Based Identification and Optimization of 5-Indazol-5-yl Pyridones as Toll-like Receptor 7 and 8 Antagonists Using a Biochemical TLR8 Antagonist Competition Assay, *J Med Chem*, 63 (2020) 8276-8295, doi:10.1021/acs.jmedchem.0c00130.
- [197] P.B. Alper, J. Deane, C. Betschart, D. Buffet, G. Collignon Zipfel, P. Gordon, J. Hampton, S. Hawtin, M. Ibanez, T. Jiang, T. Junt, T. Knoepfel, B. Liu, J. Maginnis, U. McKeever, P.Y. Michellys, D. Mutnick, B. Nayak, S. Niwa, W. Richmond, J.S. Rush, P. Syka, Y. Zhang, X. Zhu, Discovery of potent, orally bioavailable in vivo efficacious antagonists of the TLR7/8 pathway, *Bioorg Med Chem Lett*, 30 (2020) 127366, doi:10.1016/j.bmcl.2020.127366.

Bibliography

- [198] C.P. Mussari, D.S. Dodd, R.K. Sreekantha, L. Pasunoori, H. Wan, S.L. Posy, D. Critton, S. Ruepp, M. Subramanian, A. Watson, P. Davies, G.L. Schieven, L.M. Salter-Cid, R. Srivastava, D.M. Tagore, S. Dudhgaonkar, M.A. Poss, P.H. Carter, A.J. Dyckman, Discovery of Potent and Orally Bioavailable Small Molecule Antagonists of Toll-like Receptors 7/8/9 (TLR7/8/9), *ACS Med Chem Lett*, 11 (2020) 1751-1758, doi:10.1021/acsmchemlett.0c00264.
- [199] L. Pluta, B. Yousefi, B. Damania, A.A. Khan, Endosomal TLR-8 Senses microRNA-1294 Resulting in the Production of NFkB Dependent Cytokines, *Front Immunol*, 10 (2019) 2860, doi:10.3389/fimmu.2019.02860.
- [200] A.T. Bender, E. Tzvetkov, A. Pereira, Y. Wu, S. Kasar, M.M. Przetak, J. Vlach, T.B. Niewold, M.A. Jensen, S.L. Okitsu, TLR7 and TLR8 Differentially Activate the IRF and NF-kappaB Pathways in Specific Cell Types to Promote Inflammation, *Immunohorizons*, 4 (2020) 93-107, doi:10.4049/immunohorizons.2000002.
- [201] S. Jiang, H. Tanji, K. Yin, S. Zhang, K. Sakaniwa, J. Huang, Y. Yang, J. Li, U. Ohto, T. Shimizu, H. Yin, Rationally Designed Small-Molecule Inhibitors Targeting an Unconventional Pocket on the TLR8 Protein-Protein Interface, *J Med Chem*, 63 (2020) 4117-4132, doi:10.1021/acs.jmedchem.9b02128.
- [202] H.M. Berman, J. Westbrook, Z. Feng, G. Gilliland, T.N. Bhat, H. Weissig, I.N. Shindyalov, P.E. Bourne, The Protein Data Bank, *Nucleic Acids Res*, 28 (2000) 235-242, doi:10.1093/nar/28.1.235.
- [203] P. Labute, Protonate3D: assignment of ionization states and hydrogen coordinates to macromolecular structures, *Proteins*, 75 (2009) 187-205, doi:10.1002/prot.22234.
- [204] F. Sievers, A. Wilm, D. Dineen, T.J. Gibson, K. Karplus, W. Li, R. Lopez, H. McWilliam, M. Remmert, J. Soding, J.D. Thompson, D.G. Higgins, Fast, scalable generation of high-quality protein multiple sequence alignments using Clustal Omega, *Mol Syst Biol*, 7 (2011) 539, doi:10.1038/msb.2011.75.
- [205] C. UniProt, UniProt: a worldwide hub of protein knowledge, *Nucleic Acids Res*, 47 (2019) D506-D515, doi:10.1093/nar/gky1049.
- [206] B.J. Grant, L. Skjaerven, X.Q. Yao, The Bio3D packages for structural bioinformatics, *Protein Sci*, 30 (2021) 20-30, doi:10.1002/pro.3923.
- [207] B.J. Grant, A.P. Rodrigues, K.M. ElSawy, J.A. McCammon, L.S. Caves, Bio3d: an R package for the comparative analysis of protein structures, *Bioinformatics*, 22 (2006) 2695-2696, doi:10.1093/bioinformatics/btl461.
- [208] G. Wolber, A.A. Dornhofer, T. Langer, Efficient overlay of small organic molecules using 3D pharmacophores, *J Comput Aided Mol Des*, 20 (2006) 773-788, doi:10.1007/s10822-006-9078-7.
- [209] M.M. Mysinger, M. Carchia, J.J. Irwin, B.K. Shoichet, Directory of useful decoys, enhanced (DUD-E): better ligands and decoys for better benchmarking, *J Med Chem*, 55 (2012) 6582-6594, doi:10.1021/jm300687e.
- [210] P.C. Hawkins, A.G. Skillman, G.L. Warren, B.A. Ellingson, M.T. Stahl, Conformer generation with OMEGA: algorithm and validation using high quality structures from the Protein Databank and Cambridge Structural Database, *J Chem Inf Model*, 50 (2010) 572-584, doi:10.1021/ci100031x.

Bibliography

- [211] J.A. Grant, M.A. Gallardo, B.T. Pickup, A fast method of molecular shape comparison: A simple application of a Gaussian description of molecular shape, *J Comput Chem*, 17 (1996) 1653-1666, doi:10.1002/(sici)1096-987x(19961115)17:14<1653::aid-jcc7>3.0.co;2-k.
- [212] P. Mark, L. Nilsson, Structure and Dynamics of the TIP3P, SPC, and SPC/E Water Models at 298 K, *J Phys Chem A*, 105 (2001) 9954-9960, doi:10.1021/jp003020w.
- [213] W.L. Jorgensen, J. Tirado-Rives, The OPLS [optimized potentials for liquid simulations] potential functions for proteins, energy minimizations for crystals of cyclic peptides and crambin, *J Am Chem Soc*, 110 (1988) 1657-1666, doi:10.1021/ja00214a001.
- [214] W. Humphrey, A. Dalke, K. Schulten, VMD: visual molecular dynamics, *J Mol Graph*, 14 (1996) 33-38, 27-38, doi:10.1016/0263-7855(96)00018-5.
- [215] M. Scheurer, P. Rodenkirch, M. Siggel, R.C. Bernardi, K. Schulten, E. Tajkhorshid, T. Rudack, PyContact: Rapid, Customizable, and Visual Analysis of Noncovalent Interactions in MD Simulations, *Biophys J*, 114 (2018) 577-583, doi:10.1016/j.bpj.2017.12.003.
- [216] N. Michaud-Agrawal, E.J. Denning, T.B. Woolf, O. Beckstein, MDAAnalysis: a toolkit for the analysis of molecular dynamics simulations, *J Comput Chem*, 32 (2011) 2319-2327, doi:10.1002/jcc.21787.

Appendix

Tables

Table S 1. Published crystal structures of human Toll-like receptor 8.

PDB ID	Ligand	Resolution (Å)	Publication	PDB ID	Ligand	Resolution (Å)	Publication
3W3G	Unliganded	2.30	[22]	4R09	ORN06S	2.69	[31]
3W3J	CL097	2.00	[22]	4R0A	uridine mononucleoside	1.90	[31]
3W3K	CL075	2.30	[22]	4R6A	Hybrid-2	2.10	[160]
3W3L	Resiquimod (R848) crystal form 1	2.33	[22]	5AW B	N1-3-aminomethylbenzyl (meta-amine)	2.10	[161]
3W3M	Resiquimod (R848) crystal form 2	2.70	[22]	5AW D	N1-4-aminomethylbenzyl (IMDQ)	2.05	[161]
3W3N	Resiquimod (R848) crystal form 3	2.10	[22]	5AW A	MB-568	2.20	[161]
3WN4	DS-877	1.81	[96]	5AW C	MB-564	2.50	[161]
4QBZ	DS-802	2.00	[104]	5AZ5	MB-343	2.40	[98]
4QC0	XG-1-236	2.10	[104]	5HDH	Unliganded with uncleaved Z-loop	2.60	[47]
4R07	ORN06	2.00	[31]	5WY X	CU-CPT8m	2.40	[49]
4R08	ssRNA40	2.40	[31]	5WYZ	CU-CPT9b	2.30	[49]

Table S 2. Interaction frequency of residues between two TLR8 monomers throughout molecular dynamics simulations. Simulations for unliganded TLR8 (PDB ID:3W3G), TLR8 bound to agonist

Appendix

CL097 (PDB ID: 3W3J) and TLR8 bound to antagonist CU-CPT9b (PDB ID: 5WYZ) were done in triplicates.

Bond type	Aa pair	Unliganded_1	Unliganded_2	Unliganded_3	antagonist_1	Antagonist_2	Antagonist_3	Agonist_1	Agonist_2	Agonist_3
hbond	VAL100 , s. A - LYS677 , s. B--2							68.0	33.0	80.0
hbond	TYR182 , s. A - ASP627 , s. B--2							98.0	33.0	100.0
hydrophobic	PHE183 , s. A - ALA571 , s. B--1	96.0	94.0	96.0						
hbond	ASN184 , s. A - ASP627 , s. B--2							100.0	45.0	100.0
hbond	ASN184 , s. A - ASP628 , s. B--2							99.0	34.0	100.0
saltbr	LYS185 , s. A - ASP628 , s. B--0				96.0	47.0	97.0			
saltbr	LYS185 , s. A - ASP627 , s. B--0				49.0	58.0	64.0	100.0	100.0	100.0
hbond	PHE261 , s. A - GLY572 , s. B--2							95.0	48.0	79.0
hydrophobic	PHE261 , s. A - VAL520 , s. B--1				100.0	98.0	99.0			
hbond	ASN262 , s. A - TYR567 , s. B--2	100.0	100.0	100.0						
hbond	ASN262 , s. A - VAL573 , s. B--2							98.0	99.0	100.0
hbond	ASN262 , s. A - THR574 , s. B--2							48.0	85.0	81.0
hbond	ASN262 , s. A - HIE575 , s. B--2							98.0	55.0	100.0

Appendix

hbond	ASN262 , s. A - ALA571 , s. B--2				100.0	44.0	100.0
hbond	ASN262 , s. A - THR600 , s. B--2				100.0	100.0	100.0
hbond	ASN262 , s. A - GLY572 , s. B--2				100.0	99.0	100.0
hbond	ASN262 , s. A - THR598 , s. B--2				100.0	35.0	100.0
hbond	ALA263 , s. A - ARG630 , s. B--2				53.0	53.0	62.0
hbond	PRO264 , s. A - ARG630 , s. B--2				41.0	83.0	98.0
hydro phobic	PRO264 , s. A - ALA571 , s. B--1				42.0	68.0	100.0
hbond	PHE265 , s. A - ARG630 , s. B--2				87.0	100.0	93.0
hydro phobic	PRO266 , s. A - TYR597 , s. B--1		89.0	91.0	89.0		
hbond	CYS267 , s. A - ALA571 , s. B--2	100.0	100.0	100.0			
hbond	CYS267 , s. A - ARG569 , s. B--2	98.0	96.0	43.0			
hbond	VAL268 , s. A - ALA571 , s. B--2	98.0	99.0	90.0			
hydro phobic	PRO269 , s. A - ILE570 , s. B--1	100.0	100.0	100.0			
hydro phobic	PRO269 , s. A - VAL573 , s. B--1	69.0	85.0	86.0			
hydro phobic	PHE320 , s. A - PHE568 , s. B--1				94.0	78.0	67.0

Appendix

hydro phobic	PHE320 , s. A - TYR567 , s. B--1				70.0	58.0	77.0			
hydro phobic	PHE346 , s. A - PHE568 , s. B--1				100.0	97.0	86.0			
hydro phobic	PHE346 , s. A - TYR567 , s. B--1				49.0	68.0	68.0			
hbond	TYR348 , s. A - GLY572 , s. B--2							74.0	77.0	50.0
hydro phobic	TYR348 , s. A - TYR567 , s. B--1				61.0	91.0	100.0			
hydro phobic	TYR353 , s. A - PHE494 , s. B--1	100.0	100.0	100.0	100.0	100.0	100.0			
hydro phobic	TYR353 , s. A - PHE495 , s. B--1	100.0	100.0	100.0	99.0	99.0	99.0			
hydro phobic	TYR353 , s. A - PRO432 , s. B--1	100.0	100.0	100.0	100.0	100.0	100.0			
hydro phobic	VAL378 , s. A - PHE494 , s. B--1	96.0	98.0	95.0	100.0	99.0	100.0			
hydro phobic	ILE403 , s. A - ILE570 , s. B--1							100.0	76.0	64.0
hydro phobic	ILE403 , s. A - VAL573 , s. B--1							93.0	86.0	96.0
hydro phobic	PHE405 , s. A - VAL573 , s. B--1							99.0	98.0	100.0
hydro phobic	PHE405 , s. A - PHE494 , s. B--1	100.0	100.0	100.0	100.0	100.0	100.0			
hydro phobic	PHE405 , s. A - TYR567 , s. B--1							100.0	99.0	100.0
hbond	LYS407 , s. A - ARG429 , s. B--2	66.0	91.0	76.0						

Appendix

hbond	LYS407 , s. A - SER431 , s. B--2	98.0	83.0	99.0			
saltbr	GLU427 , s. A - ARG541 , s. B--0				70.0	41.0	83.0
hbond	GLU427 , s. A - TYR567 , s. B--2						99.0 98.0 97.0
hbond	GLU427 , s. A - HIP566 , s. B--2						100.0 100.0 100.0
hbond	ARG429 , s. A - ARG429 , s. B--2	99.0	100.0	100.0			
hbond	ARG429 , s. A - SER492 , s. B--2	88.0	98.0	96.0			
hbond	ARG429 , s. A - ALA518 , s. B--2						34.0 90.0 40.0
hbond	ARG429 , s. A - VAL520 , s. B--2						75.0 100.0 99.0
hbond	SER431 , s. A - ARG429 , s. B--2	100.0	100.0	100.0			
hydro phobic	PRO432 , s. A - TYR353 , s. B--1	100.0	100.0	98.0	100.0	100.0	100.0
hbond	ACE457 , s. A - LYS652 , s. B--2						91.0 35.0 94.0
hbond	GLH460 , s. A - ASN625 , s. B--2						66.0 83.0 100.0
hydro phobic	PHE461 , s. A - ILE570 , s. B--1				92.0	98.0	92.0
hydro phobic	PHE467 , s. A - ILE570 , s. B--1				86.0	98.0	96.0
hydro phobic	PHE467 , s. A - PHE568 , s. B--1				98.0	99.0	100.0

Appendix

hbond	LEU490 , s. A - ARG541 , s. B--2							98.0	59.0	97.0
hbond	SER492 , s. A - ARG429 , s. B--2	90.0	99.0	99.0						
hydro phobic	PHE494 , s. A - VAL378 , s. B--1	81.0	98.0	35.0	100.0	100.0	100.0			
hydro phobic	PHE494 , s. A - TYR353 , s. B--1	100.0	100.0	100.0	100.0	100.0	100.0			
hydro phobic	PHE494 , s. A - PHE494 , s. B--1							100.0	100.0	100.0
hydro phobic	PHE494 , s. A - PHE405 , s. B--1	100.0	100.0	100.0	100.0	100.0	100.0			
hydro phobic	PHE495 , s. A - TYR353 , s. B--1	100.0	100.0	100.0	99.0	100.0	100.0			
hbond	ALA514 , s. A - ARG541 , s. B--2							88.0	70.0	100.0
hbond	ASN515 , s. A - ARG541 , s. B--2							88.0	83.0	98.0
hbond	SER516 , s. A - ARG541 , s. B--2							99.0	99.0	90.0
hbond	SER516 , s. A - SER516 , s. B--2							100.0	100.0	100.0
hbond	ALA518 , s. A - ARG429 , s. B--2							37.0	50.0	99.0
hbond	VAL520 , s. A - ARG429 , s. B--2							95.0	100.0	100.0
hydro phobic	VAL520 , s. A - PHE261 , s. B--1				100.0	100.0	100.0			
hbond	ARG541 , s. A - LEU490 , s. B--2							100.0	92.0	95.0

Appendix

hbond	ARG541 , s. A - ASN515 , s. B--2				33.0	100.0	99.0
saltbr	ARG541 , s. A - GLU427 , s. B--0		89.0	54.0	72.0		
hbond	ARG541 , s. A - ALA514 , s. B--2				79.0	100.0	100.0
hbond	HIE566 , s. A - GLU427 , s. B--2				100.0	100.0	100.0
hydro phobic	TYR567 , s. A - PHE320 , s. B--1		100.0	100.0	100.0		
hydro phobic	TYR567 , s. A - PHE405 , s. B--1				96.0	100.0	92.0
hydro phobic	TYR567 , s. A - PHE346 , s. B--1		92.0	76.0	59.0		
hbond	TYR567 , s. A - ASN262 , s. B--2	98.0	100.0	100.0			
hydro phobic	TYR567 , s. A - TYR348 , s. B--1		99.0	100.0	100.0		
hbond	TYR567 , s. A - ARG429 , s. B--2				32.0	69.0	100.0
hydro phobic	PHE568 , s. A - TYR468 , s. B--1		96.0	89.0	91.0		
hydro phobic	PHE568 , s. A - PHE320 , s. B--1		92.0	94.0	96.0		
hydro phobic	PHE568 , s. A - PHE346 , s. B--1		100.0	100.0	100.0		
hydro phobic	PHE568 , s. A - PRO264 , s. B--1		73.0	85.0	90.0		
saltbr	ARG569 , s. A - GLU427 , s. B--0				98.0	100.0	100.0

Appendix

hydro phobic	ILE570 , s. A - PRO264 , s. B--1				99.0	99.0	99.0			
hydro phobic	ILE570 , s. A - ILE403 , s. B--1							100.0	88.0	92.0
hydro phobic	ILE570 , s. A - PHE467 , s. B--1				93.0	92.0	95.0			
hydro phobic	ILE570 , s. A - PRO269 , s. B--1	100.0	100.0	100.0						
hbond	ALA571 , s. A - CYS267 , s. B--2	100.0	100.0	100.0						
hbond	GLY572 , s. A - ASN262 , s. B--2							100.0	100.0	99.0
hbond	VAL573 , s. A - ASN262 , s. B--2							100.0	100.0	96.0
hbond	THR574 , s. A - ASN262 , s. B--2							96.0	97.0	100.0
hydro phobic	TYR597 , s. A - PHE461 , s. B--1				56.0	94.0	97.0			
hbond	THR600 , s. A - ASN262 , s. B--2							100.0	100.0	92.0
hbond	ASP627 , s. A - ASN184 , s. B--2							56.0	100.0	100.0
hbond	ASP627 , s. A - TYR182 , s. B--2							100.0	79.0	100.0
saltbr	ASP627 , s. A - LYS185 , s. B--0							100.0	100.0	100.0
saltbr	ASP628 , s. A - LYS185 , s. B--0				93.0	96.0	38.0			
hbond	ASP628 , s. A - ASN184 , s. B--2							34.0	98.0	96.0

Appendix

hbond	ASN629 , s. A - ASN184 , s. B--2			36.0	56.0	95.0
hbond	LYS677 , s. A - VAL100 , s. B--2			44.0	82.0	84.0
hbond	LYS749 , s. A - ARG810 , s. B--2			66.0	37.0	58.0
saltbr	GLU775 , s. A - ARG810 , s. B--0			93.0	51.0	97.0

Table S 3. Collected agonists of TLR8 from the literature.

SMILES	Publication
<chem>CCCCC1=CC2=C(O1)C(N)=NC1=C2C=CC=C1</chem>	[165]
<chem>CC1=CC2=C(O1)C(N)=NC1=C2C=CC=C1</chem>	[165]
<chem>CCCC1=CC2=C(O1)C(N)=NC1=C2C=CC=C1</chem>	[165]
<chem>CCCCCCC1=CC2=C(O1)C(N)=NC1=C2C=CC=C1</chem>	[165]
<chem>CCCCCCC1=CC2=C(O1)C(N)=NC1=C2C=CC=C1</chem>	[165]
<chem>CCCC1=CC2=C(O1)C(N)=NC=C2</chem>	[165]
<chem>CCCCC1=CC2=C(O1)C(N)=NC=C2</chem>	[165]
<chem>CC1=NC2=C(N)N=C3C=CC=CC3=C2S1</chem>	[102]
<chem>CCC1=NC2=C(N)N=C3C=CC=CC3=C2S1</chem>	[102]
<chem>CCCC1=NC2=C(N)N=C3C=CC=CC3=C2S1</chem>	[102]
<chem>CCCCC1=NC2=C(N)N=C3C=CC=CC3=C2S1</chem>	[102]
<chem>CCCCCCC1=NC2=C(N)N=C3C=CC=CC3=C2S1</chem>	[102]
<chem>CC(C)C1=NC2=C(N)N=C3C=CC=CC3=C2S1</chem>	[102]
<chem>CC(C)CC1=NC2=C(N)N=C3C=CC=CC3=C2S1</chem>	[102]
<chem>CCC(C)C1=NC2=C(N)N=C3C=CC=CC3=C2S1</chem>	[102]
<chem>CCC(C)CC1=NC2=C(N)N=C3C=CC=CC3=C2S1</chem>	[102]
<chem>NC1=C2N=C(CCC(F)(F)F)SC2=C2C=CC=CC2=N1</chem>	[102]
<chem>NC1=C2N=C(CCCC(F)(F)F)SC2=C2C=CC=CC2=N1</chem>	[102]
<chem>CCCC1=NC2=C(N)N=C3C=CC(=CC3=C2S1)N1C=C(N=N1)[Si](C)(C)C</chem>	[102]
<chem>CCCC1=NC2=C(NC(C)=O)N=C3C=CC=CC3=C2S1</chem>	[102]
<chem>CCCC(=O)NC1=C2N=C(CCC)SC2=C2C=CC=CC2=N1</chem>	[102]
<chem>CCCC1=NC2=C(NC(=O)CN=[N+]=[N-])N=C3C=CC=CC3=C2S1</chem>	[102]
<chem>CCCC1=NC2=C(NC(=O)CCN=[N+]=[N-])N=C3C=CC=CC3=C2S1</chem>	[102]
<chem>CCCC1=NC2=C(NC(=O)CCC#C)N=C3C=CC=CC3=C2S1</chem>	[102]
<chem>CCCC1=NC2=C(NC(=O)OC)N=C3C=CC=CC3=C2S1</chem>	[102]

Appendix

CCCC1=NC2=C(NS(C)(=O)=O)N=C3C=CC=CC3=C2S1	[102]
CCCCC1=NC2=C(NC=O)N=C3C=CC=CC3=C2S1	[102]
CCCCC1=NC2=C(NC(=O)CCC)N=C3C=CC=CC3=C2S1	[102]
CCCCC1=C(CC2=CC=CC(CN)=C2)C2=CC=CC=C2N=C1N	[161]
CCCCC1=C(CC2=CC=C(CN)C=C2)C2=CC=CC=C2N=C1N	[161]
CCCCC1=C(CCCCN)C2=CC=CC=C2N=C1N	[161]
CCCCC1=C(CCCCCN)C2=CC=CC=C2N=C1N	[161]
CCCCC1=CC2=C(CC3=CC(CN)=CC=C3)C=CC=C2N=C1N	[161]
CCCCC1=CC2=C(CC3=CC=C(CN)C=C3)C=CC=C2N=C1N	[161]
CCCCC1=CC2=C(CC3=C(CN)C=CC=C3)C=CC=C2N=C1N	[161]
CCCCC1=CC2=C(C=CC=C2N=C1N)C1=CC=C(CN)C=C1	[161]
CCCCC1=CC2=C(CCCN)C=CC=C2N=C1N	[161]
CCCCC1=CC2=C(CCCCN)C=CC=C2N=C1N	[161]
CCCCC1=CC2=C(CCCCCN)C=CC=C2N=C1N	[161]
CCCCC1=CC2=C(CCCCCCN)C=CC=C2N=C1N	[161]
CCCCC1=CC2=C(CCCC(N)=O)C=CC=C2N=C1N	[161]
CCCCC1=CC2=C(CCCCNC(N)=N)C=CC=C2N=C1N	[161]
CCCCC1=CC2=CC(CCCCN)=CC=C2N=C1N	[161]
CCCCC1=CC2=CC(CCCCCN)=CC=C2N=C1N	[161]
CCCCC1=CC2=CC(CCCCCCN)=CC=C2N=C1N	[161]
CCCCC1=CC2=CC=C(CCCCN)C=C2N=C1N	[161]
CCCCC1=CC2=CC=C(CCCCCN)C=C2N=C1N	[161]
CCCCC1=CC2=C(CCCCCN)C=C(CCCCCN)C=C2N=C1N	[161]
CCCCC1=NC2=C(N1CC1=CC=C(CN)C=C1)C1=CC=CC=C1N=C2N	[161]
CCCCC1=NC2=C(N1CC1=CC(CN)=CC=C1)C1=CC=CC=C1N=C2N	[161]
CCCCC1=CC2=CC=CC=C2N=C1N	[161]
CCCCOC1=CC2=CC=CC=C2N=C1N	[96]
CCCCNC1=CC2=CC=CC=C2N=C1N	[96]
CCCCSC1=CC2=CC=CC=C2N=C1N	[96]
CCCCC1=CC2=CC=CC=C2N=C1N	[96]
CCC\C=C\C1=CC2=CC=CC=C2N=C1N	[96]
NC1=NC2=CC=CC=C2C=C1CCCC=C	[96]
CCCC#CC1=CC2=CC=CC=C2N=C1N	[96]
COC1=CC2=CC=CC=C2N=C1N	[96]
CCOC1=CC2=CC=CC=C2N=C1N	[96]
CCCOC1=CC2=CC=CC=C2N=C1N	[96]
CCCCCOC1=CC2=CC=CC=C2N=C1N	[96]
CCCCCOC1=CC2=CC=CC=C2N=C1N	[96]

Appendix

<chem>CC(C)OC1=CC2=CC=CC=C2N=C1N</chem>	[96]
<chem>CC(C)COC1=CC2=CC=CC=C2N=C1N</chem>	[96]
<chem>CC(C)CCOC1=CC2=CC=CC=C2N=C1N</chem>	[96]
<chem>CCC(C)COC1=CC2=CC=CC=C2N=C1N</chem>	[96]
<chem>CCCCN1C(N)=NC2=CC=CC=C12</chem>	[97]
<chem>CCCCCN1C(N)=NC2=CC=CC=C12</chem>	[97]
<chem>CCCCCCN1C(N)=NC2=CC=CC=C12</chem>	[97]
<chem>CCCCCN1C(N)=NC2=C3C=CC=CC3=CC=C12</chem>	[97]
<chem>CCCCCN1C(N)=NC2=C(C)C=CC=C12</chem>	[97]
<chem>CCCCCN1C(N)=NC2=CC(C)=CC=C12</chem>	[97]
<chem>CCCCCN1C(N)=NC2=CC=C(C)C=C12</chem>	[97]
<chem>CCCCCN1C(N)=NC2=CC=CC(C)=C12</chem>	[97]
<chem>CCCCCN1C(N)=NC2=C(OC)C=CC=C12</chem>	[97]
<chem>CCCCCN1C(N)=NC2=C(CC)C=CC=C12</chem>	[97]
<chem>CCCCCN1C(N)=NC2=C(C=CC=C12)N(C)C</chem>	[97]
<chem>CCCCCN1C(N)=NC2=C(O)C=CC=C12</chem>	[97]
<chem>CCCCCN1C(N)=NC2=C(N)C=CC=C12</chem>	[97]
<chem>CCCCC1=NC2=C(O1)C1=CC=CC=C1N=C2N</chem>	[104]
<chem>CCCNC1=NC2=C(S1)C1=CC=CC=C1N=C2N</chem>	[104]
<chem>CCCCC1=NC2=C(O1)C(N)=NC1=CC=CC=C21</chem>	[104]
<chem>CCCCC1=CN2C(=N1)C(N)=NC1=CC=CC=C21</chem>	[104]
<chem>CCCCN1C=C2C(=N1)C(N)=NC1=CC=CC=C21</chem>	[104]
<chem>CCOCC1=NC2=C(N1CC(C)(C)O)C1=CC=CC=C1N=C2N</chem>	[103]
<chem>CCCCC1=NC2=C(N1CC(C)(C)O)C1=C(C=C(C=C1)C(=O)OC)N=C2N</chem>	[103]
<chem>CCCCC1=NC2=C(N1CC(C)(C)O)C1=C(C=C(C=C1)C(=O)OC)N=C2N</chem>	[103]
<chem>CCCCC1=NC2=C(N1CCO)C1=C(C=C(C=C1)C(=O)OC)N=C2N</chem>	[103]
<chem>CCCCC1=NC2=C(N1CCOCC1=CC=CC=C1)C1=C(C=C(C=C1)C(=O)OC)N=C2N</chem>	[103]
<chem>CCCCCN1C=CN=C1N</chem>	[98]
<chem>CCCCCN1C=C(N=C1N)C1=CC=CC=C1</chem>	[98]
<chem>CCCCCN1C=C(N=C1N)C1=CC=CC=C1C</chem>	[98]
<chem>CCCCCN1C=C(N=C1N)C1=CC=CC=C1CC</chem>	[98]
<chem>CCCCCN1C=C(N=C1N)C1=CC=CC(C)=C1</chem>	[98]
<chem>CCCCCN1C=C(N=C1N)C1=CC=C(C)C=C1</chem>	[98]
<chem>CCCCCN1C=C(N=C1N)C1=CC=CC(C)=C1C</chem>	[98]
<chem>CCCCCN1C=C(N=C1N)C1=CC=C(C)C=C1C</chem>	[98]
<chem>CCCCCN1C=C(N=C1N)C1=CC(C)=CC=C1C</chem>	[98]
<chem>CCCCCN1C=C(N=C1N)C1=C(C)C=CC=C1C</chem>	[98]
<chem>CCCCCN1C=C(CC2=CC=CC=C2)N=C1N</chem>	[98]

Appendix

<chem>CCCCCN1C=C(CCC2=CC=CC=C2)N=C1N</chem>	[98]
<chem>CCCCCN1C=C(N=C1N)C1=C2C=CC=CC2=CC=C1</chem>	[98]
<chem>CCCCCN1C=C(N=C1N)C1=CC=C2C=CC=CC2=C1</chem>	[98]
<chem>CCCCCN1C=C(N=C1N)C1=CC=C(C=C1)C1=CC=CC=C1</chem>	[98]
<chem>CCCCCN1C=C(N=C1N)C1=CN=CC=C1</chem>	[98]
<chem>CCCCCN1C=C(N=C1N)C1=C(C)ON=C1C</chem>	[98]
<chem>CCCCCN1C=C(N=C1N)C1=CC=CC=C1O</chem>	[98]
<chem>CCCCCN1C=C(N=C1N)C1=CC=CC=C1CO</chem>	[98]
<chem>CCCCCN1C=C(N=C1N)C1=CC=C(N)C=C1</chem>	[98]
<chem>CCCCCN1C=C(N=C1N)C1=CC=C(C=C1)C(N)=O</chem>	[98]
<chem>CCCCCN1C=C(N=C1N)C1=CC=C(C=C1)C(=O)OC</chem>	[98]
<chem>CCCCCN1C=C(N=C1N)C1=CC=CC=C1C(=O)OC</chem>	[98]
<chem>CCCCCN1C=C(N=C1N)C1=CC=CC=C1OC</chem>	[98]
<chem>CCCCCN1C=C(N=C1N)C1=CC=CC(OC)=C1</chem>	[98]
<chem>CCCCCN1C=C(N=C1N)C1=CC=C(OC)C=C1</chem>	[98]
<chem>CCCCCN1C=C(N=C1N)C1=CC=C(OC)C=C1C</chem>	[98]
<chem>CCCCCN1C=C(N=C1N)C1=CC=CC(C)=C1OC</chem>	[98]
<chem>CCCCCN1C=C(N=C1N)C1=CC=CC(OC)=C1OC</chem>	[98]
<chem>CCCCCN1C=C(N=C1N)C1=CC(OC)=C(OC)C(OC)=C1</chem>	[98]
<chem>CCCCCN1C=C(N=C1N)C1=CC=CC=C1Cl</chem>	[98]
<chem>CCCCCN1C=C(N=C1N)C1=CC=CC(Cl)=C1</chem>	[98]
<chem>CCCCCN1C=C(N=C1N)C1=CC=C(Cl)C=C1</chem>	[98]
<chem>CCCCCN1C=C(N=C1N)C1=CC=CC=C1F</chem>	[98]
<chem>CCCCCN1C=C(N=C1N)C1=CC=CC(F)=C1</chem>	[98]
<chem>CCCCCN1C=C(N=C1N)C1=CC=C(F)C=C1</chem>	[98]
<chem>CCCCCN1C=C(N=C1N)C1=CC=C(F)C=C1C</chem>	[98]
<chem>CCCCCN1C=C(N=C1N)C1=CC=CC=C1C(F)(F)F</chem>	[98]
<chem>CCCCCN1C=C(N=C1N)C1=CC=CC(=C1)C(F)(F)F</chem>	[98]
<chem>CCCCCN1C=C(N=C1N)C1=CC=C(C=C1)C(F)(F)F</chem>	[98]
<chem>CCCCN1C=NC(N)=NC(C)=C1I</chem>	[99]
<chem>CCCCN1C=NC(N)=NC(C)=C1I</chem>	[99]
<chem>CCCCN1C=NC(N)=NC(C)=C1Cl</chem>	[99]
<chem>CCCCN1C=NC(N)=NC(C)=C1Br</chem>	[99]
<chem>CCCCN1C=NC(N)=NC(C)=C1F</chem>	[99]
<chem>CCCCN1C=NC(N)=NC(C)=C1</chem>	[99]
<chem>CCCCN1C=NC(N)=NC=C1</chem>	[99]
<chem>CCCCN1C=NC(N)=NC(C)=C1CC1=CC=CC=C1</chem>	[99]
<chem>CCCCN1C=NC(N)=NC(C)=C1CCCN</chem>	[99]
<chem>CCCCN1C=NC(N)=NC(C)=C1CCCCN</chem>	[99]

Appendix

<chem>CCCCNC1=NC(N)=NC(C)=C1CCCCN</chem>	[99]
<chem>CCCCNC1=NC(N)=NC(=C1)C1=CC=CC=C1</chem>	[99]
<chem>CCCCNC1=NC(N)=NC(=C1CCCCN)C1=CC=CC=C1</chem>	[99]
<chem>CCCCNC1=NC(N)=NC(=C1CCCCCN)C1=CC=CC=C1</chem>	[99]
<chem>CCCCNC1=C(OCC2=CC=CC=C2)C=NC(N)=N1</chem>	[106]
<chem>CCCCNC1=C(OCCC)C=NC(N)=N1</chem>	[106]
<chem>CCCCNC1=C(OCCCC2=CC=CC=C2)C=NC(N)=N1</chem>	[106]
<chem>CCCCNC1=C(OC(C)C)C=NC(N)=N1</chem>	[106]
<chem>CCCCNC1=C(OCC2=C(C)ON=C2C)C=NC(N)=N1</chem>	[106]
<chem>CCCCNC1=C(OCC2=CN(C)N=C2)C=NC(N)=N1</chem>	[106]
<chem>CCCCNC1=C(OCC2=NC=CO2)C=NC(N)=N1</chem>	[106]
<chem>CCCCNC1=C(OCC2=C(C)OC(C)=N2)C=NC(N)=N1</chem>	[106]
<chem>CCCCNC1=C(OCC2=CC(C)=NN2C)C=NC(N)=N1</chem>	[106]
<chem>CCCCNC1=C(OCC2=CSC(C)=N2)C=NC(N)=N1</chem>	[106]
<chem>CCCCNC1=C(OCC2=C(OC)C(OC)=CC=N2)C=NC(N)=N1</chem>	[106]
<chem>CCCCNC1=C(OCC2=NC=CN=C2)C=NC(N)=N1</chem>	[106]
<chem>CCCCNC1=C(OCC2=NN=CC=C2)C=NC(N)=N1</chem>	[106]
<chem>CCCCNC1=NC(N)=NC=C1OCC1=CC=C2C=CC=CC2=N1</chem>	[106]
<chem>CCCCNC1=NC(N)=NC=C1OCC1=C2C=CC=CC2=CC=N1</chem>	[106]
<chem>CCCCNC1=NC(N)=NC=C1OCC1=NN(C)C2=CC=CC=C12</chem>	[106]
<chem>CCCCNC1=NC(N)=NC=C1OCC1=NC2=CC=CC=C2N1</chem>	[106]
<chem>CCCCNC1=NC(N)=NC=C1OCC1=NN2C=CC=CC2=C1</chem>	[106]
<chem>CCCCNC1=NC(N)=NC=C1OCC1=NC2=CC=CC=C2S1</chem>	[106]
<chem>COC1=CN=C(N)N=C1NCC=C</chem>	[106]
<chem>COC1=CN=C(N)N=C1NCCC1CC1</chem>	[106]
<chem>CCCC(C)NC1=NC(N)=NC=C1OC</chem>	[106]
<chem>COC1=CN=C(N)N=C1NCCCC(F)(F)F</chem>	[106]
<chem>CC[C@H](C)CNC1=NC(N)=NC=C1OC</chem>	[106]
<chem>CCC[C@H](CO)NC1=NC(N)=NC=C1OC</chem>	[106]
<chem>CCC[C@@H](CO)NC1=NC(N)=NC=C1OC</chem>	[106]
<chem>COC1=CN=C(N)N=C1N[C@H](CO)CC(C)C</chem>	[106]
<chem>CC[C@H](C)[C@@H](CO)NC1=NC(N)=NC=C1OC</chem>	[106]
<chem>CCCC[C@@H](CO)NC1=NC(N)=NC=C1OC</chem>	[106]
<chem>COC1=CN=C(N)N=C1N[C@H](CCO)CC(C)C</chem>	[106]
<chem>CCC(C)[C@H](CCO)NC1=NC(N)=NC=C1OC</chem>	[106]
<chem>CCC[C@@H](CCO)NC1=NC(N)=NC=C1OC</chem>	[106]
<chem>CCCC[C@@H](CCO)NC1=NC(N)=NC=C1OC</chem>	[106]

Appendix

Table S 4. Collected antagonists of TLR8 from the literature.

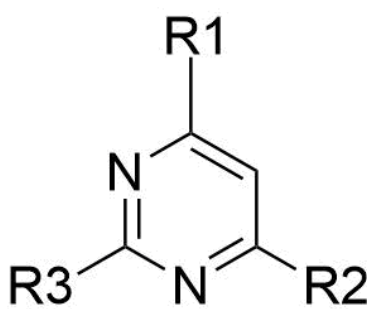
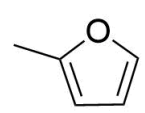

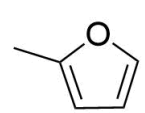
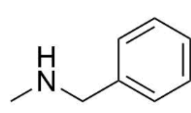
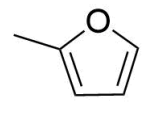
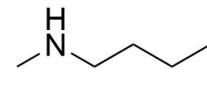
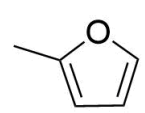
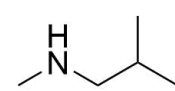
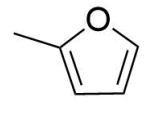
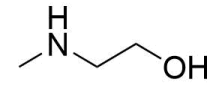
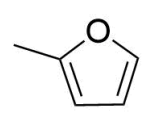
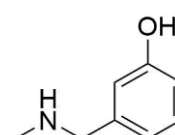
SMILES	Publication
<chem>CC1=CC=CC(=C1)C1=CC=NC2=C(C=NN12)C(N)=O</chem>	[49]
<chem>CCOC(=O)C1=C2N=CC=C(N2N=C1)C1=CC(=CC=C1)C(F)(F)F</chem>	[49]
<chem>CCOC(=O)C1=C2N=CC=C(N2N=C1)C1=CC(C)=CC=C1</chem>	[49]
<chem>NC(=O)C1=C2N=CC=C(N2N=C1)C1=CC(=CC=C1)C(F)(F)F</chem>	[49]
<chem>NC(=O)C1=C2N=CC=C(N2N=C1)C1=C(C=CC=C1)C(F)(F)F</chem>	[49]
<chem>NC(=O)C1=C2N=CC=C(N2N=C1)C1=CC=C(C=C1)C(F)(F)F</chem>	[49]
<chem>NC(=O)C1=C2N=CC=C(N2N=C1)C1=CC=CC=C1</chem>	[49]
<chem>NC(=O)C1=C2N=CC=C(N2N=C1)C1=CC(=CC=C1)N(=O)=O</chem>	[49]
<chem>NC(=O)C1=C2N=CC=C(N2N=C1)C1=CC(F)=CC=C1</chem>	[49]
<chem>NC(=O)C1=C2N=CC=C(N2N=C1)C1=CC(Cl)=CC=C1</chem>	[49]
<chem>NC(=O)C1=C2N=CC=C(N2N=C1)C1=CC(=CC(=C1)C(F)(F)F)C(F)(F)F</chem>	[49]
<chem>COC1=C(C=CC=C1)C1=CC=NC2=C(C=NN12)C(N)=O</chem>	[49]
<chem>COC1=CC=CC(=C1)C1=CC=NC2=C(C=NN12)C(N)=O</chem>	[49]
<chem>CCOC1=CC=CC(=C1)C1=CC=NC2=C(C=NN12)C(N)=O</chem>	[49]
<chem>CNC(=O)C1=C2N=CC=C(N2N=C1)C1=CC(=CC=C1)C(F)(F)F</chem>	[49]
<chem>CC1=CC(=CC=C1O)C1=CC=NC2=C1C=CC(O)=C2</chem>	[49]
<chem>CC1=NC2=C(C=CC=C2)C(=C1)C1=CC=C(O)C(C)=C1</chem>	[49]
<chem>CC1=C(O)C=CC(=C1)C1=NNC(=O)C2=CC=CC=C12</chem>	[49]
<chem>COC1=CC=C(C2=CC(C)=C(O)C=C2)C2=CC=CC=C12</chem>	[49]
<chem>CC1=C(O)C=CC(=C1)C1=CC=C(O)C2=CC=CC=C12</chem>	[49]
<chem>CC1=C(O)C=CC(=C1)C1=CC=C(N)C2=CC=CC=C12</chem>	[49]
<chem>CN1N=C(C2=CC(O)=C(O)C(C)=C2)C2=CC=CC=C2C1=O</chem>	[49]
<chem>COC(=O)C1=C(C)C=C(C=C1)C1=NNC(=O)C2=CC=CC=C12</chem>	[109]
<chem>CC(=O)OC1=C(C)C=C(C=C1)C1=NNC(=O)C2=CC=CC=C12</chem>	[109]
<chem>CC(=O)OC1=C(C)C=C(C=C1)C1=NNC(=O)C2=CC=CC=C12</chem>	[109]
<chem>CC1=CC(=CC(C)=C1O)C1=NNC(=O)C2=CC=CC=C12</chem>	[109]
<chem>CCC1=C(O)C=CC(=C1)C1=NNC(=O)C2=CC=CC=C12</chem>	[109]
<chem>CN1N=C(C2=CC(O)=C(O)C=C2)C2=CC=CC=C2C1=O</chem>	[109]
<chem>CC1=CC(=CC(C)=C1O)C1=CC=NC2=CC=CC=C12</chem>	[109]
<chem>CC1=C(O)C=CC(=C1)C1=CC=NC2=CC=CC=C12</chem>	[109]
<chem>CC1=C(O)C=CC(=C1)C1=NC=NC2=CC=CC=C12</chem>	[109]
<chem>CC1=C(O)C=CC(=C1)C1=CN=CC2=CC=CC=C12</chem>	[109]
<chem>CC1=CC(=CC(C)=C1O)C1=NN=CC2=CC=CC=C12</chem>	[109]
<chem>CC1=C(O)C=CC(=C1)C1=NN=CC2=CC=CC=C12</chem>	[109]
<chem>CC1=CC(=CC(C)=C1O)C1=CC=CC2=CC=CC=C12</chem>	[109]
<chem>CC1=C(O)C=CC(=C1)C1=CN=NC2=CC=CC=C12</chem>	[109]

Appendix

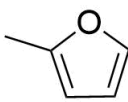
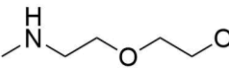
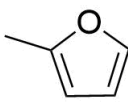
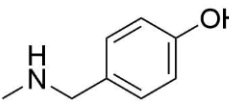
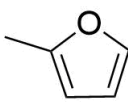
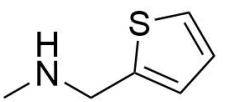
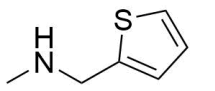
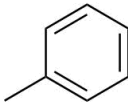
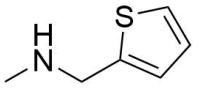
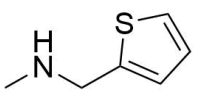
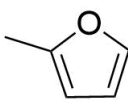
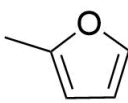
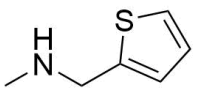
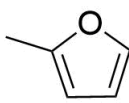
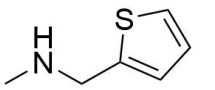
<chem>CC1=C(O)C=CC(=C1)C1=CNC2=CC=CC=C12</chem>	[109]
<chem>CC1=C(O)C=CC(=C1)C1=C2C=CNC2=NC=C1</chem>	[109]
<chem>CC1=C(O)C=CC(=C1)C1=C2N=CC=CC2=NC=C1</chem>	[109]
<chem>CC1=NC2=CC=CC=C2C(=C1)C1=CC(C)=C(O)C(C)=C1</chem>	[109]
<chem>CC1=C(O)C=CC(=C1)C1=CC(=NC2=CC=CC=C12)C(F)(F)F</chem>	[109]
<chem>COC1=NC2=CC=CC=C2C(=C1)C1=CC(C)=C(O)C=C1</chem>	[109]
<chem>COC(=O)C1=C(C=CC(OC)=C1C)C1=CC=NC2=CC=CC=C12</chem>	[109]
<chem>COC(=O)C1=C(C=CC(OC)=C1C)C1=CC=NC2=CC(OC)=CC=C12</chem>	[109]
<chem>COC1=CC=C2C(=C1)N=CC=C2C1=CC(C)=C(O)C=C1</chem>	[109]
<chem>CC1=C(O)C=CC(=C1)C1=CC=NC2=CC(Cl)=CC=C12</chem>	[109]
<chem>COC1=C(C)C=C(C=C1)C1=CC=NC2=CC(=CC=C12)C1=CC=CC=C1</chem>	[109]
<chem>COC1=C(C)C=C(C=N1)C1=CC=NC2=CC=CC=C12</chem>	[109]
<chem>CC1=C(O)N=CC(=C1)C1=CC=NC2=CC(O)=CC=C12</chem>	[109]
<chem>COC1=CC=C2C(=C1)N=CC=C2C1=CC(C)=C(OC)N=C1</chem>	[109]
<chem>COC1=CC=C2C(=C1)N=CC=C2C1=CC(C)=C(O)N=C1</chem>	[109]
<chem>COC1=C(C)C=C(C=N1)C1=CC=NC2=CC(O)=CC=C12</chem>	[109]
<chem>COC1=CC=C2C(=C1)N=CC=C2C1=CC(C)=C(OCC2=CC=CC=C2)N=C1</chem>	[109]
<chem>CC1=C(C=O)C=CC(=C1)C1=CC=NC2=CC=CC=C12</chem>	[109]
<chem>CC(=O)C1=C(C)C=C(C=C1)C1=CC=NC2=CC=CC=C12</chem>	[109]
<chem>CC1=C(N)C=CC(=C1)C1=CC=NC2=CC=CC=C12</chem>	[109]
<chem>COC1=C(C)C=C(C=C1)C1=CC=NC2=CC=CC=C12</chem>	[109]
<chem>CC1=C(O)C=CC(=C1)C1=CC2=CC=CC=C2N=C1</chem>	[109]
<chem>COC1=CC=C(C=C1)C(=O)C1=CC=NC2=CC=CC=C12</chem>	[109]
<chem>CC1=C(O)C=CC(CC2=CC=NC3=CC(O)=CC=C23)=C1</chem>	[109]
<chem>CC1=C(O)C=CC(=C1)C1=CC(N)=NC2=CC=CC=C12</chem>	[109]
<chem>CC1=CC(=CC(C)=C1O)C1=CC(N)=NC2=CC=CC=C12</chem>	[109]
<chem>CC1=C(O)C=CC(=C1)C1=CC2=CC=CC=C2N=C1N</chem>	[109]

Appendix

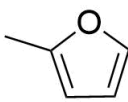
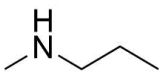
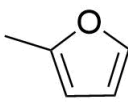
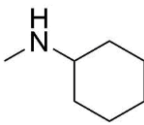
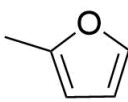
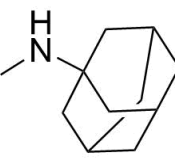
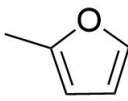
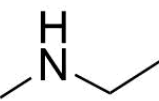
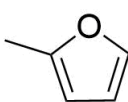
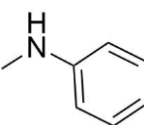
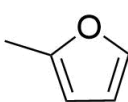
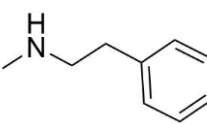
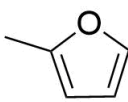
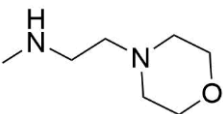
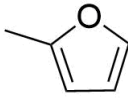
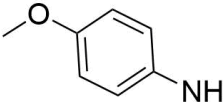
Table S 5. Synthesised analogues of **5**.

				
ID	R1	R2	R3	
15	CF ₃			
16	CF ₃			
17	CF ₃			
18	CF ₃			
19	CF ₃			
20	CF ₃			

Appendix

21	CF ₃		
22	CF ₃		
5	CF ₃		
23	CF ₃	CH ₃	
14	CF ₃		
24	CF ₃	-	
25	CF ₃		-
26	-		
27	CH ₃		

Appendix

28	CF ₃		
29	CF ₃		
30	CF ₃		
31	CF ₃		
32	CF ₃		
33	CF ₃		
34	CF ₃		
35	CF ₃		

Appendix

Appendix

Figures

Appendix

<i>TLR3_HUMAN</i> /1-693	1 - - - - - MRQTLP CIYFWGGLLPFGMLCASSTTKKTVS - - -	31
<i>TLR7_HUMAN</i> /1-830	1 MVFPMWTLKRQILILFNILISKLLGARWFKTLPQDVTLDV	42
<i>TLR9_HUMAN</i> /1-806	1 -MGFCRSALHPLSLLVQAIMLAMTLALGTLPAPFLPQEL - - -	37
<i>TLR8_HUMAN</i> /1-819	1 MENMFLQSSMLTCTIFLLISGSCELCAEENFSRSYPQDE - - KK	40
<i>TLR3_HUMAN</i> /1-693	32 - - - HEVADCSHLKLTQVP - - - DDLPTNITVNLNTHNQLRRL	66
<i>TLR7_HUMAN</i> /1-830	43 PKNHVIVDCTDKHLTEIP - - - GGIPNTNTNLTLTINHLPDI	80
<i>TLR9_HUMAN</i> /1-806	38 - QPHGLVNCNWLFLKSVPHFSMAAPRGNVTSLSLSSNRHHL	78
<i>TLR8_HUMAN</i> /1-819	41 QNDSVIAECSNRRLQEVF - - - QTVGKYVTELDLSDNFITHI	78
<i>TLR3_HUMAN</i> /1-693	67 PAANFTRYSQLTSLDVGFN - - - - - TISKLEPEL	94
<i>TLR7_HUMAN</i> /1-830	81 SPASFHRLDHLVEIDFRNCVPIPLGSKNNMCIKRLQIKPRS	122
<i>TLR9_HUMAN</i> /1-806	79 HDSDFAHLPRLHNLKWNCPVGLS - - PMHFPCHMTIEPST	118
<i>TLR8_HUMAN</i> /1-819	79 TNESFQGLQNLTKINLNHNPNVQHQNNGNPGIQSNGLNITDGA	120
<i>TLR3_HUMAN</i> /1-693	95 CQKLPMLKVLNLQHNELSQLSDKTF AFCTNLTELHLMSNSIQ	136
<i>TLR7_HUMAN</i> /1-830	123 FSGLTYLKSLYLDGNQLEIPQ - - - GLPPSLQLLSLEANNIF	161
<i>TLR9_HUMAN</i> /1-806	119 FLAVPTLEELNLSYNNIMTVP - - - ALPKSLISLSLSHTNIL	156
<i>TLR8_HUMAN</i> /1-819	121 FLNLKKNLRELLLEDNQLPQIPS - - - GLPESLTELISLIQNNIY	159
<i>TLR3_HUMAN</i> /1-693	137 KIKNNPFVKQKNLITDLSHNGLSSTKLGTQVQLENLQELL	178
<i>TLR7_HUMAN</i> /1-830	162 SIRKENLTELANEILYLGQNCYRNPCYVSYSIEKDAFLNL	203
<i>TLR9_HUMAN</i> /1-806	157 MLDSASLAGLHALRFLFMDGNCYYKNPQRQALEVAPGALLGL	198
<i>TLR8_HUMAN</i> /1-819	160 NITKEGISRLINKNLYLAWNCYFNKVC EKTN - IEDGVFET	200
<i>TLR3_HUMAN</i> /1-693	179 SNNKIQALKSEELDIFAN - - - SSLKKLELSSNQIKESPGCF	217
<i>TLR7_HUMAN</i> /1-830	204 TKLKVLSLKDNNVTAVPTVLPSTLTLEYLYNNMIKIQEDDF	245
<i>TLR9_HUMAN</i> /1-806	199 GNLTHTLSLKYNNTLVVPRNLPSSLEYLLLSYNNRIVKLAPEDL	240
<i>TLR8_HUMAN</i> /1-819	201 TNLELLSLSFNSLSHVPPKLPSSLRKLFLSNTQIKYISEEDF	242
<i>TLR3_HUMAN</i> /1-693	218 HAIGRLFGLFLNNVQLGPSLTEKLCLELAN - - - - -	247
<i>TLR7_HUMAN</i> /1-830	246 NNLNQLQILDLSGNCPRCYNAPFPAPCKNNSPLQIPVNAFD	287
<i>TLR9_HUMAN</i> /1-806	241 ANLTALRVLDVGGNCRRCDHAPNPMCPCPR - HFPQLHPDTFS	281
<i>TLR8_HUMAN</i> /1-819	243 KGLINLTLLDLSGNCPRCFNAPFPCVPCDGGASINIDRFAFQ	284
<i>TLR3_HUMAN</i> /1-693	248 - - TSIRNLSLSNSQLSTTSNTTFLGLKWTNLTMLDLSYNNLN	287
<i>TLR7_HUMAN</i> /1-830	288 ALTELKVLRLHSNSLQHVPPRWFKNINKLQELDL SQNFLAKE	329
<i>TLR9_HUMAN</i> /1-806	282 HLSRLEGLVLKDSLSWLNASWFRGLGNLRVLDLSENFYKLC	323
<i>TLR8_HUMAN</i> /1-819	285 NLTQLRYLNLSSTSLRKINAAWFKNMPHLKVLDLEFNLYLVGE	326
<i>TLR3_HUMAN</i> /1-693	288 VVGNDSFAPWLQLEYFFLEYNNIQHLFSHSLGLFNVRYNL	329
<i>TLR7_HUMAN</i> /1-830	330 IGDAKFLHFLPSLIQLDLSFNFEQLQVYRASMNLSQAFSSLSKS	371
<i>TLR9_HUMAN</i> /1-806	324 ITKTKAFAQGLTQLRKLNLSFNQYQKRVSAHLSLAPSFGLVA	365
<i>TLR8_HUMAN</i> /1-819	327 IASGAFLTMLPRLEILDLSFNQYIKGSYPQHINISRNFSKLS	368
<i>TLR3_HUMAN</i> /1-693	330 KRSFTKQSSLASLPKIDDFSQWLKCLEHLNMEENDIPGIK	371
<i>TLR7_HUMAN</i> /1-830	372 LKILRIRGYVFKELKSFNLSPLHNLQNLVLDLGTNFIKIAN	413
<i>TLR9_HUMAN</i> /1-806	366 LKELDMHGIFFRSLDETTLRPLARLPMLQTLRLQMNFINDAQ	407
<i>TLR8_HUMAN</i> /1-819	369 LRALHLRGYVFEQELREDDFQPLMQLPNLSTINLGINFKQID	410
<i>TLR3_HUMAN</i> /1-693	372 SNMFTGLINLKLYLSLS - - - - -	387
<i>TLR7_HUMAN</i> /1-830	414 LSMFKQFKRLKVIDLSVNKISP SGDSSEVGFCSNARTSVESY	455
<i>TLR9_HUMAN</i> /1-806	408 LGIFRAFPGLRYVDLSNRI SGASELTATMG EADGGEKVWLQ	449
<i>TLR8_HUMAN</i> /1-819	411 FKLFGNFSNLEIILYLS - - - - -	452
<i>TLR3_HUMAN</i> /1-693	388 - - - - - NSFTSLRTLNET - - - - - FVSLAHSPLHI	411
<i>TLR7_HUMAN</i> /1-830	456 EPQVLEQLHYFRYDKYARSCRFKNKEASFMSVNESCYKYGQT	497
<i>TLR9_HUMAN</i> /1-806	450 P - - - - - GD LAPAPVDT PSSE - - - DFRPNCSTLNFT	476
<i>TLR8_HUMAN</i> /1-819	453 K - - - - - RRSTDFEFDPHSNFYHFTRP - - - - - LIKPQCAAYGKA	485

Appendix

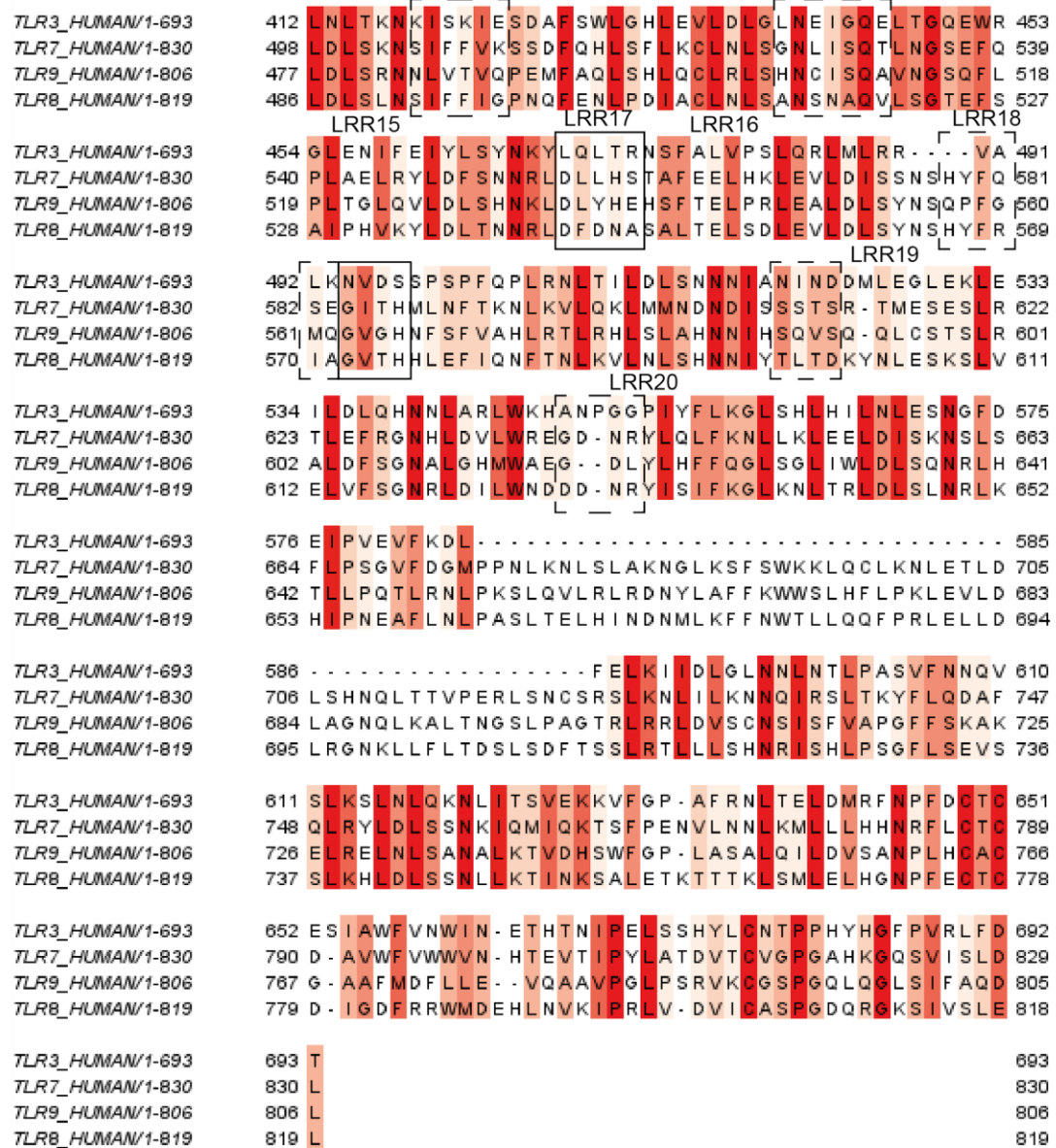


Figure S 1. Multiple sequence alignment of human TLR3, TLR7, TLR8 and TLR9. The sequences are colored according to the conservation. The binding site residues and residues implicated in the receptor dimerisation are highlighted in the lined and dashed boxes, respectively.

Appendix

Species	Accession	Position	Sequence	Position
TLR8_HUMAN	1-819	1	MENMFLQSSMLTCLFLLISGSCELC AEENFSRSYPCDE	42
TLR8_MOUSE	1-810	1	MENMPPQSWILTCFCLLSSGTS AIFHKANYSRSYPCDE	42
A5H300_RAT	1-807	1	---MSPQSWILTCFCLLSSGTS AVFLKGNFSRSYPCDE	39
B3XXC2_PIG	1-808	1	---MTLHFLLLTCLFLLIIPDSCEFFTGANYSRSYPCDE	39
A5H622_BOVIN	1-811	1	---MTLHFLLLTCLFLLISDSCEFFTEASYPRSYPCDE	39
W5Q9N5_SHEEP	1-813	1	ENMTLRFLLLTCLFLLIISDSCEFFTEASYPRSYPCDE	41
ABQM58_HORSE	1-816	1	---MILQPLLLTCLFLLIISDSCEFFTETNYSRSYPCDE	39
B2BE52_FELCA	1-817	1	---MTLQSLLLTCLFLLISDSREFFTEANYSRSYPCDE	39
TLR8_HUMAN	1-819	43	DSVIAECNSNRRLQEVPTVGKYVTELDLSDNFI	84
TLR8_MOUSE	1-810	43	SLVIAECNHRQLHEVPQTIGKYVTNIDLSDNAI	84
A5H300_RAT	1-807	40	ALVTAECNHRQLHEVPQTIGKYVTDVDSDNIT	81
B3XXC2_PIG	1-808	40	GSVIAECNHRQLQEVPRRVGNVTELDLSDNFI	81
A5H622_BOVIN	1-811	40	GSFIAECNGRRRLQEVPTVDKDVTEVDSDNFI	81
W5Q9N5_SHEEP	1-813	42	GSFIAECNSNRRLQEVPTVDKAVTEVDSDNFI	83
ABQM58_HORSE	1-816	40	VSVIAECNDRRLQEVPTVGKYVTELDLSDNFI	81
B2BE52_FELCA	1-817	40	GSIIAQCNDRRLQEVPTVSKYVTDALDSYNFI	81
TLR8_HUMAN	1-819	85	GLQNLTKINLNHNPNVQHQNGNPGIQSNGLNIT	126
TLR8_MOUSE	1-810	85	KLQNLTKIDLNHNKQKQHPNEN---KNGMNI	122
A5H300_RAT	1-807	82	KFRNLTKINLNHNKQKQHPNEN---KNGMNI	119
B3XXC2_PIG	1-808	82	GLQNLTKINLNHNKQKQHPNEN---KNGMNI	117
A5H622_BOVIN	1-811	82	GLQNLTKINLNHNKQKQSGNPAV---KKAMTI	120
W5Q9N5_SHEEP	1-813	84	GLQNLTKINLNHNKQKQSGNPAV---KKAMTI	122
ABQM58_HORSE	1-816	82	GLQNLTKINLNHNKQKQSGNPAV---KKAMTI	123
B2BE52_FELCA	1-817	82	GLQNLTTRINLNHNKQKQHLNENPDINRSGMNI	123
TLR8_HUMAN	1-819	127	RELLELEDNQLPQIPSGLPESLTEL SLIQNNI	168
TLR8_MOUSE	1-810	123	LTVLLELEDNQLYTI PAGLPESLKE LSLIQNNI	164
A5H300_RAT	1-807	120	LTELLELEDNQLYTI PAGLPESLKE LSLIQNNI	161
B3XXC2_PIG	1-808	118	RELLELEDNQLREIPTGLPESLREL SLIQNKI	159
A5H622_BOVIN	1-811	121	RELLELEDNQLQQIPAGLPESLKKL SLIQNNI	162
W5Q9N5_SHEEP	1-813	123	RELLELEDNQLQEIPAGLPESLKE LSLIQNNI	164
ABQM58_HORSE	1-816	124	RELLELEDNQLDKIPTGLPESLREL SLIQNRIT	165
B2BE52_FELCA	1-817	124	LNQLLELEDNQLDQIPAGLPESLREL SLIQNNI	165
TLR8_HUMAN	1-819	169	LINLKNLYLAWNCYFNKVC E--KTNI	208
TLR8_MOUSE	1-810	165	LRNLERLYLGWNCYFK--CN-QTFKVEDGAFKNL	203
A5H300_RAT	1-807	162	LRNLERLYLGWNCYFK--CN-QIFKVEDGAFNNL	200
B3XXC2_PIG	1-808	160	LRKLESLYLGWNCYFT--CN-ETFI	198
A5H622_BOVIN	1-811	163	LGNLESYLGWNCYFA--CD-KKFTI	201
W5Q9N5_SHEEP	1-813	165	LGNLERLYLGWNCYFA--CN-KKFSI	203
ABQM58_HORSE	1-816	166	LMNLEYLYLGWNCYFGNICH-KTFDIEDGT	206
B2BE52_FELCA	1-817	166	LTNLQRLYLSWNCYFGNNCNNKTFDIEDGT	207
TLR8_HUMAN	1-819	209	SFNSLSHVPRKLPSSLRKLF LSNQTQIKYI	250
TLR8_MOUSE	1-810	204	SFNNLFYVPRKLPSSLRKLF LSNAKIMNI	245
A5H300_RAT	1-807	201	SFNNLFYVPRKLPSSLRKLF LSNAKISTIT	242
B3XXC2_PIG	1-808	199	SFNTLYRVPRKLPSSLTKLYLSNTKIRNIN	240
A5H622_BOVIN	1-811	202	SFNPLHSVPRSLPSSLTELYLSNTHIGNV	243
W5Q9N5_SHEEP	1-813	204	SFNPLHSVPRSLPSSLTELYLSNTHIGNV	245
ABQM58_HORSE	1-816	207	SFNNLSHVPRKLPNSLRELYLSNTKIKNIT	248
B2BE52_FELCA	1-817	208	SFNKLHVHPRKLPNSLRELYLSNAKIKVIS	249
TLR8_HUMAN	1-819	251	LDLSGNCPRCFNAPFPVPCDGGASINIDRF	292
TLR8_MOUSE	1-810	246	LDLSGNCPRCFNAPFPCTPCCKENSSIH	287
A5H300_RAT	1-807	243	LDLSGNCPRCFNAPFPCCNLSASIRIH	284
B3XXC2_PIG	1-808	241	LDLSGNCPRCFNAPFPCCNPGDASIQIH	282
A5H622_BOVIN	1-811	244	LDLSGNCPRCFNAPFPVPCQGDASIQIH	283

Appendix

W5Q9N5_SHEEP/1-813	246	LDLSGNCPRCFNAPFPCTPQGGASIQIHPLAFQT	LTQLRYL	287
A8QM58_HORSE/1-816	249	LDLSGNCPRCFNAPFPCTPQERDSSIQIHPLAFQD	LTQLRYL	290
B2BE52_FELCA/1-817	250	LDLSGNCPRCFNAPFPCTPQEGGSSIQIHPLAFQT	LTQLRYL	291
TLR8_HUMAN/1-819	293	NLSSTSLRKINAAWFKNMPHLKVL	DLEFNLYLVGEIASGAFLT	334
TLR8_MOUSE/1-810	288	NLSSTSLRTIPSTWFENLSNLKEL	HLEFNLYLVQEIASGAFLT	329
A5H300_RAT/1-807	285	NLSSTSLRTIPSTWFENLNLKEL	HLEFNLYLVQEIASGAFLT	326
B3XXC2_PIG/1-808	283	NLSSTSLRRIPATWFENLHHLKVL	HLEFNLYLMDEIASGEFLA	324
A5H622_BOVIN/1-811	286	NLSSTSLRKVPASWFDNMHNLKVL	DLEFNLYLMDEIASGEFLT	327
W5Q9N5_SHEEP/1-813	288	NLSSTSLRKVPASWFDNMHNLKVL	DLEFNLYLMDEIASGEFLT	329
A8QM58_HORSE/1-816	291	NLSSTSLRKVPAPAIWFDNMHHLKVL	HLEFNLYLVQEIASGEFLT	332
B2BE52_FELCA/1-817	292	NLSSTSLQKIPAMWFQSMHNLKVL	HLEFNLYLVDEIASGEFLT	333
TLR8_HUMAN/1-819	335	MLPRLEILDLSFNFIKGSYPQHINISRNFSKLLSLRALHLRG		376
TLR8_MOUSE/1-810	330	KLPSLQILDLSFNFIKQKEYLQFINISSNFSKLLSLKHLHLRG		371
A5H300_RAT/1-807	327	KLPSLQILDLSFNFIHKEYLQYITISPNFSMLRSLRKLHLKG		368
B3XXC2_PIG/1-808	325	KLPSLEILDLSYNYEQKKYPQYINISHYFANLTSQILHLRA		366
A5H622_BOVIN/1-811	328	KLPSLEILDLSYNYELKKYPQHINISKNFSKLLSLQMLHLRG		369
W5Q9N5_SHEEP/1-813	330	KLPSLEILDLSYNYELKKYPQYINISKNFSKLLSLQMLHLRG		371
A8QM58_HORSE/1-816	333	KLPSLEILDLSFNFIKQKEYLQFINISSNFSKLLSLQMLHLRG		374
B2BE52_FELCA/1-817	334	KLPSLEILDLSYNYVKKAKYPRYINISQNFSLKLLQTLHLRG		375
TLR8_HUMAN/1-819	377	YVFQELREDDFQPLMQLPNLTSTINLGINFIKQIDFKLFQNF	FS	418
TLR8_MOUSE/1-810	372	YVFRELKKKHFEHLQSLPNLATINLGINFIEKIDFKAFQNF	FS	413
A5H300_RAT/1-807	369	YVFRELKKEHFKPLQNLPNLTSTINLGINFIEKIDFKAFQDF	FP	410
B3XXC2_PIG/1-808	367	YVFQELRKEDFQPLRNLHLKFINLGINFIKQIDFTIFSEFS		408
A5H622_BOVIN/1-811	370	YVFQELRMEDFEPLRHLNLTSTINLGVNFIKQIDFSIFQWFP		411
W5Q9N5_SHEEP/1-813	372	YVFQELRRKDFKPLQHLNLTSTINLGVNFIKQIDFSIFHWFP		413
A8QM58_HORSE/1-816	375	YVFQEVRRKEHFRPLMSLSNLKTINLGVNFIKQIDFTFFQHF	FP	416
B2BE52_FELCA/1-817	376	YVFQELRAEDFQPLMNLNLTSTINLGINFIKQIDFTLQNF	FS	417
TLR8_HUMAN/1-819	419	NLEIIYLSENRISPLVKDTRQSYANSSSFQRHIRKRRSTDF	-	459
TLR8_MOUSE/1-810	414	KLDVIYLSGNRIASVLDG----	TDYSSWRNRLRKPLSTDD	450
A5H300_RAT/1-807	411	NLKVIYLSGNRIASVIDG----	TDHSSWRNRLRKPLSTDYD	447
B3XXC2_PIG/1-808	409	NLSIIYLSENRISPLVNNTGQKNGDRPSFQSHVLKPRSATP	-	449
A5H622_BOVIN/1-811	412	NLKIIYLSENRISPLVSDTEQHDANGTSFQSHILKRRSADI	-	452
W5Q9N5_SHEEP/1-813	414	NLKIVYLSENRISPLVSDTEQHDANGTFFQSHILKRRSADI	-	454
A8QM58_HORSE/1-816	417	NLTVIYLSENRISPLVNDLSQNYTNGSAFQSHILKRRSADF	-	457
B2BE52_FELCA/1-817	418	NLSIIYLSENRISPLVNDIKQNDMSGSSSQSHIRLR	SADT	458
TLR8_HUMAN/1-819	480	EFDPHSNFYHFTRPLIKPQCAAYGKALDLSLNSIFFIGPNQF		501
TLR8_MOUSE/1-810	451	EFDPHVNIFYHSTKPLIKPQCTAYGKALDLSLNNIFIIQKSQF		492
A5H300_RAT/1-807	448	EFDPHMNFYHSTKPLIKPQCTTYGKALDLSLNNIFVIGKSQF		489
B3XXC2_PIG/1-808	450	KFDPHSNFYHNTKPLIKPQCSRYGKALDLSLNSIFFIGPNQF		491
A5H622_BOVIN/1-811	453	QFDPHSNFYHNTKPLIKTECSRNLGNALDLSLNSIFFIGVNQF		494
W5Q9N5_SHEEP/1-813	455	QFDPHSNFYHNTKPLIKTECSRNLGNALDLSLNSIFFIGVNQF		496
A8QM58_HORSE/1-816	458	EFNPHSNFYHNTNPLIKPQCTAYGKALDLSLNSIFFIGQKQF		499
B2BE52_FELCA/1-817	459	EFDPHSNFYHNTNPLIKPQCTVYGKALDLSLNSIFFIGREQF		500
TLR8_HUMAN/1-819	502	ENLPDIACLNLSANSNAQVLSGTEFSAIPHVKYLDLTNNRLD		543
TLR8_MOUSE/1-810	493	EGFQDIACLNLSFNANTQVFNGTEFSSMPHIKYLDLTNNRLD		534
A5H300_RAT/1-807	490	EGFQDIACLNLSFNANGQVLNGTEFSSMPHIKYLDLTNNRLD		531
B3XXC2_PIG/1-808	492	EAFKDIACLNLSNNGNGQVLHGSEFSLPGIKYLDLTNNRLD		533
A5H622_BOVIN/1-811	495	KDFGNIACLNLSNNGNGQVLNGTEFSCLSGIKYLDLTNNRLD		536
W5Q9N5_SHEEP/1-813	497	KDFGNIACLNLSNNGNGQVLNGTEFSRLSGIKYLDLTNNRLD		538
A8QM58_HORSE/1-816	500	KAFHDIACLNLSNNGIGQPLHGTEFSAPPHIKYLDLTNNRLD		541
B2BE52_FELCA/1-817	501	KAFHDIACLNLSNNGNGQVLHGTEFSAPPHIKYLDLTNNRLD		542
TLR8_HUMAN/1-819	544	FDNASALTTELSDLEVLDLSYNHYFRIAGVTHHLEFIQNFTN		585
TLR8_MOUSE/1-810	535	FDDNNAFSDLDHLEVLDLSHNAHYFSIAGVTHRLGFIQNLIN		576

Appendix

A5H300_RAT/1-807	532	FDDNQTFSDLD	LEVLDLSHNAHYFSIAGVTHRLGFIQNLIK	573
B3XXC2_PIG/1-808	534	FDDDAAFSELPL	LEVLDLSYNSHYFRIAGVTHRLGFIQNLPQ	575
A5H622_BOVIN/1-811	537	FDDDAAFSELPL	LEVLDLSYNNAHYFRIAGVTHRLGFIHLTN	578
W5Q9N5_SHEEP/1-813	539	FDDDAAFSELPL	LEVLDLSYNNAHYFRIAGVTHRLGFIHLTN	580
A8QM58_HORSE/1-816	542	FDDDNALRELPE	LEVLDLSYNNAHYFRIAGVTHRLGFIQNLTQ	583
B2BE52_FELCA/1-817	543	FDDDNALSDLE	LEVLDLSYNNAHYFRIAGVTHRLGFIQNLTQ	584
LRR19				
TLR8_HUMAN/1-819	586	LKVLNLSHNNIY	TLTDKYNLESKSLVELVFSGNRLDLWNDD	627
TLR8_MOUSE/1-810	577	LRVLNLSHNGIY	TLTESELKSLKELVFSGNRLDLWNAN	618
A5H300_RAT/1-807	574	LKVLNLSHNGIY	TLTDEYKLQSKSLKELVFSGNRLDLWNAN	615
B3XXC2_PIG/1-808	576	LRVLNLSHNSIY	TLTETYLKSTSLKELVFSGNRLDLWNAQ	616
A5H622_BOVIN/1-811	579	LRVLNLSNNDIY	TLTETQLKSSASLGELVFSGNRLDLWNAQ	619
W5Q9N5_SHEEP/1-813	581	LRVLNLSNNDIY	TLTETQLKSSASLGELVFSGNRLDLWNAQ	621
A8QM58_HORSE/1-816	584	LRVLNLSHNSIY	TLTEYNMNSMSLEELVFSGNRLDLWNAE	624
B2BE52_FELCA/1-817	585	LKVLNLSHNSIY	TLTEQDLRSMSELKELVFSGNRLDLWNAE	625
LRR20				
TLR8_HUMAN/1-819	628	DNRYSIFKGL	KNLTRLDLSLNRLKHIPNEAFLNLPASLTTEL	669
TLR8_MOUSE/1-810	619	DGKYWSIFKSL	QNLIRLDLSYNNLQQIPNGAFLNLPQSLQEL	660
A5H300_RAT/1-807	616	DGKYWSIFTS	LETTLRLDLSYNNLQQIPNEAFLNLPQSLQEL	657
B3XXC2_PIG/1-808	617	DDRYWDIFKNL	STLTHLDLSNNLQHIPPSEAFLNLPQTLET	658
A5H622_BOVIN/1-811	620	DVRYWQIFQNL	TNLTRLDLARNNLRHISSQAFLNLPRTLTDL	661
W5Q9N5_SHEEP/1-813	622	DVRYWQIFQNL	TNLTRLDLARNNLRHISSQAFLNLPRTLTDL	663
A8QM58_HORSE/1-816	625	DRRYRKIFKCL	RNLTRLDLSFNNLQHIPPDEAFLNLPQNLTTEL	666
B2BE52_FELCA/1-817	626	GDKYWKIFTN	LGNLTWLDLSSNNLRHIPNEAFLNLPQSLTKL	667
TLR8_HUMAN/1-819	670	HINDNMLKFF	NWTLTLLQQFPRLELLDLRGNKLLFLTDSLSDF	711
TLR8_MOUSE/1-810	661	LISGNKLRFF	NWTLTLLQYFPHLHLLDLSRNELYFLPNCLSKFA	702
A5H300_RAT/1-807	658	HINDNRLRFF	NWTLTLLQYFPHLHVLDLGRNELYFLTNCLSKFT	699
B3XXC2_PIG/1-808	659	YISDNRLNFF	NWSLLQQFPNLTLLDLSGNELSFLTDSLSKFT	700
A5H622_BOVIN/1-811	662	YINDNMLNFF	NWSLLEYFPHLRLLDLSGNQLFFLTNSLSTFA	703
W5Q9N5_SHEEP/1-813	664	YINDNMLNFF	NWSLLEYFPHLRLLDLSGNQLFFLTNSLSTFA	705
A8QM58_HORSE/1-816	667	YINDNRLHFF	NWTLTLLQHFPHLHLLDLSRNKLSSLTNLSKFS	708
B2BE52_FELCA/1-817	668	YIRDNVNLSF	NWTLTLLQLFPHLQLLDLSGNRLSSLTNLSKFT	709
TLR8_HUMAN/1-819	712	SLRRTLLLSHNR	ISHLPSGFLSEVSSLKHLDLSSNLLKKTINK	753
TLR8_MOUSE/1-810	703	HSLETLLLSHNF	SHLPSGFLSEARNLVHLDLSFNTIKMINK	744
A5H300_RAT/1-807	700	HSLEKTLNHNH	SHLPAGFLSEARNLVYLDLSFNTIKMINK	741
B3XXC2_PIG/1-808	701	TSLETLILSRNR	ISYLPAGFLSEASSLTHLDLSSNQLKMNVI	742
A5H622_BOVIN/1-811	704	SSLETLLLSRNR	ISHLPSDFLSGASSLIHLDLSSNQLKMLNR	745
W5Q9N5_SHEEP/1-813	706	SSLETLLLSRNR	ISHLPSDFLSGASSLIHLDLSSNQLKMLNR	747
A8QM58_HORSE/1-816	709	PSLRTLLLSQNK	ISHLPSGFFSEASGLIHLDLRFNRLKMINK	750
B2BE52_FELCA/1-817	710	PSLRTLLLSRRNR	ISHLPSNFLSEASSLIHLDLSSNLLKMINK	751
TLR8_HUMAN/1-819	754	SALETKTITTKL	SMLELHGNNPFECTCDIGDFRRWMDENLVKI	795
TLR8_MOUSE/1-810	745	SSLQTKMKTNLS	ILELHGNYFDCTCDISDFRSWLDENLNITI	786
A5H300_RAT/1-807	742	SSLQTETKTNLS	VLDLQGNHFDCTCDISDFRSWLEENPHVRI	783
B3XXC2_PIG/1-808	743	SKLHAKTTTNLA	LKLDRNPFDCDIDFRKWMDENLKVITI	784
A5H622_BOVIN/1-811	746	STFETKTATKLT	VLELGGNPFDCDLDGDFLEWMDRNLNVRV	787
W5Q9N5_SHEEP/1-813	748	STFETKTATKLT	VLELGGNPFDCDLDGDFLEWMDRNLNVRV	789
A8QM58_HORSE/1-816	751	TTLQTKTTINLA	VLELGGNPFDCDIDGDFRRWMDENLNIAI	792
B2BE52_FELCA/1-817	752	STLQTKTATNLT	VLELGGNPFDCDIDGDFRRWMDENLDVTI	793
TLR8_HUMAN/1-819	796	PRLVDVICASPG	DQRGKSI VSL	819
TLR8_MOUSE/1-810	787	PKLVNVVICSNP	GDQKSKS IMSLDL	810
A5H300_RAT/1-807	784	PRLVDVICSNP	GDQRWKSVM SLDL	807
B3XXC2_PIG/1-808	785	PRLTDVICASPG	DQRGRS I VSL	808
A5H622_BOVIN/1-811	788	PRLTDVICASPG	DQEGKSI VSL	811
W5Q9N5_SHEEP/1-813	790	PRLTDVICASPG	DQEGKSI VSL	813
A8QM58_HORSE/1-816	793	PRLADVICASPG	DQRGKSI VSL	816
B2BE52_FELCA/1-817	794	PRLADVICSSPG	DQRGKSI VSL	817

Figure S 2. Multiple sequence alignment of human, mouse, rat, pig, cow, sheep, horse and cat TLR8. The sequences are colored according to the conservation scores [164]. The binding site residues and

Appendix

residues implicated in the receptor dimerisation are highlighted in the lined and dashed boxes, respectively.

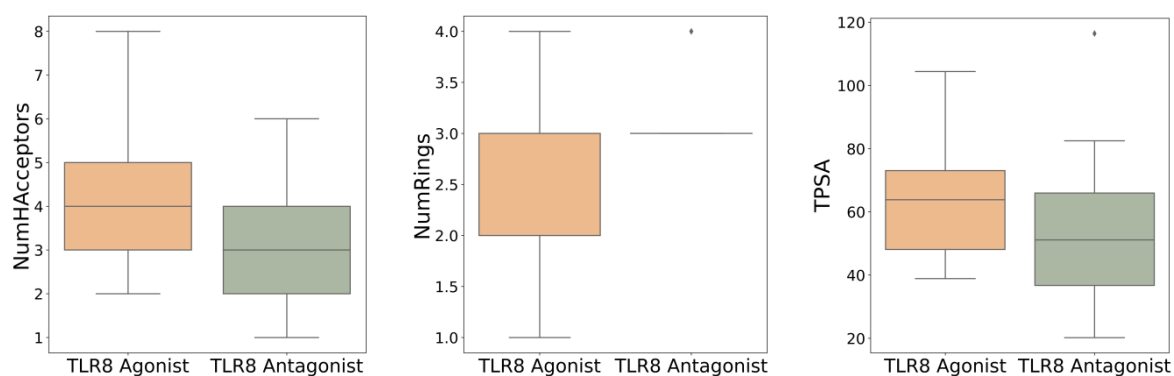
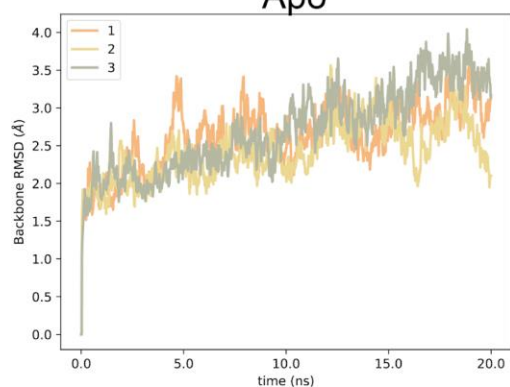


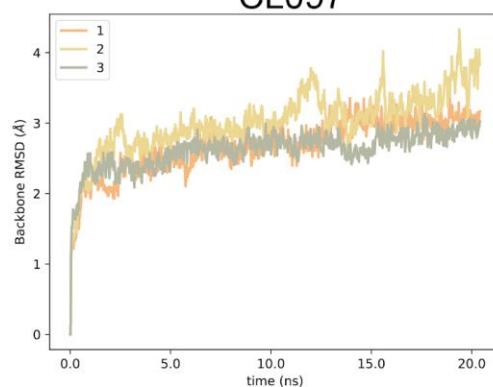
Figure S 3. Distribution of number of hydrogen bond acceptors, number of rings and TPSA for different TLR8 agonists and antagonists.

Appendix

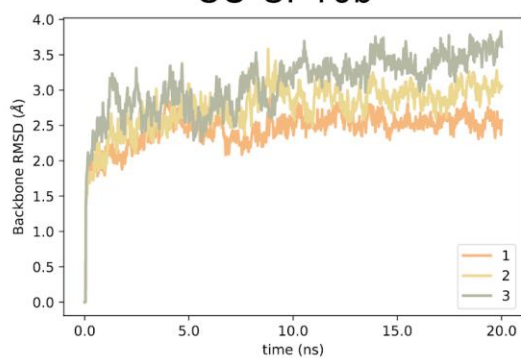
Apo



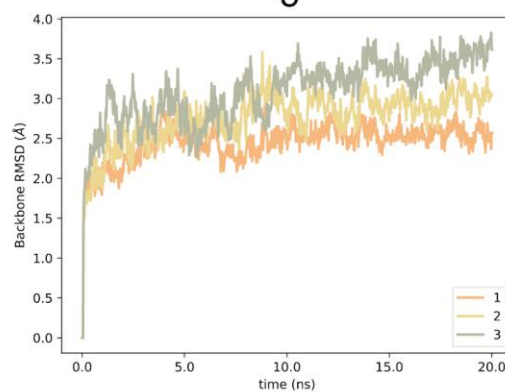
CL097



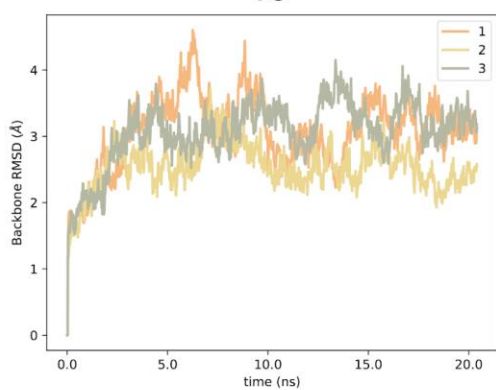
CU-CPT9b



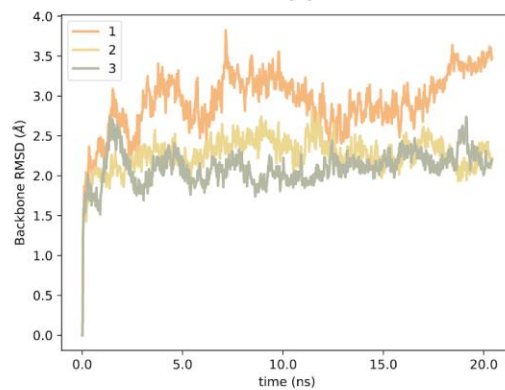
5



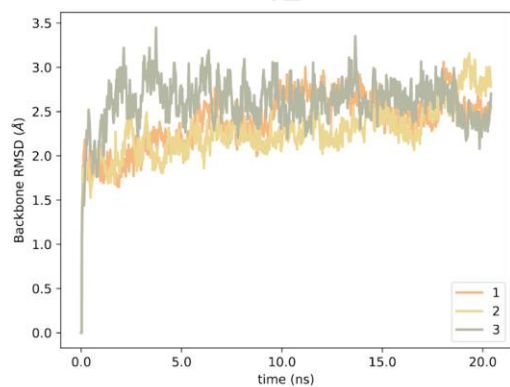
10



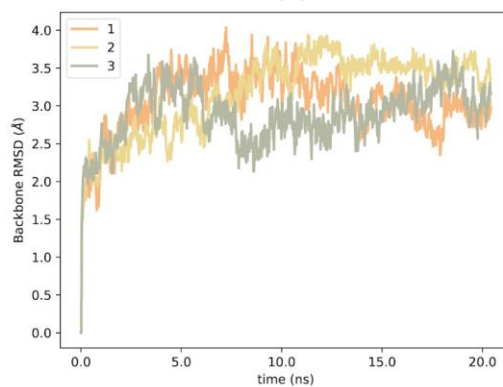
11



12



14



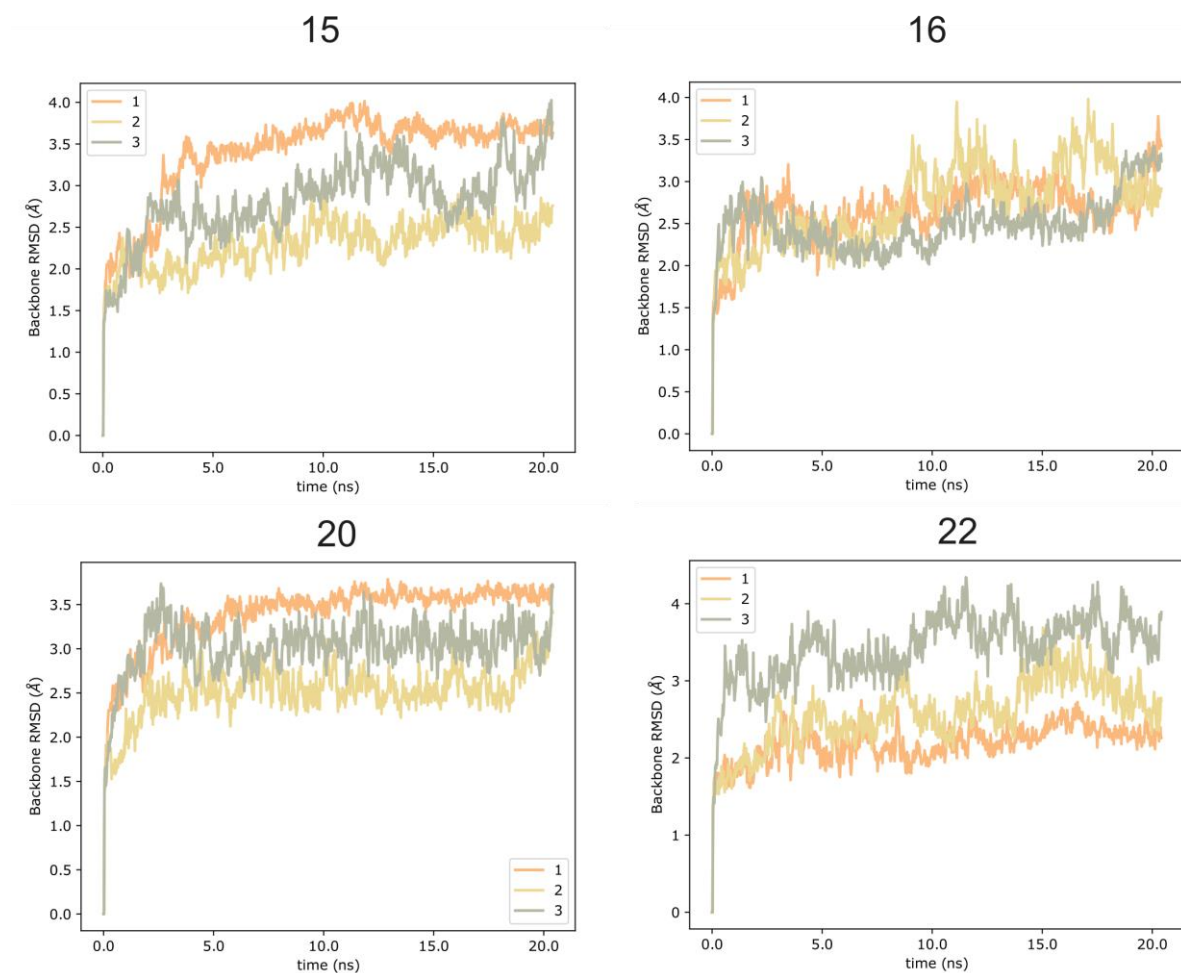


Figure S 4. Plots of root mean square deviation (RMSD) for the simulated systems. All the frames were superimposed to the starting frame and RMSD was calculated.

List of figures

Figure 1. Pattern-recognition receptors (PRRs) recognise pathogen-associated molecular patterns (PAMPs) and damage-associated molecular patterns (DAMPs) from pathogens and endogenous cells.	1
Figure 2. Roles of TLR8 in antigen-presenting cells (APC), Treg (T regulatory cells), hepatocytes and neurons.	4
Figure 3. Structure of TLR8. Schematic representation of the TLR8 ectodomain, transmembrane domain and cytoplasmic TIR domain (A). Cartoon representation of the ectodomain (B) with leucine-rich repeats (LRR) and Z-loop (PDB ID: 3W3J) [22].	5
Figure 4. Schematic representation of the dimerisation of TLR8 monomers upon Z-loop cleavage, and subsequent activation of the dimer by the binding of natural ligands.....	6
Figure 5. Schematic representation of the stabilisation of inactive state by small-molecule antagonists.....	6
Figure 6. Overview of TLR8-mediated signalling pathways. Upon activation of the receptor, downstream signalling cascades, which involve various adapter molecules and kinases, transmit the signal. As a result, transcription factors NF- κ B, AP-1, and IRF7 activate subsequent transcription of genes coding for pro-inflammatory cytokines and type I interferons.	8
Figure 7. Aberrant TLR8 signalling is involved in various pathological conditions. In allergic disorders and asthma (A) activation of TLR8 shifts the allergic state, characterised by T-helper cell type 2 cells response (Th2), into the non-allergic Th1 response. In cancer (B), TLR8 activation in, e.g pancreatic and lung cancer cells, leads to the secretion of pro-inflammatory cytokines and cell death inhibition, which promotes chronic inflammation and neoplastic transformation in pre-cancerogenic and cancerogenic cells. The opposite effect is observed in squamous carcinoma, where TLR8 activation leads to cell death and subsequent activation of the repair mechanisms.	9
Figure 8. Previously described TLR8 agonists.....	11
Figure 9. Previously described TLR8 antagonists.....	12

List of figures

Figure 10. A simple representation of molecular docking. Molecular docking is a method for the prediction of the ligand conformation and orientation in the macromolecular binding site. 15

Figure 11. A simple representation of a molecular dynamics simulation. Molecular dynamics simulations are atomic-level computer simulations that capture the dynamic behaviour of different molecular systems through time. 17

Figure 12. 3D pharmacophores describe the nature and location of the chemical moieties in ligands involved in interactions with macromolecular targets (A). The molecular interaction pattern between ligand and macromolecular target through molecular dynamics simulation can be described with dynophores (B). 18

Figure 13. Overview of TLR8 (PDB ID: 4R09) (orange and green cartoons for the two monomers) with the depicted binding sites for small-molecule (yellow sticks) and dinucleotide (grey sticks) agonists, side view (left) and front view (right). 22

Figure 14. Heatmap of average root-mean-square deviation (RMSD) values for alpha carbons between superimposed structures of TLR8 monomers. For the sake of clarity, only representative structures were selected: unliganded TLR8 (PDB ID: 3W3G), unliganded TLR8 with uncleaved Z-loop (PDB ID: 5HDH), small-molecule agonist-bound TLR8 (PDB ID: 3W3L, 5AWC and 4QBZ), uridine-bound TLR8 (PDB ID: 4R0A), dinucleotide- and uridine-bound TLR8 (PDB ID: 4R09) and small-molecule antagonist-bound TLR8 (PDB ID: 5WYX). 23

Figure 15. Superposed crystal structures of unliganded (PDB ID: 3W3G), small-molecule agonist-bound (PDB ID: 3W3J), uridine-bound (PDB ID: 4R0A), small-molecule antagonist-bound (PDB ID: 5WYZ) and TLR8 with uncleaved Z-loop (PDB ID: 5HDH). Frontal view of the lateral face of TLR8, with enlarged view on loops in LRR18 and LRR8. 24

Figure 16. Overview of TLR8 (PDB ID: 5WYZ) (orange and green cartoons) with depicted binding sites for small-molecule (yellow sticks) antagonists, side view (left) and front view (right). 25

Figure 17. Overview of unliganded TLR8 (PDB ID: 3W3G) (grey cartoons) with depicted dimerisation patches (orange and green cartoons for each monomer), side view (left) and front view of the monomer (right). 26

List of figures

Figure 18. Overview of the antagonist-bound TLR8 (PDB ID: 5WYZ) (grey cartoons) with depicted dimerisation patches (orange and green cartoons for each monomer), side view (left) and front view of the monomer (right). The antagonist (yellow sticks) is also depicted.27

Figure 19. Overview of the agonist-bound TLR8 (PDB ID: 3W3J) (grey cartoons) with depicted dimerisation patches (orange and green cartoons for each monomer), side view (left) and front view of the monomer (right). The agonist (yellow sticks) is also depicted.28

Figure 20. Overview of the workflow for computationally-assisted identification of novel TLR8 modulators. The number of compounds after each step is represented on the arrows..32

Figure 21. Scatter Plot of SlogP and Weight for the reported TLR8 agonists and antagonists.....33

Figure 22. Distribution of the number of rotatable bonds (left) and the number of hydrogen bond donors (right) for TLR8 agonists and antagonists.34

Figure 23. Overlay of binding poses of synthetic small-molecule agonists (grey and white sticks) in the left panel and uridine (orange sticks) in the right panel from the superimposed crystal structures. For the sake of clarity, only following structures of TLR8 bound to selected ligands are depicted: DS-802 (PDB ID: 4QBZ), IMDQ (PDB ID: 5AWD), MB-564 (PDB ID: 5AWC), MB-343 (PDB ID: 5AZ5), dinucleotide and uridine (PDB ID:4R07).....35

Figure 24. A binding pose of small-molecule agonist CL097 (grey sticks) with interacting TLR8 residues (orange and green sticks for each monomer) (PDB ID: 3W3J) in 3D (left) and 2D representation (right). Hydrophobic and aromatic interactions are represented as yellow and blue spheres/circles. Hydrogen bond acceptor and donor interactions are represented as red and green arrows, respectively.36

Figure 25. Final structure-based pharmacophore based on interaction pattern of TLR8 agonists (A) and associated ROC curve on the validation set (B). AR1 - aromatic interaction, HBD1 - hydrogen bond donor, HBA1, 2 - hydrogen bond acceptor 1 and 2, HYD1, 2 - hydrophobic feature 1 and 2.37

Figure 26. Selected virtual screening hits from the pharmacophore-based virtual screening.38

List of figures

Figure 27. Modulation of hTLR8-mediated NF- κ B/AP-1 activation for virtual screening hits. (A) HEK-Blue hTLR8 cells were stimulated with CL075 or the compounds (5 and 25 μ M) for 24 h. Mean + SD (n=3). (B) HEK-Blue hTLR8 cells were preincubated with ODN2088 (1 μ M) or the compounds (10 and 25 μ M) for 1 h and afterwards stimulated with CL075 (8 μ M) for 24 h. Supernatants were analysed for TLR8-mediated NF- κ B/AP-1 activation by secreted embryonic alkaline phosphatase (SEAP) reporter assay using QuantiBlue (OD640). Mean + SD (n=4).40

Figure 28. Concentration-response curves of the ODN2088 and 5. HEK-Blue hTLR8 cells were incubated with increasing concentrations of ODN2088 or 5 for 1 h and stimulated with CL075 for 24 h. SEAP production was detected by QUANTI-Blue and OD was measured at 640 nm. Mean \pm SD (n = 3). Nonlinear regression with variable slope (four parameters) was used to fit the curve.....41

Figure 29. Selected virtual screening hits from shape- and atom-based similarity search.42

Figure 30. Modulation of hTLR8-mediated NF- κ B/AP-1 activation for the selected hits from the shape- and atom-based similarity search. (A) HEK-Blue hTLR8 cells were stimulated with CL075 or the compounds (5 and 25 μ M) for 24 h. Mean +SD (n=3). (B) HEK-Blue hTLR8 cells were preincubated with ODN2088 (1 μ M) or the compounds (10 and 25 μ M) for 1 h and afterwards stimulated with CL075 (8 μ M) for 24 h. Supernatants were analysed for TLR8-mediated NF- κ B/AP-1 activation by SEAP reporter assay using QuantiBlue (OD640). Mean +SD (n=3).43

Figure 31. Concentration-response curves of the 11 and 14. HEK-Blue hTLR8 cells were incubated with increasing concentrations of 11 or 14 for 1 h and additionally stimulated with CL075 for 24 h. SEAP production was detected by QUANTI-Blue and OD was measured at 640 nm. Mean \pm SD (n = 3). Nonlinear regression with variable slope (four parameters) was used to fit the curve.....44

Figure 32. Modulation of hTLR8-mediated cytokine secretion in THP-1 cells. THP-1 cells were pre-incubated with ODN2088 (1 μ M) or the compounds 5, 11 and 14 for 1 h and then additionally incubated with CL075 (8 μ M) for 24 h (A) or 4 h (B). Cytokine secretion into the culture medium was assessed by enzyme-linked immunosorbent assay (ELISA). Mean + SD (n=3).....45

List of figures

Figure 33. A binding pose of small-molecule antagonist CU-CPT9b (grey sticks) with interacting TLR8 residues (orange and green sticks for each monomer) (PDB ID: 5WYZ) in 3D (A) and 2D representation with the frequency of the formed interactions across triplicates of molecular dynamics simulation (B). Hydrophobic and aromatic interactions are represented as yellow and blue spheres/circles. Hydrogen bond acceptor and donor interactions are represented as red and green arrows, respectively.47

Figure 34. A predicted binding pose of 5 (grey sticks) with interacting TLR8 residues (orange and green sticks for each monomer) (PDB ID: 5WYZ) in 3D (A) and 2D representation with the frequency of the formed interactions during the molecular dynamics simulation (B). Hydrophobic and aromatic interactions are represented as yellow and blue spheres/circles. Hydrogen bond acceptor and donor interactions are represented as red and green arrows, respectively.48

Figure 35. The 3D representation of the dynamic 3D pharmacophore derived from the MD simulations of 5 (A) and 10 (B) (grey sticks). Hydrophobic and aromatic interactions are represented as yellow and blue clouds of points. Hydrogen bond acceptor and donor interactions are represented as red and green clouds of points.49

Figure 36. Bar code series representing hydrophobic interaction occurrence sequence of CU-CPT9b, 5 and 12 with Ala518 and Tyr348* during MD simulation. Simulation with each ligand was performed in triplicates.50

Figure 37. General optimisation strategy for 5 (grey sticks) with three main parts of the interest depicted in the 3D view of the binding site (left) and 2D depiction of 5 (right).51

Figure 38. Induction of hTLR8-mediated NF- κ B/AP-1 activation of the synthesised analogues. HEK-Blue hTLR8 cells were stimulated with TL8-506 or the compounds (10 and 25 μ M) for 24 h. Mean +SD (n=3).52

Figure 39. Inhibition of hTLR8-mediated NF- κ B/AP-1 activation of the synthesised analogues. HEK-Blue hTLR8 cells were preincubated with ODN2088 (1 μ M) or the compounds (10 and 25 μ M) for 1 h and afterwards stimulated with TL8-506 (0.6 μ M) for 24 h. Supernatants were analysed for TLR8-mediated NF- κ B/AP-1 activation by SEAP reporter assay using QuantiBlue (OD640). Mean +SD (n=3).53

List of tables

Figure 40. A predicted binding pose of 15 (grey sticks) with interacting TLR8 residues (orange and green sticks for each monomer) (PDB ID: 5WYZ) in 3D (A) and 2D representation with the frequency of the formed interactions during the molecular dynamics simulation (B). Hydrophobic and aromatic interactions are represented as yellow and blue spheres/circles. Hydrogen bond acceptor and donor interactions are represented as red and green arrows, respectively.55

Figure 41. Predicted binding pose of 20 (grey sticks) with interacting TLR8 residues (orange and green sticks for each monomer) (PDB ID: 5WYZ) in 3D (A) and 2D representation with the frequency of the formed interactions during the molecular dynamics simulation for 20 (B), 22 (C) and 16 (D). Hydrophobic and aromatic interactions are represented as yellow and blue spheres/circles. Hydrogen bond acceptor and donor interactions are represented as red and green arrows, respectively.56

Figure S 1. Multiple sequence alignment of human TLR3, TLR7, TLR8 and TLR9. The sequences are colored according to the conservation. The binding site residues and residues implicated in the receptor dimerisation are highlighted in the lined and dashed boxes, respectively. 115

Figure S 2. Multiple sequence alignment of human, mouse, rat, pig, cow, sheep, horse and cat TLR8. The sequences are colored according to the conservation scores [164]. The binding site residues and residues implicated in the receptor dimerisation are highlighted in the lined and dashed boxes, respectively. 118

Figure S 3. Distribution of number of hydrogen bond acceptors, number of rings and TPSA for different TLR8 agonists and antagonists..... 119

Figure S 4. Plots of root mean square deviation (RMSD) for the simulated systems. All the frames were superimposed to the starting frame and RMSD was calculated..... 121

List of tables

Table 1. Toll-like receptors, their localisation in cells and their respective natural ligands [9].....2

List of tables

Table 2. Protein sequence similarity between ectodomains and TIR domains in human TLR8 and TLR3, TLR7 and TLR9.....	29
Table 3. Protein sequence similarity between ectodomains and TIR domains in human TLR8 and TLR8s from animals.....	29
Table 4. Average interaction frequencies for 10, 11, 12, and 14 through MD simulations triplicates. AR - aromatic interaction, HBD - hydrogen bond donor, HBA - hydrogen bond acceptor, HYD - hydrophobic feature.....	48
Table S 1. Published crystal structures of human Toll-like receptor 8.....	94
Table S 2. Interaction frequency of residues between two TLR8 monomers throughout molecular dynamics simulations. Simulations for unliganded TLR8 (PDB ID:3W3G), TLR8 bound to agonist CL097 (PDB ID: 3W3J) and TLR8 bound to antagonist CU-CPT9b (PDB ID: 5WYZ) were done in triplicates.....	94
Table S 3. Collected agonists of TLR8 from the literature.....	102
Table S 4. Collected antagonists of TLR8 from the literature.....	107
Table S 5. Synthesised analogues of 5.....	109